Mechanistic Insights into the Interaction of Conformationally Distinct Amyloid-β Oligomers with the Prion Protein and Lipid Membranes

Priyanka Madhu

A thesis submitted for the partial fulfillment
of Doctor of Philosophy

Department of Chemical Sciences
Indian Institute of Science Education and Research Mohali
Knowledge City, Sector 81, SAS Nagar, Manauli PO, Mohali 140306, Punjab, India

December 2020

Dedicated to My Father,

Late Mr. Dharampal Madhu

Declaration

The work presented in this thesis has been carried out by me under the guidance of Dr. Samrat Mukhopadhyay at the Indian Institute of Science Education and Research Mohali. This work has not been submitted in part or in full for a degree, a diploma, or a fellowship to any other university or institute. Whenever contributions of others are involved, every effort is made to indicate this clearly, with due acknowledgement of collaborative research and discussions. This thesis is a bonafide record of original work done by me and all sources listed within have been detailed in the bibliography.

Priyanka Madhu

In my capacity as the supervisor of the candidate's thesis work, I certify that the above statements by the candidate are true to the best of my knowledge.

Dr. Samrat Mukhopadhyay
(Supervisor)

Acknowledgments

I express sincere thanks to all who have been there with me throughout my long journey of Ph.D.

First of all, I would like to thank my Ph.D. supervisor, Dr. Samrat Mukhopadhyay, whom I always admire for his vast knowledge not only on science but on a variety of topics. His excitement towards the research and his various quotes like “killer data,” “have clarity of thoughts,” kept me motivated in my Ph.D. The kind of training that I received from him, whether it is about the designing experiments, giving presentations, or writing a manuscript, will always be cherishable to me. I am very fortunate to have him as my academic father.

I want to thank my doctoral committee members, Dr. Angshuman Roy Choudhury and Dr. Santanu Kumar Pal, for their evaluation and valuable comments on my work.

Dr. Karishma Bhasne and Dr. Hema M. Swasthi taught me the basics of research, how to plan experiments, and the nitty-gritty associated with the work. They have taught me how well one should be prepared before coming on the working bench. An awesome post-doc, Dr. Anupa Majumdar, whom I admire for her keen knowledge. Various discussions with her had always remained fruitful for me. I thank Dr. Priyanka Dogra for teaching me the handling of pipette, expression, and purification of proteins and various other techniques associated with my work.

I acknowledge Debapriya Das for helping me with the time-resolved fluorescence anisotropy studies and Dr. Anupa Majumdar for teaching me the lipid vesicles preparation for my amyloid-β-lipid work. I thank Dr. Prashant Pandit and Dr. Shambhu Yadav for helping me with creating deletion constructs of the prion protein and Dr. Mahak Sharma and Dr. Devashish Dwivedi for helping me with the cell viability assay in my amyloid-β-prion protein work. I thank Prof. Witold Surewicz (Case Western Reserve University, U.S.A.) and Prof. Purnananda Guptasarma for their kind gifts of DNA plasmids. I thank Prof. Nigel M. Hooper (University of Manchester, U.K.) for guiding with the preparation of amyloid-β oligomers. I would also like to thank Dr. Santanu Kumar Pal, Ipshita Pani, Aayush, and Najiya for the collaborative work. I appreciate Dr. Anupa Majumdar, Debapriya Das, and Sayanta Mahapatra to involve me in their research works as a coworker. I thank IISER Mohali, Centre for Protein Science, Design, and Engineering (CPSDE), and Council of Scientific and Industrial Research (CSIR) for providing financial support and the

European Molecular Biology Organisation (EMBO) for the travel grant and additional support to attend the international conference.

I am very fortunate to have fantastic and fabulous labmates, Dr. Anupa Majumdar, Dr. Sourav Sinha Roy, Dr. Swapnil Singh, Dr. Shruti Arya, Dr. Karishma Bhasne, Dr. Hema M. Swasthi, Dr. Priyanka Dogra, Aishwarya Agarwal, Debapriya Das, Sayanta Mahapatra, Anamika Avni, Lisha Arora, Sandeep Rai, Ashish Joshi, Anusha Sarbahi, and Swastik P. G. I would like to thank all my labmates, from seniors to juniors, to maintain lab coherence and unity. I thank Dr. Neha Jain, Dr. Shruti Arya, and Dr. Mily Bhattacharya, who were not my direct work associates but have always given me useful suggestions and advice for my research career. I would also like to thank Vidya bhaiya for his efforts to keep the lab clean.

My Ph.D. journey has remained joyful and stress-free because of the fantastic people that I met here, who have become my family. The names are as Sudhanshu S. Chaurasia, Arnob Mukherjee, Avinash Singh, Ankit Singh, Satyam Ravi, Swagatam Nayak, Ayushi Singhania, and Pooja Munjal. Various discussions on current affairs and science over tea will always be my cherishable memories. I have learned a lot from them, whether it's about science, playing games, intellectual knowledge, or making fun. Badminton, another source of my enjoyment, had given me very good friends, Rajneesh, Vishavdeep, Nitish, Nishant, Shubham, Shubhendu, Vikas, Arnob, Ankit, Swagatam, Karishma, and Hema, with whom I had a lot of fun. I have also had the pleasure of being friends with Nitika, Komal, Nitin, Aman, Shivangi, Jyotsana, Shambhu, Deepak, Garima, and Jasleen. My labmates cum friends, Aishwarya Agarwal, Debapriya Das, Sayanta Mahapatra, and Anupa Majumdar, were always there in my all ups and downs. I also thank my college friends from University of Delhi, Elisha Kumari, Aditi Bharadwaj, Bhuvnesh Saini, and Manisha Yadav, who were always there to listen to all my stories and thoughts. I don't have to think before saying or sharing anything with them.

Last but not least, whatever endeavor I have put into completing this work would not have been possible without the unconditional love, blessings, sacrifices, and support of my dear family members. Mummy- Mrs. Krishna Madhu, Papa- Mr. Dharampal Madhu, Didi- Mrs. Anjali Piplani, Jiju- Mr. Manoj Piplani, Bhaiya- Mr. Chirag Madhu, and Bhabhi- Mrs. Kanika Madaan. Being the youngest, I always had the advantage of coached by my elder brother and sister in

every step of my career. Sharing the same workstream with my sister-in-law allowed me to discuss my work with her and get her valuable inputs. My mother's words, "*har cheej ka ek sahi time hota hai, jaruri nahi hai jab tum chaho tab miley*" (Translation: Things have their own right time, it's not necessary that whenever you want you will get) had kept me fighting to clear the NET exam and get into the Ph.D. program. My father, who was not so educated and started working at a very early age, had made sure that his children should not face the problems that he came across. I always admire him for his thinking, his way of parenting. Whatever I am, that is because of him. His words, "*beta, pareshan mat ho, sab ache se ho jayega*" (Translation: Dear daughter, don't worry, everything will be alright) had always kept me going in my life. I am happy that I am going to fulfill one of his dreams. For all the good he gave me, the part he represents in my life, I dedicate this thesis to my father, Mr. Dharampal Madhu.

Finally, I am grateful to all those who helped me, directly and indirectly, to achieve this goal, to all those whom I have been not able to express gratitude as an individual.

Priyanka Madhu

Chapter 1. Introduction

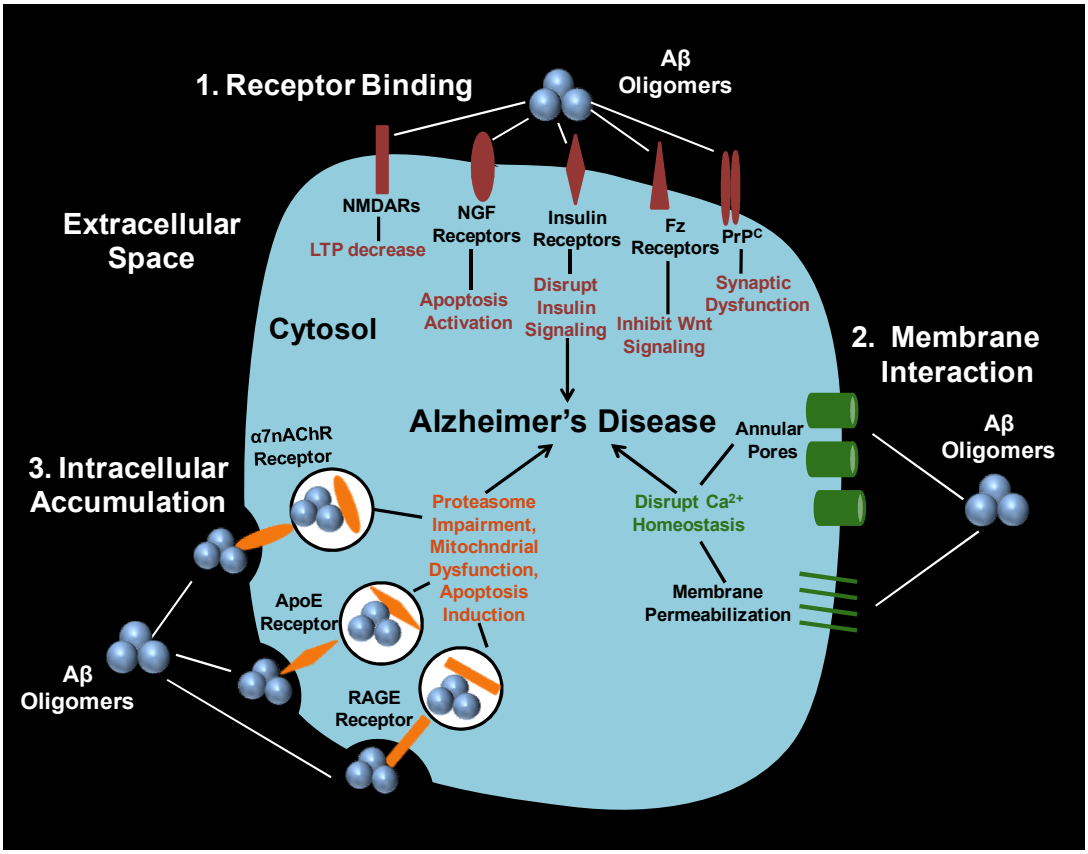

Alzheimer's disease (AD) is an age-related neurodegenerative disorder which is characterized by memory dysfunctions and cognitive decline. Two pathological alterations illustrate the brain of AD patients; one is the formation of amyloid plaques which are present in the extracellular space, and another is the neurofibrillary tangles (NFTs) that are present within the neurons. Amyloid plaques are formed from the deposition of fibrillar amyloid-β (Aβ) peptide, while NFTs are the aggregates of hyperphosphorylated tau protein. The accumulation of Aβ peptide plays an important role and is considered as the central event in AD pathology. Aβ peptide is a small amphipathic peptide whose length varies from 37-42 amino acid residues. While the most abundant variant of Aβ in a healthy brain is $A\beta_{40}$, the amyloid plaques found in the AD brain constitutes $A\beta_{42}$. $A\beta_{42}$ is more hydrophobic and aggregation-prone as compared to $A\beta_{40}$ because of the presence of two additional amino acids, isoleucine, and alanine at residue positions 41 and 42, respectively. Aggregation of Aβ produces a variety of species, such as oligomers, protofibrils, and fibrils. Among the various kinds of aggregated forms, soluble Aβ oligomers are the real culprits in the pathogenesis of AD. Soluble oligomers of Aβ peptide are considered as

the potent neurotoxic species that inhibit long-term potentiation and cause synaptic dysfunction in AD. Soluble Aβ oligomers trigger a downstream signaling cascade of events via interacting with a multitude of receptors, which further result in cellular toxicity. An array of soluble Aβ oligomers are produced both *in vitro* and *in vivo*. These various kinds of soluble oligomers exhibit their neurotoxic effects mainly by three mechanisms: 1) binding to the receptors, 2) interacting with the lipid membrane, and 3) intracellular accumulation. Mounting evidence suggests many receptors for binding to Aβ oligomers such as N-methyl-D-aspartate receptors (NMDARs), nerve growth factor (NGF) receptors, insulin receptors, frizzled (Fz) receptors and cellular prion protein (PrP^C). Binding of Aβ oligomers to PrP^C activates the Fyn kinase, which results in tau phosphorylation and causes synaptic impairments. Interaction of soluble Aβ oligomers with the lipid membrane leads to the formation of annular pores and also causes membrane permeabilization. In this thesis, the efforts were directed towards elucidating the molecular mechanism by which Aβ oligomers interact with the prion protein and the lipid membrane and cause toxicity.

Chapter 2. Structural Classification of Amyloid-β oligomers

The accumulation of soluble oligomers of Aβ peptide exhibit pronounced toxic effects in AD. A plethora of studies has shown that a wide variety of soluble Aβ oligomers are present in AD patients, APP transgenic mice, *in vivo*, and *in vitro*. The putative soluble Aβ oligomers that are believed to be involved in AD are dimers, trimers, dodecamers (Aβ*56), globulomers, prefibrillar aggregates, Aβ-derived diffusible ligands (ADDLs), annular protofibrils, and protofibrils. Many different laboratories produce different types of Aβ oligomers that vary based on morphology, size, toxicity, methods of preparations, and structure, and so on. This raises the question of structural relationships among the different oligomers. A rational classification of oligomers based on the structure has been emerged to identify the fundamental structural attributes of soluble oligomers. Two conformation-specific antibodies, namely, anti-amyloid oligomer (A11) antibody and anti-amyloid fibril (OC) antibody, have been produced which recognize mutually exclusive structural epitopes of two structurally distinct oligomers, prefibrillar and fibrillar oligomers, respectively. As a prelude, we first standardized the preparation of two structurally different Aβ oligomers. Using an array of biophysical and

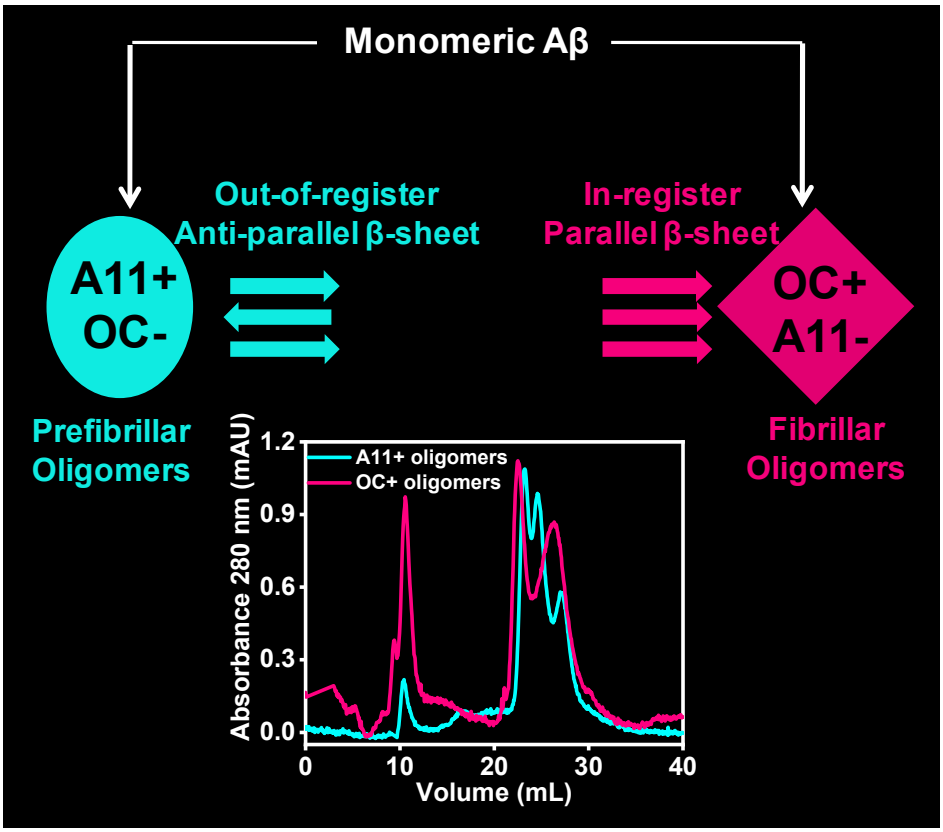

biochemical tools involving dot-blot assay, atomic force microscopy (AFM), dynamic light scattering (DLS) and size-exclusion chromatography (SEC), we characterize the two different oligomeric preparations. Our study revealed that the two oligomeric preparations produce conformationally distinct Aβ oligomers of different size distributions.

Chapter 3. Preferential Recruitment of Conformationally Distinct Amyloid-β Oligomers by the Human Prion Protein

Amyloid-β (Aβ) oligomers are known to cause synaptic dysfunction in Alzheimer's disease (AD) and have been shown to mediate the downstream cellular toxicity by binding to one of the cell-surface receptors, the prion protein (PrP). Human prion protein (PrP) is a glycophosphatidyl-inositol (GPI) membrane-anchored protein that undergoes misfolding into a disease-associated deadly scrapie prion. However, the mechanism of interaction between conformationally distinct Aβ oligomers and PrP is poorly understood. In this work, we dissect the mechanism of intermolecular association between conformationally distinct, prefibrillar (A11-positive) and

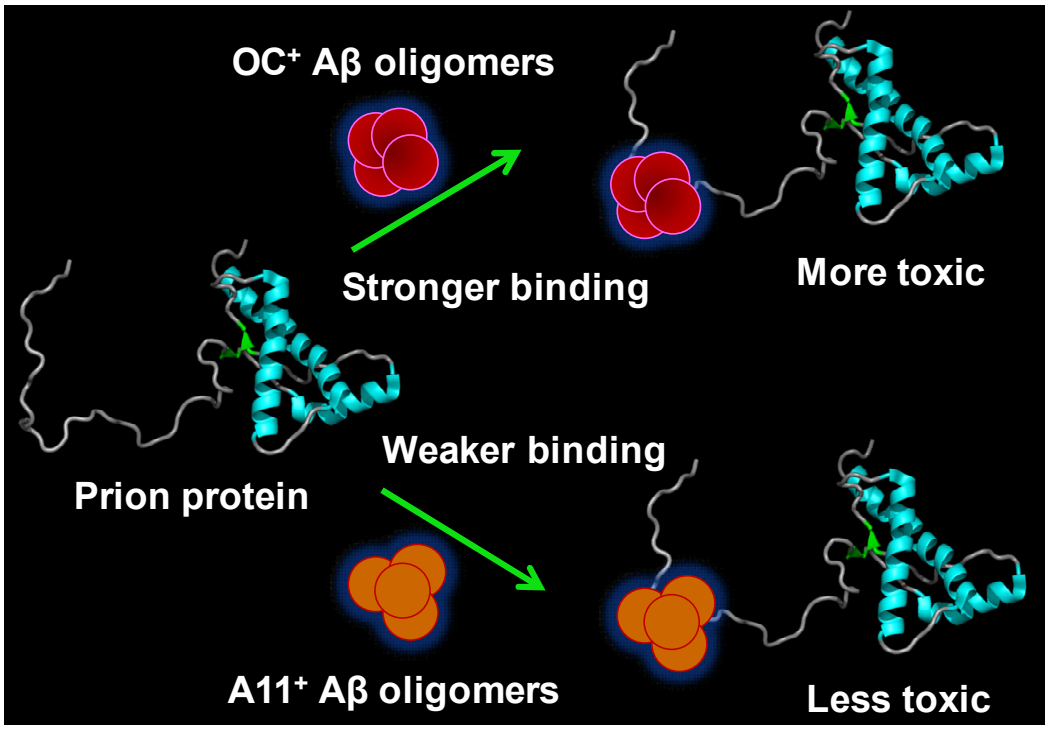

fibrillar (OC-positive) Aβ oligomers and PrP by using an array of biophysical and biochemical tools. Our site-specific binding titrations using fluorescence polarization and quenching measurements demonstrate that the heterotypic association of Aβ oligomers and PrP primarily occurs via the N-terminal intrinsically disordered region of PrP. We determine the binding affinities of OC-positive oligomers having an in-register parallel β-sheet structure and A11-positive oligomers possessing an anti-parallel β-sheet structure, with PrP. Our studies also demonstrate the toxic effects of Aβ oligomers on binding PrP in mammalian cells. Taken together, our results revealed the electrostatic interactions between the intrinsically disordered region of PrP and Aβ oligomers drive the preferential recruitment mediating the deleterious effects of OC-positive oligomers. Our studies also underscore the importance of designing the therapeutic strategies that target the interaction between OC-positive oligomers and PrP.

Chapter 4. Impact of Conformationally Distinct Alzheimer's Amyloid-β Oligomers on the Dynamics of Lipid Membrane Comprising Brain Total Lipid Extract

Soluble oligomers of Aβ are considered to exhibit toxic effects in Alzheimer's disease (AD). Studies have shown that the interaction of Aβ oligomers with the lipid membrane is one of the

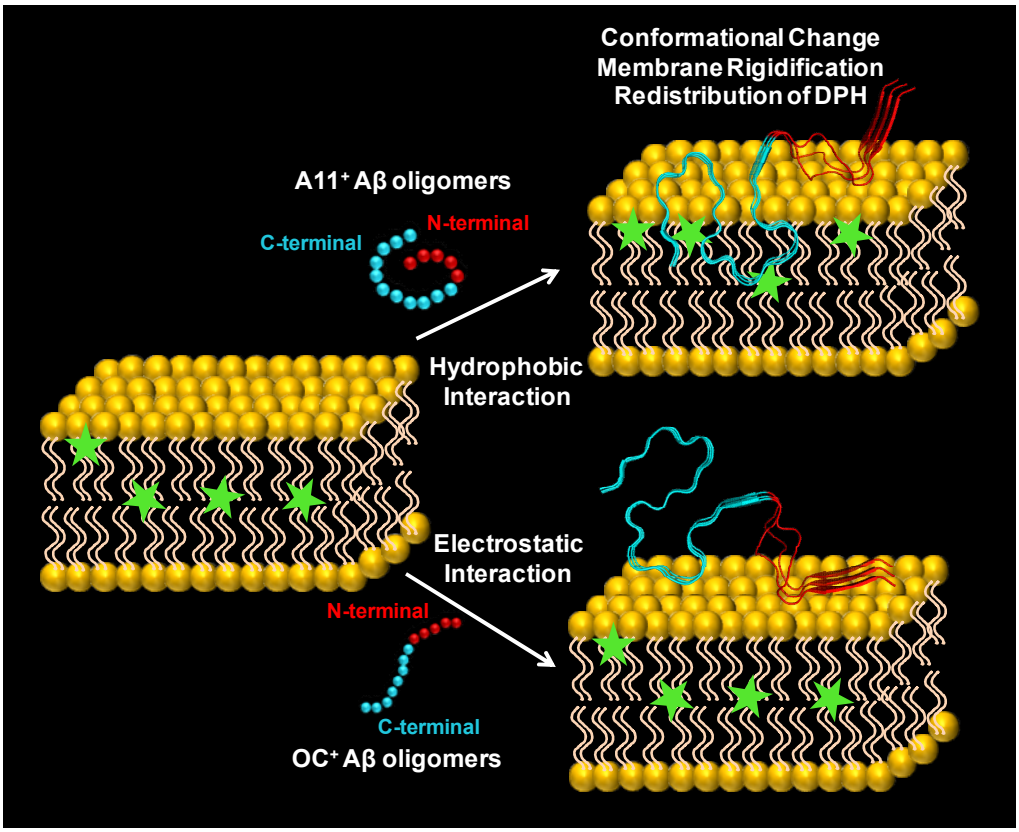

key mechanisms of toxicity produced by Aβ oligomers. However, the mechanism by which structurally distinct Aβ oligomers interact with the lipid membrane remains elusive. In this work, we elucidate the mechanism of interaction of conformationally distinct, A11-positive prefibrillar and OC-positive fibrillar oligomers with the lipid membrane derived from brain total lipid extract. Our steady-state and time-resolved fluorescence study demonstrates that the A11-positive Aβ oligomers interact with the non-aqueous hydrophobic core of the membrane, resulting in an increase in the membrane micro-viscosity. In contrast, the interaction between OC-positive Aβ oligomers and the lipid membrane is driven electrostatically via the intrinsically disordered N-terminal region of oligomers. Our study also reveals that the A11-positive Aβ oligomers undergo a conformational change upon binding to the lipid membrane. Our findings dissect the general mechanism by which conformationally distinct oligomers of many amyloidogenic proteins interact with the lipid membrane and cause toxicity.

List of Publications

- ✓ **Madhu, P.,** and Mukhopadhyay, S. (2020) Preferential Recruitment of Conformationally Distinct Amyloid-β Oligomers by the Intrinsically Disordred Region of the Human Prion Protein. *ACS Chem. Neurosci*. **11**, 86-98.

- ✓ **Madhu, P.,** Das, D., and Mukhopadhyay, S. Conformation-Specific Perturbation of Membrane Dynamics by Structurally Distinct Oligomers of Alzheimer's Amyloid-β Peptide. (manuscript under review)

- ❖ Pani, I.*, **Madhu, P.*,** Najiya, N., Aayush, A., Mukhopadhyay, S., and Pal., S. K. (2020) Differentiating Conformationally Distinct Alzheimer's Amyloid-β Oligomers Using Liquid Crystals. *J. Phys. Chem. Lett.* **11**, 9012-9018. (*joint first authors)

- ❖ Majumdar, A.*, Das, D.*, **Madhu, P.,** Avni, A. and Mukhopadhyay, S. (2020) Excitation Energy Migration Unveils Fuzzy Interfaces within the Amyloid Architecture. *Biophys. J.* **118**, 1-6.

- ❖ Mahapatra, S., Sarbahi, A., **Madhu, P.,** Swasthi, H. M., and Mukhopadhyay. S. Scarcity of Disaggregates Inflates Yeast Prion Transmission by Modulating its Kinetics and Conformational Characteristics. (manuscript in preparation)

- ❖ Not part of thesis work.

Presentations at Conferences

- **P. Madhu** and S. Mukhopadhyay: Recruitment of Amyloid-β oligomers by the prion protein, EMBO Workshop Proteostasis: From organelles to organisms (2019), Ericeira, Portugal.

- **P. Madhu** and S. Mukhopadhyay: Interaction of Conformationally Distinct Amyloid-β oligomers with the Prion Protein, International Conference on Intrinsically Disordered Proteins: Forms, Functions and Diseases (2017), IISER Mohali, India.

- **P. Madhu** and S. Mukhopadhyay: Interaction of Conformationally Distinct Amyloid-β oligomers with the Prion Protein, Third International symposium on Protein Folding and Dynamics (2016), National Centre for Biological Sciences (NCBS), Bangalore, India.

Table of Contents

Introduction

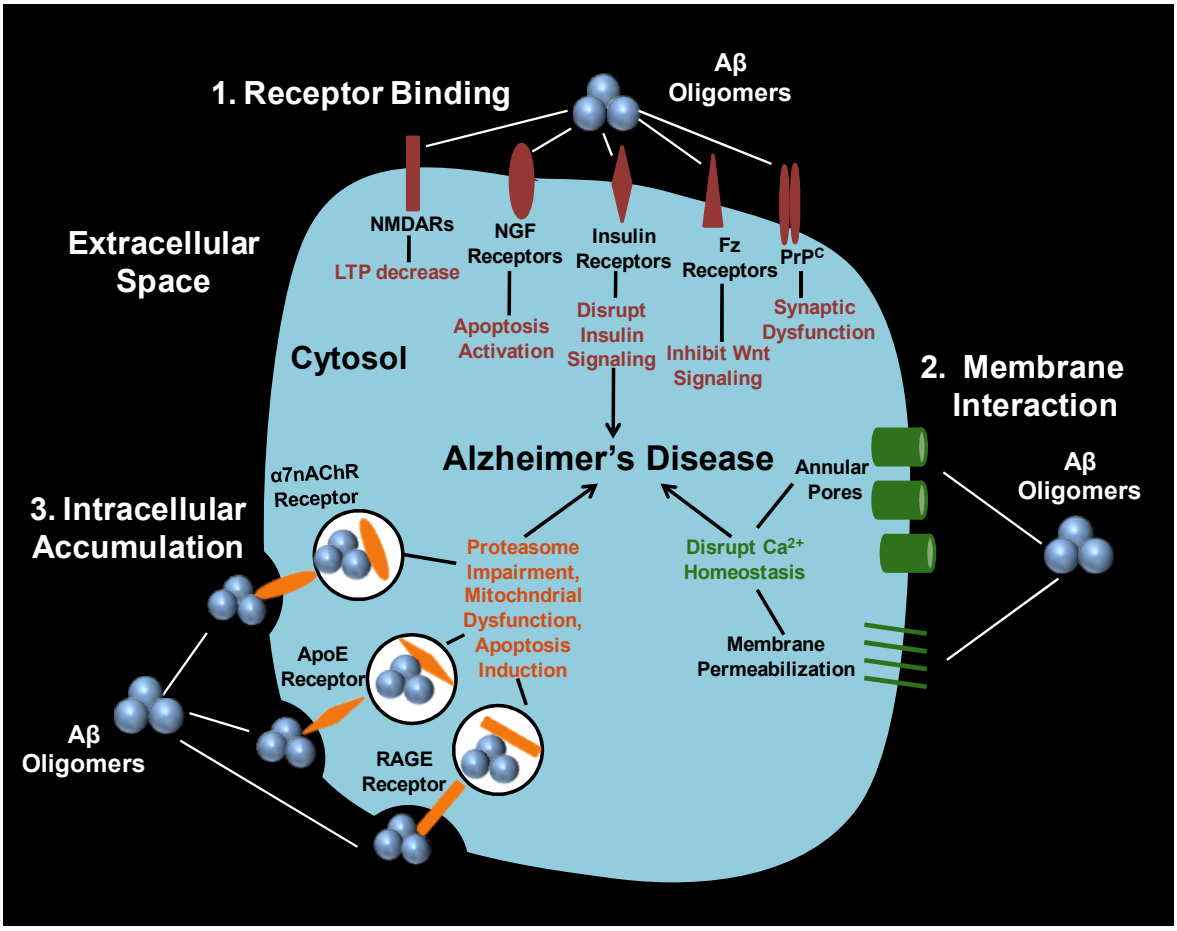

1.1 Alzheimer's disease

Alzheimer's disease (AD) is an age-related devastating neurodegenerative brain disorder from which around 50 million people are suffering worldwide (1). The disease could be sporadic or inherited in origin. Ninety-nine percent of AD cases emerge from the sporadic, late-onset AD that occurs beyond the age of 65, whereas the inherited, early-onset familial AD (FAD) that can strike prematurely occurs only in a small fraction (2). By 2050, in the United States, it is expected that every 33 seconds, one new case of AD will develop, which will increase to nearly a million new cases per year. This will increase the cost of care for AD patients. Therefore, it is necessary to devise the therapeutics by identifying the biological culprits of AD.

In 1907, Dr. Alois Alzheimer, a neuropathologist and psychiatrist, examined a woman patient named Auguste Deter (3, 4). He described her symptoms as (3):

"Her memory is seriously impaired. If objects are shown to her, she names them correctly, but almost immediately afterwards she has forgotten everything. When reading a text, she skips from line to line or reads by spelling the words individually, or by making them meaningless through her pronunciation. In writing she repeats separate syllables many times, omits others and quickly breaks down completely. In speaking, she uses gap-fills and a few paraphrased expressions ("milk-pourer" instead of cup); sometimes it is obvious she cannot go on. Plainly, she does not understand certain questions. She does not remember the use of some objects."

Early symptoms of AD are impairments in memory and confusion that interfere with the daily activities, and the following symptoms involve a decline in cognitive functions such as language, behavioral changes, and motor difficulties, which ultimately lead to death (5). The symptoms of AD develop due to neuronal atrophy, which occurs because of the neuronal cell death, shrinkage of neurons, or the loss of axons and dendrites and results in brain shrinkage (Figure 1.1). The brain atrophy starts with the medial temporal lobe and then occurs in the distinct cortical regions (2).The microscopic analysis of the AD brain reveals two pathological abnormalities in the brain (Figure 1.2). These are known as the extracellular amyloid plaques and the intracellular neurofibrillary tangles (NFTs). The extracellular amyloid plaques are formed of aggregated amyloid-β (Aβ) peptide, while NFTs are the aggregates of hyperphosphorylated tau protein (6). The deposition of NFTs is parallel in progression with the cognitive deficits, while the amyloid plaques deposition occurs before the beginning of cognitive deficits.

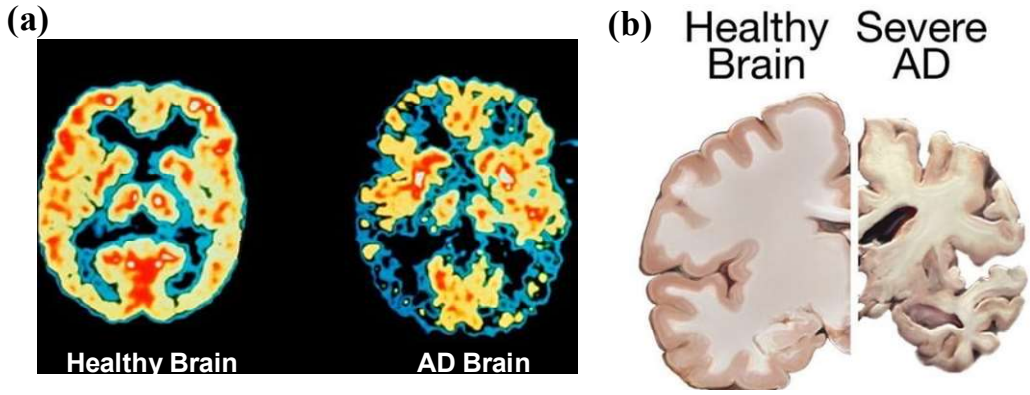

Figure 1.1: The imaging of healthy and AD brain. (a) Positron Emission Tomography (PET) scans of the healthy brain (left panel) and AD brain (right panel). The active parts of the brain are in yellow and red, which indicates the reduced activity of the AD brain. Image credit: Science Photo Library (https://www.telegraph.co.uk/science/2017/07/16/brain-scanning-could-improve-dementia-diagnosis-two-thirds-patients/) (b) Brain shrinking in AD as compared to the healthy brain. Image credit: MedlinePlus (https://medlineplus.gov/genetics/condition/alzheimer-disease/).

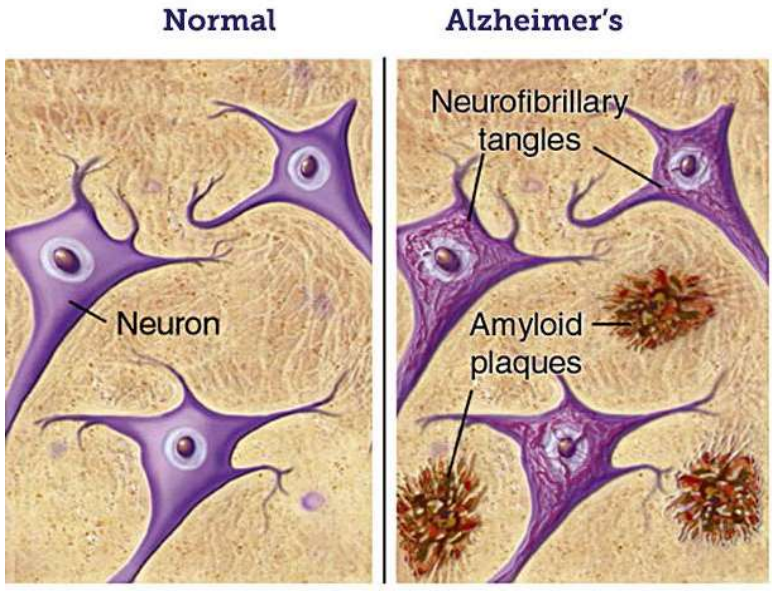

Figure 1.2: The two pathological alterations of AD: extracellular amyloid plaques and the intracellular neurofibrillary tangles. Image Credit: BrightFocus Foundation (https://www.brightfocus.org/).

The different stages of AD are classified based on the spatiotemporal occurrence of amyloid plaques and NFTs (7). Six stages are defined based on the deposition of NFTs in the different regions (Figure 1.3a). NFTs appears in:

Stage 1: Transentorhinal region,

Stage 2: Cornus Ammonis (CA1) region in the hippocampus

Stage 3: Subiculum of the hippocampal formation

Stage 4: Amygdala, thalamus, and claustrum,

Stage 5: The associative areas of all isocortical areas

Stage 6: Primary sensory, motor, and visual areas.

There are three stages of AD based on the deposition of amyloid plaques in different regions (Figure 1.3b) (8). These are:

Stage 1: Isocortical region

Stage 2: Allocortical or limbic regions,

Stage 3: Subcortical

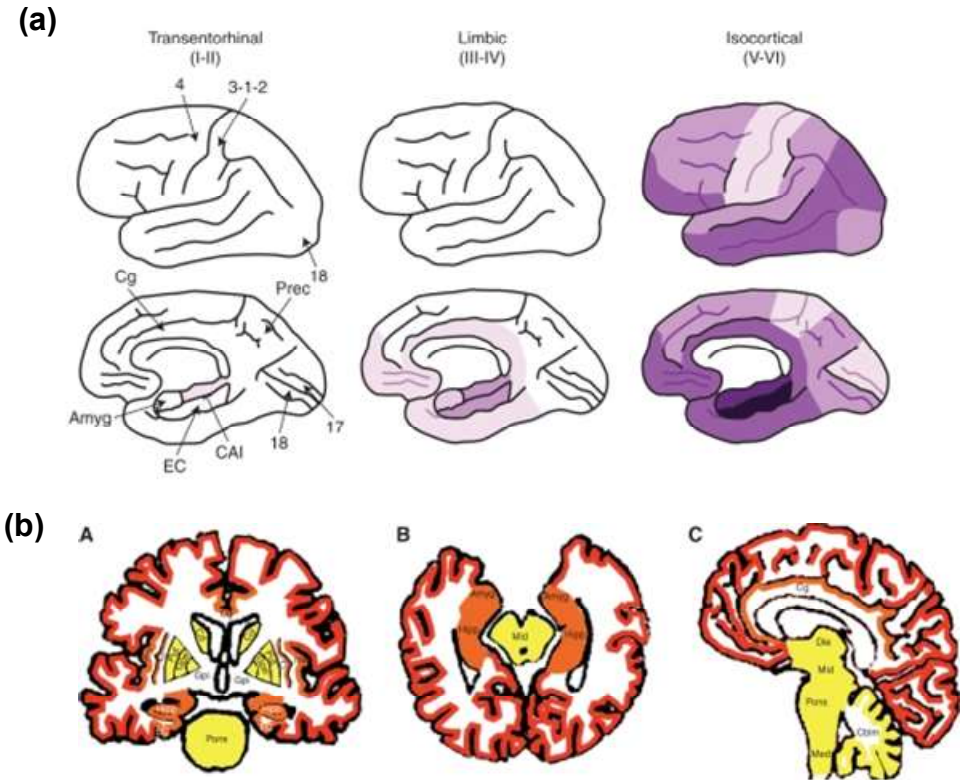

Figure 1.3: (a) Spatiotemporal relationship of NFTs deposition. The shading shows the distribution of NFTs, and the darker regions indicate the increasing densities. (b) The

spatiotemporal occurrence of amyloid plaques is shown in the Coronal (A), axial (B) and sagittal (C) views of the brain. Stage 1, stage 2 and stage 3 are indicated in red, orange and yellow, respectively. Amyg = Amygdala; EC = Entorhinal cortex; CA1 = Cornus ammonis 1; Prec = Precuneus; 4 = Primary motor cortex; 3-1-2 = Primary sensory cortex; 17 = Primary visual cortex; 18 = Associative visual cortex; Hipp = Hippocampus; Cg = Cingulate cortex; Put = Putamen; Gpe = Globus pallidus externus; Gpi = Globus pallidus internus; C1 = Claustrum; Ins = Insular cortex; Die = Diencephalon; Mid = Midbrain; Med = Medulla oblongata; Cblm = Cerebellum. Reproduced with permission from (6).

The depositions of both NFTs and amyloid plaques are involved in AD, which disrupts the various regions of the brain. However, it is not clear what initiates their depositions in these different regions of the brain.

1.2. Amyloid cascade hypothesis

In 1991, Hardy and Allosp gave the amyloid cascade hypothesis (9) and later on in 1992, Hardy and Higgins stated the amyloid cascade hypothesis as follows (10):
"Our hypothesis is that deposition of amyloid-β protein (AβP), the main component of the plaques, is the causative agent of Alzheimer's pathology and that the neurofibrillary tangles, cell loss, vascular damage, and dementia follow as a direct result of this deposition."

In AD pathology, the central event is the deposition of an aggregation-prone Aβ peptide. A body of evidence shows that the various forms of Aβ, from insoluble Aβ fibrils to soluble oligomeric species, either synthetic or extracted from AD patients, cause synaptic dysfunction and neuronal death (11). The basis of amyloid cascade hypothesis is due to the occurrence of AD in individuals (a) having autosomal-dominant mutations in the gene that encodes the γ-secretase complex proteins presenilin 1/2 (PSEN 1/2) or the amyloid precursor protein (APP), and (b) suffering from Down syndrome, a condition which is attributed with the triplication and overexpression of the chromosome 21 that encodes APP (9, 10). The next question is how APP produces Aβ peptide.

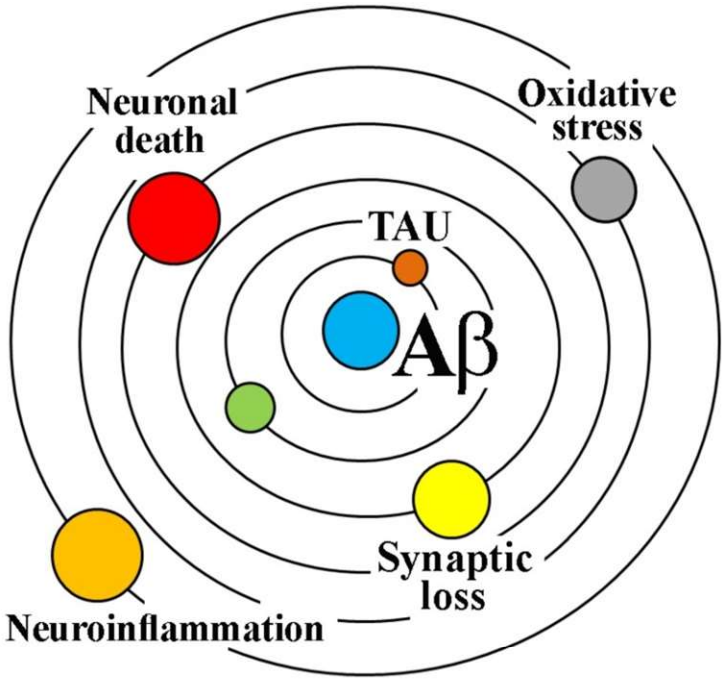

Figure 1.4: The representation of the amyloid cascade hypothesis as geocentric Ptolemy's theory, which places earth at the center of the solar system. Reproduced with permission from (11).

1.3. Generation of Aβ from APP

APP is a type I transmembrane glycoprotein, which is a precursor of Aβ peptide. The differential splicing of APP mRNA produces three major isoforms that have 695, 751, or 770 amino acid residues (12, 13). The non-neuronal cells express mainly APP having 770 or 751 amino acids (14), while the neuronal cells express APP having 695 amino acid residues (15). APP comprises a large ectodomain that contains heparin- and metal-binding ectodomain E1, an acidic domain, an ectodomain E2 which has a helical structure, the Aβ sequence, the C-terminus which is a cytoplasmic domain and a YENPTY sorting motif (12) (Figure 1.5). In the Golgi bodies, the polypeptide APP can undergo many types of post-translational modifications such as phosphorylation, glycosylation, sulphation, and palmitoylation (16, 17). Most of the APP undergoes an endosomal-lysosomal degradation pathway (18), and a portion of the APP internalizes to the cell surface where it undergoes cleavage by secretase enzymes (19). APP can undergo enzymatic cleavage via two routes: amyloidogenic and non-amyloidogenic. APP

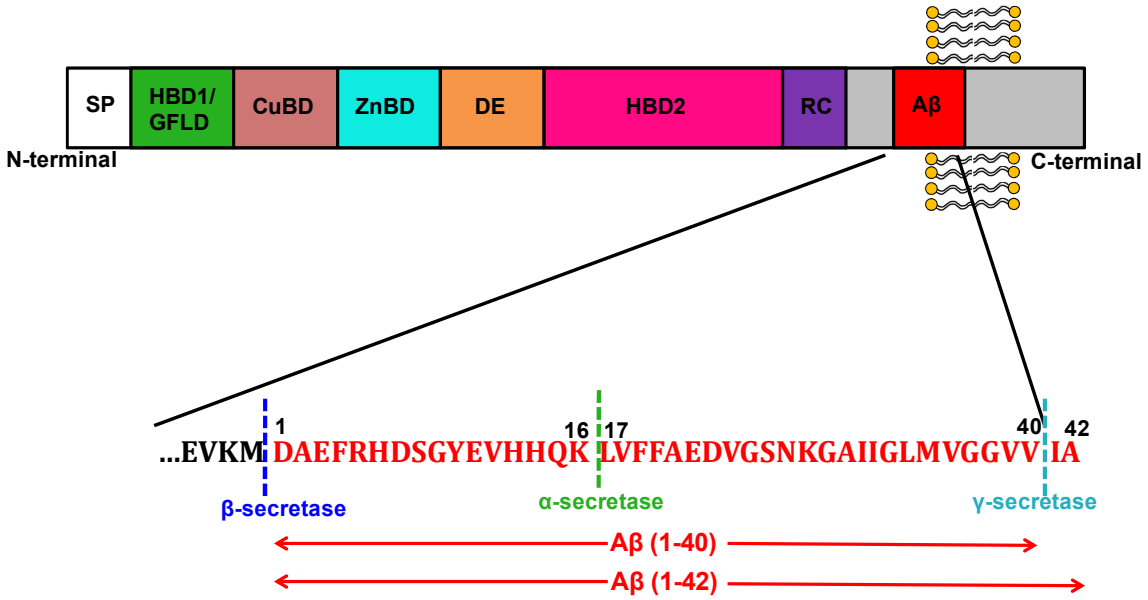

Figure 1.5: The structure of APP. APP contains heparin-binding and growth factor-like domain (HBD1/GFLD), copper- (CuBD), and zinc-binding domains (ZnBD), an acidic region (DE), second heparin-binding domain (HBD2), random coiled region (RC), Aβ domain and the C-terminus. The insert shows the sequence of Aβ (in red) in APP along with the enzymes that cleave APP. Drawn using the reference (22).

cleavage by the amyloidogenic pathway produces neurotoxic Aβ, while the non-amyloidogenic path precludes Aβ formation (20, 21). In the non-amyloidogenic pathway, APP undergoes cleavage by an integral metalloendopeptidase, α-secretase enzyme between residues K613 and L614, which are a part of the Aβ sequence and thus destroys the formation of Aβ (21). The ADAM (a disintegrin and metalloprotease) family with ADAM 9, 10, 17, and 19 are involved in mediating the activity of α-secretase (23, 24). The activity of non-amyloidogenic α-secretase can be either inducible or constitutive, depending on its subcellular localization. Most of the proteolytic processing of APP by the non-amyloidogenic pathway happens at the cell surface, and α-secretase is constitutively active at the cell surface (25). A small amount of α-secretase is present in the trans-Golgi network (TGN), where protein kinase C regulates its activity. In TGN, α-secretase competes with a large amount of β-secretase present (26). Therefore, a minimal amount of APP is cleaved by α-secretase in TGN. The α-secretase cleavage produces an amino-terminal fragment known as secreted APP α (sAPPα), and a carboxyterminal fragment (CTF), CTF83 (20, 21) (Figure 1.6). The fragment sAPPα has a beneficial role, such as promoting

neurite growth and survival (27, 28). The neuronal membrane-tethered CTF83 undergoes cleavage by γ-secretase that produces p3 and an amino-terminal APP intracellular domain (AICD). The multi-protein complex mediates the activity of γ-secretase. Four proteins, presenilin (PS) 1 or 2, anterior pharynx defective-1 (Aph-1), presenilin enhancer (Pen2), and nicastrin (Nct), are required to form the multi-protein complex (29). Presenilin is an aspartyl protease that cleaves the membrane-anchored APP fragment. γ-secretase matures in different steps. First, Nct and Aph-1 form a complex, which further binds to PS, followed by binding of Pen2 (30). In the

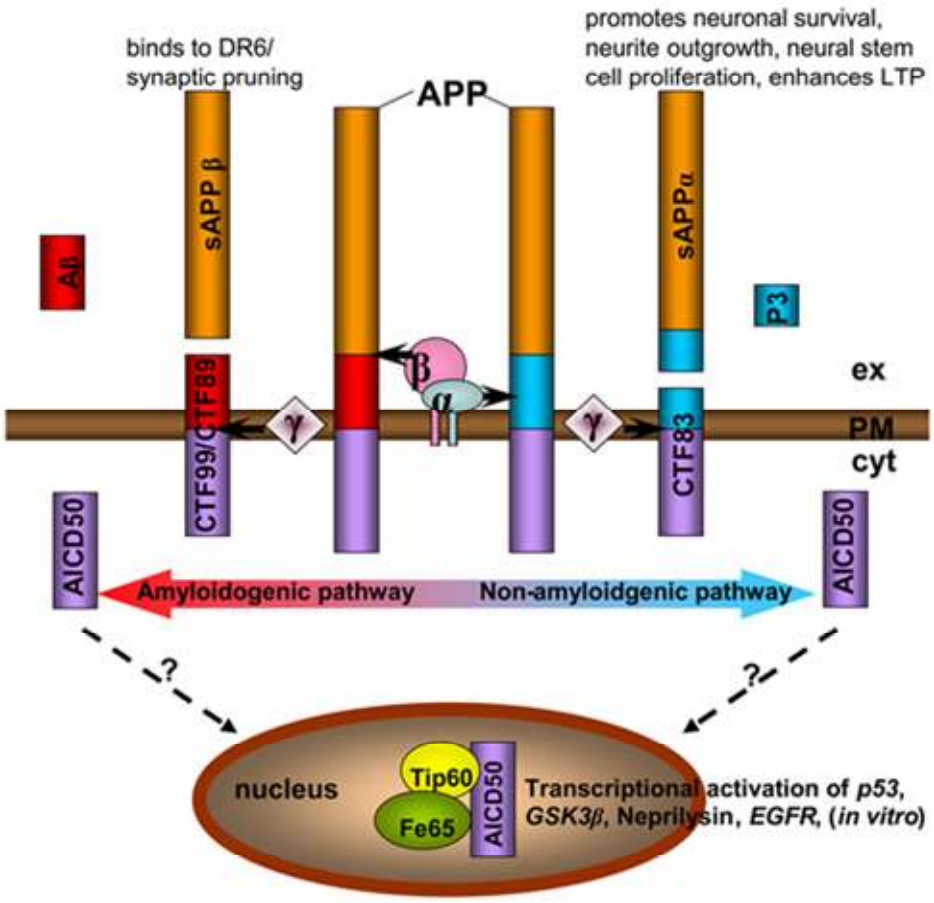

Figure 1.6: The proteolytic processing of APP by two pathways. The amyloidogenic path (left side/red) where β- and γ-secretases cleave APP which result in the formation of a secreted form of APP β and C-terminal fragments (CTF99/CTF89, Aβ and AICD50). The non-amyloidogenic pathway (right side/blue) where α- and γ-secretases cleave APP that results in the formation of secreted APP α (sAPPα) and C-terminal fragments (CTF83, p3 and AICD50) along with the

products that are produced on cleavage. ex: extracellular; PM: Plasma membrane; cyt: cytoplasm. Reproduced with permission from (21).

amyloidogenic pathway, APP undergoes cleavage by β-secretase enzyme between residues M597 and D598, which produces an amino-terminal fragment, sAPPβ, and CTF99 (20, 21). The β-site APP cleaving enzyme 1 (BACE1) mediates the activity of β-secretase. BACE1 is majorly present in TGN and the endosomal compartments (31). Due to vesicle trafficking, BACE1 reaches the plasma membrane, but it quickly recycles inside the cell. So, only a minimal amount of APP cleavage occurs by BACE1 at the plasma membrane surface. The cleavage of APP by BACE1 occurs primarily in the endocytic vesicles due to the optimum acidic pH required for the BACE1 activity, which is present in the endosomes. Unlike sAPPα, sAPPβ does not have neuroprotective roles (28), but it helps in the pruning of synapses during neuronal development (32). The CTF99 undergoes cleavage by γ-secretase that produces Aβ and free AICD (Figure 1.6). Cleavage by γ-secretase can occur at various sites that result in the generation of Aβ and AICD of different lengths. The length of Aβ varies from 38-43 amino acid residues, and mainly Aβ (1-40) is being produced in a healthy brain. The site for the cleavage by γ-secretase has physiological effects as the generation of Aβ (1-42), which is more hydrophobic, is mainly involved in AD (33). The free AICD translocates into the nucleus (34), where it binds to the adaptor proteins like Fe65 due to the presence of consensus motif YENPTY in AICD (35). The Fe65-bound AICD complex combines with Tat-interactive protein 60 (Tip60) (36) and causes transcriptional activation of genes such as p53 (37), glycogen-synthase kinase-3β (GSK3β) (38), neprilysin (39) and many others. The next question is, what the fate of Aβ is.

1.4. Amyloid-β (Aβ) peptide

Aβ is a small aggregation-prone peptide that is produced from APP, and the length of the peptide varies from 39 to 43 depending on the site where γ-secretase cleaves APP. The most abundant species of Aβ that is produced by cells is Aβ (1-40) (Aβ40), which is ~ 80-90 %, followed by Aβ (1-42) (Aβ42), which is ~ 5-10 % (40). Under normal conditions, Aβ peptide can undergo degradation, and the two main enzymes that are involved for degradation are insulin-degrading enzyme (IDE) and neprilysin (NEP). IDE is a metalloprotease that has a higher binding affinity for insulin than Aβ, but the rate of insulin hydrolysis is slower. NEP is a cell membrane-bound

type II metalloprotease, which is extracellularly active in degradation, while IDE is both intracellularly and extracellularly active. Most of Aβ degradation occurs by these two enzymes. Both the two enzymes decrease in aging and in disease condition, which results in the accumulation of Aβ. The undegraded Aβ is transferred to the blood-brain barrier (BBB) and finally lead into the circulation. On the brain side, the low-density lipoprotein receptor-related protein (LRP) and the receptor for advanced glycation end products (RAGE) on the blood side are involved in the transport of soluble Aβ across BBB. Disruption in the transportation of Aβ across BBB will lead to the build-up of Aβ in the brain.

The amyloid plaques deposited in AD patients majorly consist of the longer form of Aβ, Aβ42. Aβ42 plays a central role in the severity of AD pathogenesis. This is supported by the genetic studies which have identified mutations in *presenilin* 1 and 2 genes of AD patients that modify the enzymatic cleavage sites of APP and results in an increase in the ratio of Aβ42 / Aβ40 (41). Aβ42 is more hydrophobic and fibrillogenic than Aβ40 because of the presence of two extra amino acids that are isoleucine and alanine, which results in the different aggregation behavior of both the peptides. Previous studies have shown that the non-aggregated form of Aβ, i.e., monomeric Aβ is non-neurotoxic. Aβ peptide is present in the brain and cerebrospinal fluid (CSF) of healthy individuals throughout the whole life, which indicates that the peptide is physiologically active (42, 43). Recent studies have shown that the monomeric Aβ plays a neuroprotective role in the brain by protecting the mature neurons against excitotoxic death. Also, the Aβ40 peptide regulates the voltage-gated potassium channels (44). The non-aggregated neuroprotective Aβ peptide becomes neurotoxic upon aggregation and results in AD pathology.

1.5. Aggregation of Aβ

Aβ is an amphipathic peptide that has a hydrophilic N-terminal and a hydrophobic C-terminal. Monomeric Aβ is considered as an intrinsically disordered peptide that poses difficulty in the crystallization. The 3D-solution structures of different Aβ fragments have been resolved using X-ray crystallography, NMR spectroscopy, and molecular dynamics (MD) techniques. Aβ (1-40) and Aβ (1-39) have been found unstructured in aqueous solution while Aβ (1-42) rapidly adopts a β-sheet structure at physiological pH due to its high propensity of aggregation (45, 46).

Aggregation of Aβ in an aqueous medium produces a variety of species that includes oligomers, protofibrils, and fibrils. Amyloid fibrils can further assemble and form insoluble amyloid plaques

that are linked with AD. Oligomers are the soluble forms of Aβ that spread throughout the brain (47). Most of the studies suggest that Aβ undergoes aggregation via a nucleation-dependent polymerization pathway that involves a lag phase, rate-limiting step, which is followed by a growth phase. The nucleus is formed in the rate-limiting step, and once it is formed, the aggregation progresses by the incorporation of more Aβ molecules. Aggregation of Aβ into amyloid fibrils requires a minimal concentration of Aβ, which is higher for Aβ40 and around five-fold lower for Aβ42. At a very high supersaturated Aβ concentration, Aβ can undergo non-specific aggregation and prevent the specific Aβ polymerization (48). The aggregation of Aβ is very much dependent on the reaction conditions such as pH, ionic strength, initial concentration, solvent hydrophobicity, temperature, buffer, presence of pre-aggregated forms of Aβ, and also the pre-dissolved solvent for Aβ monomerization. Recent studies have shown the monomer-dependent secondary nucleation of Aβ42 peptide in which the surfaces of existing aggregates are involved in catalyzing the nucleus construction by the addition of monomers (49). In this pathway, the rate of aggregation depends both on the Aβ fibrils and Aβ monomers. FAD-linked point mutations, including Dutch (E22Q), Arctic (E22G), Iowa (D23N), and Italian (E22K), have been shown to aggregate at a faster rate than wild type Aβ (48). Under the *in vitro* condition (cell culture, test tube), the aggregation process involves the micromolar concentration of Aβ and timescales from minutes to days for the amyloid fibril formation. However, *in vivo* (clinical trials), the amyloid plaque formation takes 40-60 years in humans, and the concentration of Aβ is in the nanomolar range (50). Although the two conditions are quite different, the morphologies and the biochemical properties of Aβ fibrils produced *in vitro* are quite similar to those found *in vivo* (51).

1.6. Structure of amyloid fibril

The term “amyloid” was given by Schleiden, followed by Virchow to characterize the iodine-stained deposits observed in the liver autopsy, which was believed to be a carbohydrate in nature (52). Later on, the high content of nitrogen in amyloid established the proteinaceous characteristics of these deposits, but the inaccurate descriptive name was retained. Amyloids are known to show specific binding to the dye Congo red and thioflavin T. The X-ray fiber diffraction indicates that the amyloid fibrils formed from the different proteins share a typical β-sheet structure. The β-strands that are held together by hydrogen bonding run perpendicular to

the fibril axis and the direction of hydrogen bonding runs parallel to the fibril axis. The

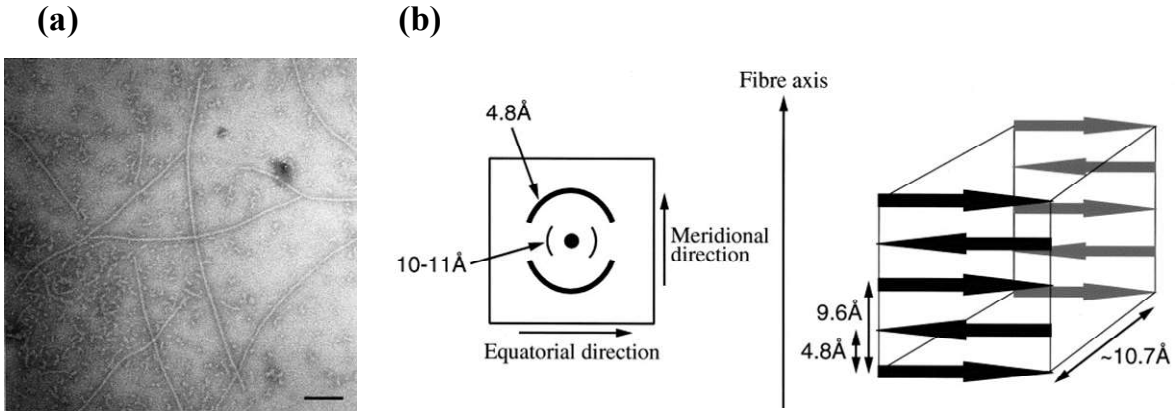

Figure 1.7: (a) Electron micrographs of amyloid fibrils of Aβ42 that show a diameter of 7-8 nm. (b) X-ray diffraction pattern of amyloid fibrils showing cross-β spacing. The reflection at 4.8 Å correspond to the spacing between two β-strands, and the reflection at 10-11 Å shows the inter-sheet spacing. Reproduced with permission from (61).

amyloid fibrils can be characterized by an array of biophysical tools involving circular dichroism (CD), nuclear magnetic resonance (NMR), electron microscopy (EM), atomic force microscopy (AFM), and X-ray fiber diffraction, and Fourier-transform infrared spectroscopy (FTIR). The AFM and EM images of amyloids display long, unbranched, and straight fibrils and are made up of subunits known as "protofilaments" (53, 54) (Figure 1.7a). The X-ray fiber diffraction display two reflections, one at 4.8 Å, which comes from the hydrogen bonding distances between two β-strands, and the other at 10 Å arise from the side-chain packing between the two sheets (55, 56) (Figure 1.7b). The interactions between the bonded β-sheets arise from the atomic structure of short-segments that form fibrils. The side chains of one sheet are interlocked with the side chains of another sheet that give rise to a tight and dry interface. This motif of pair of sheets is known as a steric zipper, and the tightly mating pair is the protofilaments of amyloid fibril (57). Cryo-electron microscopy (cryo-EM) can give information about the number of protofilaments, the degree of twist, and the atomic structure of fibrils. Cryo-EM studies indicate that the synthetic amyloid fibrils formed from many proteins like insulin, lysozyme, and Aβ40 are composed of a number of protofilaments that are twisted around one another (58–60). The number of these protofilaments vary from 2-6. Solid-state NMR (ssNMR) of amyloid fibrils reveals the arrangement of β-sheets within the protofilaments. ssNMR can measure interactions over very

short ranges (~ 6 Å) and thereby give the local information within the β-sheets (61). The amyloid fibrils of the same polypeptide chain can show alteration in the structural properties which give rise to the polymorphism in amyloids. The basic cross-β core of the polymorphs of amyloid fibrils remains conserved. The morphology of fibrils can be affected by the physico-chemical environment, such as pH, agitation, temperature, salt, or other co-solutes (62, 63). The amyloid polymorphism can mainly occur due to the variation in the methods of arrangement of protofilaments, the number of protofilaments, or the substructure of protofilaments. The cross-β structure of amyloid fibrils can exist in different conformations such as out-of-register anti-parallel β-sheets or in-register parallel β-sheets or β-helix.

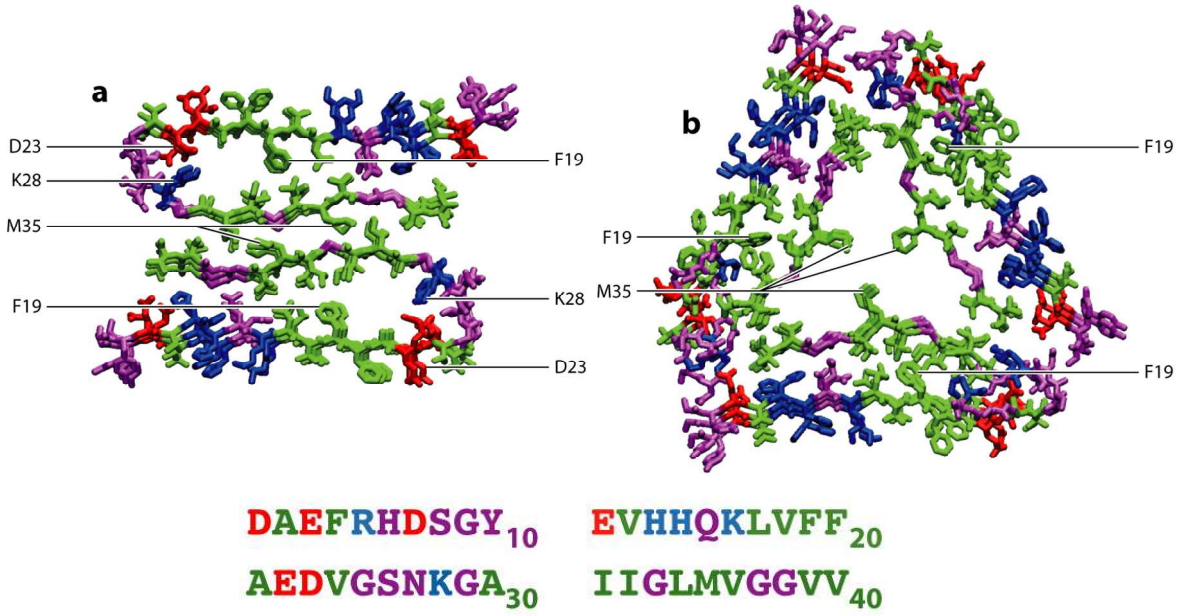

Figure 1.8: Structure of polymorphs of Aβ40 fibrils. (a) Striated-ribbon, and (b) twisted-pair Aβ40 fibrils. The hydrophobic, positively charged, polar, and negatively charged amino acid residues 9-40 are shown in green, blue, purple, and red, respectively. Reproduced with permission from (66).

Aggregation of Aβ leads to the formation of thermodynamically stable insoluble filamentous protein aggregates, amyloid fibrils. Initial ssNMR studies on the structure of amyloid fibrils of Aβ (34-42) and Aβ (10-35) shows an anti-parallel and a parallel cross-β structure, respectively (64, 65). Primarily, the full-length amyloid-β peptide is 40 or 42 residue in length. Subsequent studies on the structures of amyloid fibrils of Aβ40 and Aβ42 show that these fibrils consist of

in-register parallel-β sheets (66, 67). Subtle changes in the growth conditions of fibril formation affect the Aβ40 fibrils morphology. Fibrils of Aβ40 grown under agitation forms rod-type structure and appear as "striated-ribbon," while fibrils that are formed under quiescent condition have "twisted" morphology (68). NMR studies indicate that the two amyloid polymorphs are quite similar in the peptide conformations. The molecular structure in both the fibrils is U-shaped that consists of two β-strand segments, residues 10-22 and 30-40, which are connected by a bend or loop with residues 25-29. An unfolded segment, residues 1-9 precede the two β-strands. The quaternary contacts occur between the side chains of F19 of one β-sheet and the L34 side chains of another β-sheet within a cross-β unit (69). The two polymorphs are different in the overall symmetry of the arrangement of cross-β units. Electron microscopy studies show that the protofilaments in striated-ribbon contain two cross-β units and have two-fold rotational symmetry, while twisted-pair protofilament comprises three cross-β units that are associated via three-fold rotational symmetry (Figure 1.8). The bend segment, residues 23-29, forms a salt bridge between the positively charged residue, D23, and negatively charged residue, K28, by an electrostatic interaction in the striated-ribbon fibrils. In contrast, in the twisted-pair protofilaments, the salt bridge is not present. A recent study on the Aβ40 fibril seeded with an amyloid-enriched extract of brain tissue shows structural similarity with the three-fold symmetric structure of twisted-pair Aβ40 fibrils and D23-K28 salt bridge of striated-ribbon fibrils (70). Interestingly, amyloid fibrils formed from disease-associated Iowa mutant (D23N Aβ40) display an anti-parallel β-sheet structure (71).

In AD patients, the fragment Aβ42 is the principal species involved in amyloid plaques, which differs from Aβ40 by two amino acids, isoleucine, and alanine at residue positions 41 and 42, respectively. Studies on the structure of Aβ42 fibrils also show an in-register parallel β-sheet structure like Aβ40 fibrils (66). First, ssNMR study on the structurally homogenous sample of Aβ42 fibrils displays a unique triple β-motif which is formed from three β-sheets with residues 12-18 (β_1), 24-33 (β_2) and 36-40 (β_3). The structure is stabilized by salt bridge interactions between the residues K28 and A42, unlike Aβ40 fibril, which has a salt bridge between residues D23 and K28 (72) (Figure 1.9a). The structure of another polymorph of Aβ42 fibrils displays a significant difference within the core structure of amyloid fibrils. In this polymorph, the 3D structure consists of two Aβ42 molecules per subunit. Each Aβ42 molecule is encompassing five

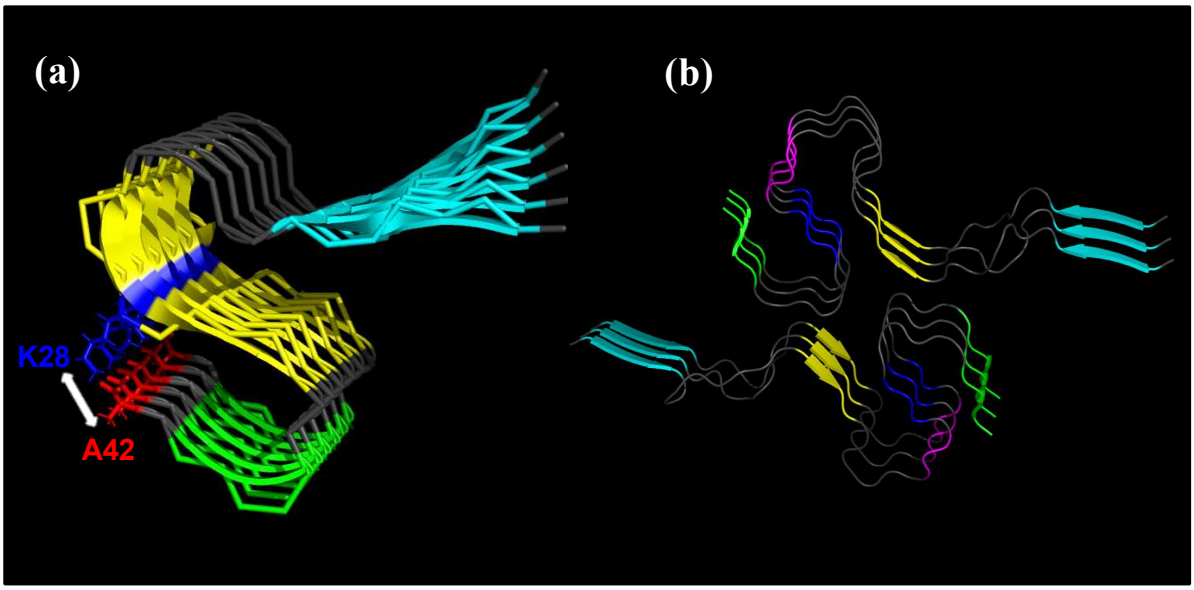

Figure 1.9: Solid-state NMR structure of Aβ42 fibrils that are generated using PyMol (Version 1.8, Schrödinger, LLC, New York, NY). (a) Structural-model with triple β-motif (PDB ID: 2MXU) (72). The structure is stabilized by salt-bridge between residues K28 and A42. Three β-sheets are shown in cyan (β1, 12-18), yellow (β2, 24-33) and green color (β3, 36-40). (b) Structure of Aβ42 fibril (PDB ID: 2NAO) (73). The fibril structure consists of two Aβ42 molecules per subunit and each molecule comprising five β-sheets that are shown in cyan (β1, 2-6), yellow (β2, 15-18), magenta (β3, 26-28), blue (β4, 30-32) and green (β5, 39-42).

in-register parallel β-strands, 2-6 (β1), 15-18 (β2), 26-28 (β3), 30-32 (β4), and 39-42 (β5) (73) that wind around the intramolecular core like a double-horseshoeshape (Figure 1.9b). The structural heterogeneity in amyloid fibrils distinguishes the amyloid from the natively folded protein structure. Therefore, the amyloid fibrils can be described as "polymer state" of the polypeptide chain, which can form different structures with less sequence specificity (74). The final state of aggregation of Aβ leads to the formation of amyloid plaques which, consists of insoluble amyloid fibrils and was assumed to mediate toxicity in AD. However, patients dying with AD exhibited a weak correlation between the amyloid plaques and the severity of dementia (75). The next question is what kind of aggregated species shows a direct relationship with the progression of AD pathogenesis.

1.7 The amyloid-β oligomer hypothesis

It was believed that the fibrillar Aβ deposited as amyloid plaques were solely responsible for AD according to the amyloid cascade hypothesis, stated in 1992. The amyloid-β oligomer hypothesis, reported in 1998, challenged the amyloid cascade hypothesis. A body of evidence suggests the involvement of soluble Aβ oligomers in AD pathogenesis rather than the

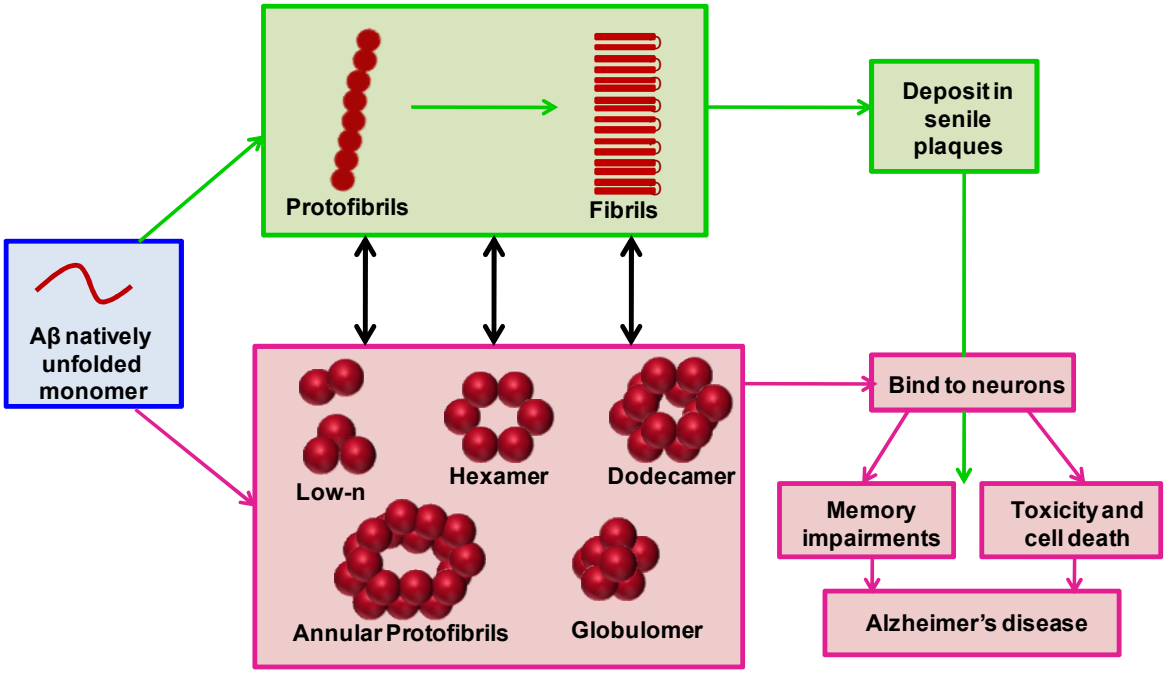

Figure 1.10: The toxic amyloid-β oligomer hypothesis. The natively unfolded aggregation-prone Aβ peptide assembles to form various types of soluble oligomers (magenta) and insoluble fibrils (green). The insoluble fibrils deposit within the extracellular senile plaques and the soluble oligomers exhibit neurotoxic effects in AD. Drawn using the concept from reference (82).

insoluble amyloid plaques, which give rise to the Aβ oligomer hypothesis. The amyloid-β oligomer hypothesis was based on the first discovery of the inhibition of long-term potentiation (LTP) and the nerve cell death by fibril-free preparation (76, 77). Subsequent studies by Lue and coworkers and McLean and coworkers in 1999 revealed that the concentration of soluble Aβ oligomers increases in AD and correlates strongly with the synaptic change in AD while insoluble Aβ did not show correlation with the disease severity (78, 79). Soon afterward, the

elevated levels of Aβ were identified in the very early stage of dementia in human AD brains, which displayed a strong correlation with the cognitive decline (80).

Aggregation of point-mutations in Aβ causes an increase in the amount of Aβ oligomers, which leads to an increase in the cytotoxicity (82). Small quantities of injection of Aβ oligomers into the non-transgenic animals cause a loss in memory. Synthetic and brain-derived both Aβ oligomers disrupt the long-term depression and long-term potentiation (LTP) in both *ex vivo* and *in vivo* (76). Therefore, an accumulating body of evidence demonstrates that soluble Aβ oligomers are the primary neurotoxic species. According to the Klein group in 2018 (76), "*Aβ oligomers are both necessary and sufficient to trigger AD-associated memory malfunction and neurodegeneration*." Thus, soluble oligomers of Aβ are the real culprit in AD, not monomers or fibrils (Figure 1.10).

1.8 Aβ oligomers

In 1996, the search for a soluble Aβ pool was initiated in the human brain. The discordance between the amyloid plaques and the severity of AD pathology and the discrepancy in the location of neuronal loss and the plaques stimulated Kuo and coworkers to search for the possible species that reconcile these differences (83). Their study suggests the role of water-soluble Aβ42 oligomers, which is 12 times higher in AD brains as compared to healthy brains. In this study, the water-soluble Aβ pool from the AD brain homogenates was extracted by using ultracentrifugation at 220,000 x g. The water-soluble Aβ oligomers vary in size from < 10 kDa to > 100 kDa, among which 40 % of the fraction is in the 30-100 kDa size range. This study gives the first evidence for the existence of elevated concentration of a varied range of soluble Aβ oligomers *in vivo*. A subsequent study in 1997 by Walsh and coworkers characterizes the fibrillogenesis intermediates of both Aβ42 and Aβ40 *in vitro* by the combination of electron microscopy, light scattering, and size-exclusion chromatography techniques (84). The kinetic and structural analysis of the intermediates revealed the existence of curved linear strings, which have a molecular weight of > 100 kDa, are ~ 200 nm in length, and 6-8 nm in diameter and these structures were termed as "protofibrils." Later on, in 1998, a new class of small diffusible Aβ oligomers had been found, which are known as Aβ-derived diffusible ligands (ADDLs) (77). The molecular weights of these ADDLs vary between 17 and 42 kDa. Subsequently, in 1999,

McLean and coworkers detected SDS-stable dimers and trimers of Aβ having molecular weights of ~ 8 kDa and ~ 12 kDa in AD brain tissue (78). These species were present in both insoluble and soluble fraction and extracted by centrifugation at 175,000 x g. After these original studies, soluble Aβ oligomers became the spotlight for studying AD pathophysiology.

Soluble oligomers have been characterized using a wide array of biophysical techniques and imaging tools. The most common method is the SDS-PAGE, which gives the molecular weights of the species based on migration in the presence of SDS (85). However, it is known that SDS induces artifacts in the determination of molecular weights. Another well-known technique is the size-exclusion chromatography (SEC), which is a non-SDS-based method that separates the proteins on the basis of Stoke's radius. SEC can also induce artifacts in the determination of molecular weights due to the interaction of proteins with the column matrix. The dynamic light scattering (DLS) method, a spectroscopic approach, gives the hydrodynamic radius of oligomeric species on the basis of the Stokes-Einstein relationship. This technique is intrinsically biased for the higher-order species. The imaging techniques such as electron microscopy (EM) and atomic force microscopy (AFM) gives the three-dimensional morphological view of the species present in the sample and also suggests that the preparation is fibril free (86). EM and AFM cannot distinguish between the dimers and trimers of small proteins. Recently, the detection of oligomers by antibodies has been studied in different laboratories. These antibodies are capable of recognizing the oligomers formed by amyloidogenic proteins, not the monomer and the fibrillar forms of protein (85). Since a single technique can misrepresent the state of oligomers, therefore, a multitude of methods is required for the correct characterization of oligomers.

A plethora of studies have indicated the existence of a variety of Aβ oligomeric species in AD brains, APP transgenic mice, *in vitro*, and *in vivo*. These Aβ assemblies vary on the basis of morphology, size, toxicity, methods of preparation, structure, reactivity towards conformation-dependent antibodies, and biological effects. Soluble Aβ oligomers have been given a wide variety of names such as ADDLs, globulomers, annular protofibrils, prefibrillar aggregates, protofibrils, and Aβ*56 (dodecamer) (87). The putative Aβ oligomers that are directly involved in AD are described in Table 1. In addition to the various oligomers that are discussed in table 1, there is another approach that allows studying the individual lower molecular weight oligomeric species based on their size distribution. This approach is known as photoinduced cross-linking of unmodified proteins (PICUP). In PICUP, monomeric Aβ is covalently cross-linked by the

photolysis of the ruthenium (II) complex (88, 89). This process is zero-length (very fast) and highly efficient, which eliminates the problem of metastability of the oligomeric assemblies. In order to avoid the heterogeneity of the mixture, the oligomers were extracted from the gel matrix. By using PICUP, the pure oligomeric species of specific size-order are produced to study the structure-activity of Aβ oligomers (88, 89). However, *in vivo*, the oligomeric pool is likely to be dynamic and heterogeneous; therefore, it is difficult to separate the oligomers on the basis of its order of neurotoxicity. Soluble oligomers are common to many amyloidogenic proteins and represent the neurotoxic species. Many amyloid-forming proteins have been shown to have structural plasticity, which indicates a possibility of the presence of distinct structures among the different oligomeric preparations. It has been demonstrated that the conformation-dependent antibodies recognize generic conformation epitopes present in the distinct aggregation states, which leads to the emergence of structural classification of oligomers.

Table1. Various types of Aβ oligomers

Name	Characteristics	Location	Biological Effects
Dimers and Trimers	SDS-stable, appeared at ~ 8 kDa and ~ 12 kDa as dimers and trimers on SDS-PAGE (78).	Found in the frontal cortex of AD brain (78), and conditioned medium of Chinese hamster ovary cells that express APP_{751} (90). Dimer is also found in the soluble extracts of 10-12 months and 10-14 months aged Tg2576 and J20 AD mice models, respectively (87, 91). Trimer is secreted *in vitro* by primary neurons.	Causes loss of dendritic spines and impair LTP (87, 92).
	SDS-stable, non-fibrillar Aβ	First purified from middle-aged Tg2576 mice (91), found	Disrupts memory of young rats (91),

Aβ*56	dodecamer, and the molecular weight is 56 kDa (91).	in mice overexpressing Arctic mutant (93), and was also synthesized *in vitro* (94).	considered as neurotoxic species (94).
Aβ-derived diffusible ligands (ADDLs)	Small diffusible oligomers of 5-6 nm (77) and appeared between 10-100 kDa on SDS-PAGE (95).	Synthetically prepared *in vitro* (77), found in Tg2576 mice (96) and AD brain extracts (97).	Inhibit LTP in rat hippocampal slices (77), and also found to inhibit LTP through cellular prion protein (98).
Globulomers	Globular, water-soluble 60 kDa oligomer (99), migrate at 38-48 kDa on SDS-PAGE (100).	Prepared by incubating Aβ42 with SDS or fatty acids (100), detected in the brain of AD patients and Tg2576 mice (99).	Block LTP in rat hippocampal slices (99), inhibit spontaneous synaptic activity in AD patients (101).
Annular Protofibrils (APFs)	Ring-shaped or pore-like appearance, 18-25 nm in diameter, stable up to months, detected by annular anti-protofibril antibody (102, 103).	Formed by Arctic variant (E22G) of Aβ40 and wild-type Aβ40 (102) and also prepared from the prefibrillar oligomers of Aβ42 by exposure to a hydrophobic-hydrophilic interface such as lipid membrane (103).	Form β-barrel structures in the lipid membrane environment (102).

1.9 Structurally distinct Aβ oligomers

Many different laboratories have produced a wide range of Aβ oligomers that vary in the ways of preparations or purification, size, morphology, toxicity, which raises the question of structural

relations among the different oligomeric preparations. Prof Glabe and coworkers have proposed that the classification of Aβ oligomers based on the structure is the most useful and biologically relevant (104). In 2003, a conformation-dependent antibody known as anti-amyloid oligomer antibody (A11) was generated, which recognizes soluble Aβ oligomers and does not recognize the monomeric or fibrillar forms of Aβ. Interestingly, Prof

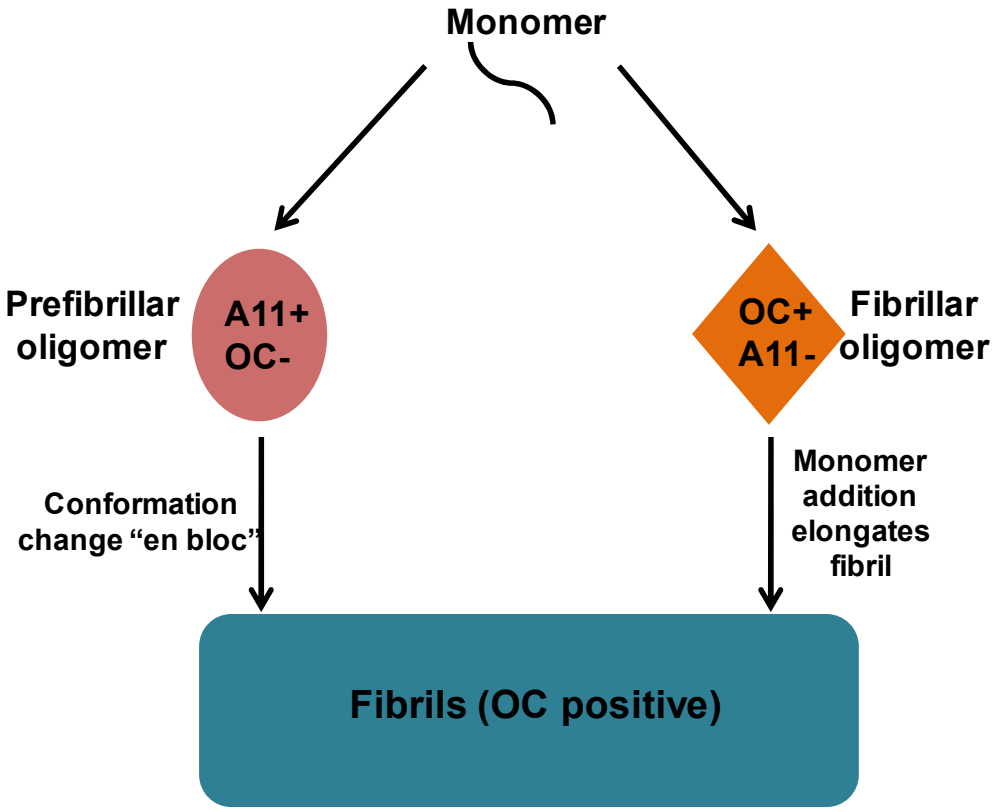

Figure 1.11: Classification of oligomers on the basis of conformation. Two conformationally distinct oligomers, prefibrillar and fibrillar oligomers. Prefibrillar oligomers are reactive to A11 antibody but do not bind to OC antibody. Fibrillar oligomers are active to OC antibody but do not react with the A11 antibody. Both the conformations of oligomers form the fibrils that are reactive to the OC antibody. Drawn using the concept from reference (104).

Glabe's group showed that the antibody equally binds to oligomers of other amyloidogenic proteins like islet amyloid polypeptide (IAPP), prion peptide (106-126), polyglutamine, α-synuclein, lysozyme, and human insulin. Other forms of these proteins do not show reactivity to the A11 antibody (105). The soluble oligomers of all these proteins display toxicity, and the

toxicity gets inhibited with the A11 antibody. This signifies that the antibody binds to a unique structural feature of the proteins, which is common to the oligomers and is independent of the amino acid sequence. The unique common structure in the oligomers might mediate a common mechanism of toxicity. Soluble oligomers that are recognized by the A11 antibody are known as prefibrillar oligomers as they preceded the formation of fibrils. Further, in 2007, Prof Glabe's group reported another conformation-specific antibody, which is known as anti-amyloid fibril antibody (OC) that recognizes soluble Aβ oligomers and the Aβ fibrils (106). The OC antibody does not bind to prefibrillar oligomers that are reactive to the A11 antibody. Also, the OC antibody recognizes the amyloid fibrils of IAPP and α-synuclein proteins. Soluble oligomers that bind to OC antibody are termed as "fibrillar oligomers" as the conformational epitope of these oligomers is similar to the fibrils. Therefore, it was proposed that many amyloids show a fundamental characteristic of the conformational difference between the two fibrillar and prefibrillar oligomers (Figure 1.11). The two structure-specific antibodies, OC and A11, recognize mutually exclusive and generic epitopes of conformationally distinct fibrillar and prefibrillar oligomers, respectively. Further, it has been shown that the OC antibody identifies the in-register parallel β-sheet structure and A11 antibody recognized out-of-register anti-parallel β-sheet structure (107, 108).

1.10 Mechanism of toxicity mediated by Aβ oligomers

So far, we understand that the soluble Aβ oligomers are the species that strongly relate to AD pathogenesis, and many different types of Aβ oligomers exist *in vitro* and *in vivo*. Now, these various types of Aβ oligomers exhibit their neurotoxic effects in AD through a number of different mechanisms. The mechanism by which Aβ oligomers mediate their toxicity is not clearly understood. Aβ oligomers are found in both extracellular and intracellular space. There are mainly three pathways by which Aβ oligomers have been proposed to exert their deleterious effects in AD (109). These are (1) receptor-mediated toxicity, (2) interaction with the cell membrane, and (3) intracellular accumulation.

1.10.1 Receptor-mediated toxicity

In 1998, when the first synthetic Aβ oligomers, ADDLs, were prepared, it was observed that the treatment of cells with trypsin abolished the binding of ADDLs to hippocampal neurons and

subsequently inhibited the toxicity. This indicated the involvement of high-affinity protein receptors for the binding of Aβ oligomers to the hippocampal neurons and the toxicity (77, 81). Successive studies have identified many putative neuronal receptors for Aβ that bind Aβ oligomers at the cell surface, which further trigger the downstream signaling pathways and lead to the synaptic dysfunctions and neurodegeneration. One of the receptors for Aβ oligomers is N-methyl-D-aspartate receptors (NMDARs). NMDARs are the ion channels that play a central role in synaptic plasticity. The opening of NMDARs channels leads to the influx of Ca^{2+} ions, which further induces LTP (92). The activation of NMDARs can induce LTP or LTD, depending on the nature of the stimulus. Mounting evidence suggested that the Aβ oligomers inhibited the NMDAR-mediated LTP and promoted the LTD. Studies also indicated that the Aβ oligomers-mediated LTP inhibition involves the activation of the GluN2B subunit of NMDARs (92, 110). Thus, NMDARs play a central role in mediating the toxic effects of Aβ oligomers. Growing evidence indicated that the lipid-raft associated protein, nerve growth factor (NGF) acts as a receptor for monosialoganglioside-induced Aβ oligomers and mediates the toxic effects of Aβ oligomers. NGF induces cell death by the involvement of p75 neurotrophin receptor (111). Recent studies suggested that the soluble Aβ oligomers inhibit the Wnt signaling pathway by binding to the frizzled (Fz) receptors, which are near to the Wnt-binding site. Wnt signaling is required for the cell movement, cell polarity, neuronal development, synaptic function, and synaptic plasticity. Binding of Aβ oligomers to Fz receptors block the Wnt signaling, which further results in phosphorylation of tau protein and neurofibrillary tangles formation (112). A body of evidence has shown that impaired insulin signaling is also involved in AD. Aβ oligomers bind to the insulin receptors and cause the internalization of insulin receptors from dendritic spines. Perturbation in the insulin signaling pathway may inhibit the memory formation process (113). In 2009, a recent study by Prof Stritmater and coworkers identified the cellular prion protein (PrP^C) as a high-affinity binding receptor for Aβ oligomers (98). Studies have shown that PrP^C binds Aβ oligomers with nanomolar affinity, and PrP^C mediates the Aβ oligomers-induced inhibition of LTP in hippocampal neurons. PrP^C is a C-terminal glycophosphatidylinositol-anchored protein that is expressed at axons and synapses where it localized in the lipid rafts. PrP^C undergoes misfolding into the scrapie prion $PrP^{Sc,}$ which is a disease-related amyloid isoform. PrP^{Sc} is involved in fatal transmissible neurodegenerative diseases, which is known as Creutzfeldt-Jakob disease in humans and bovine spongiform

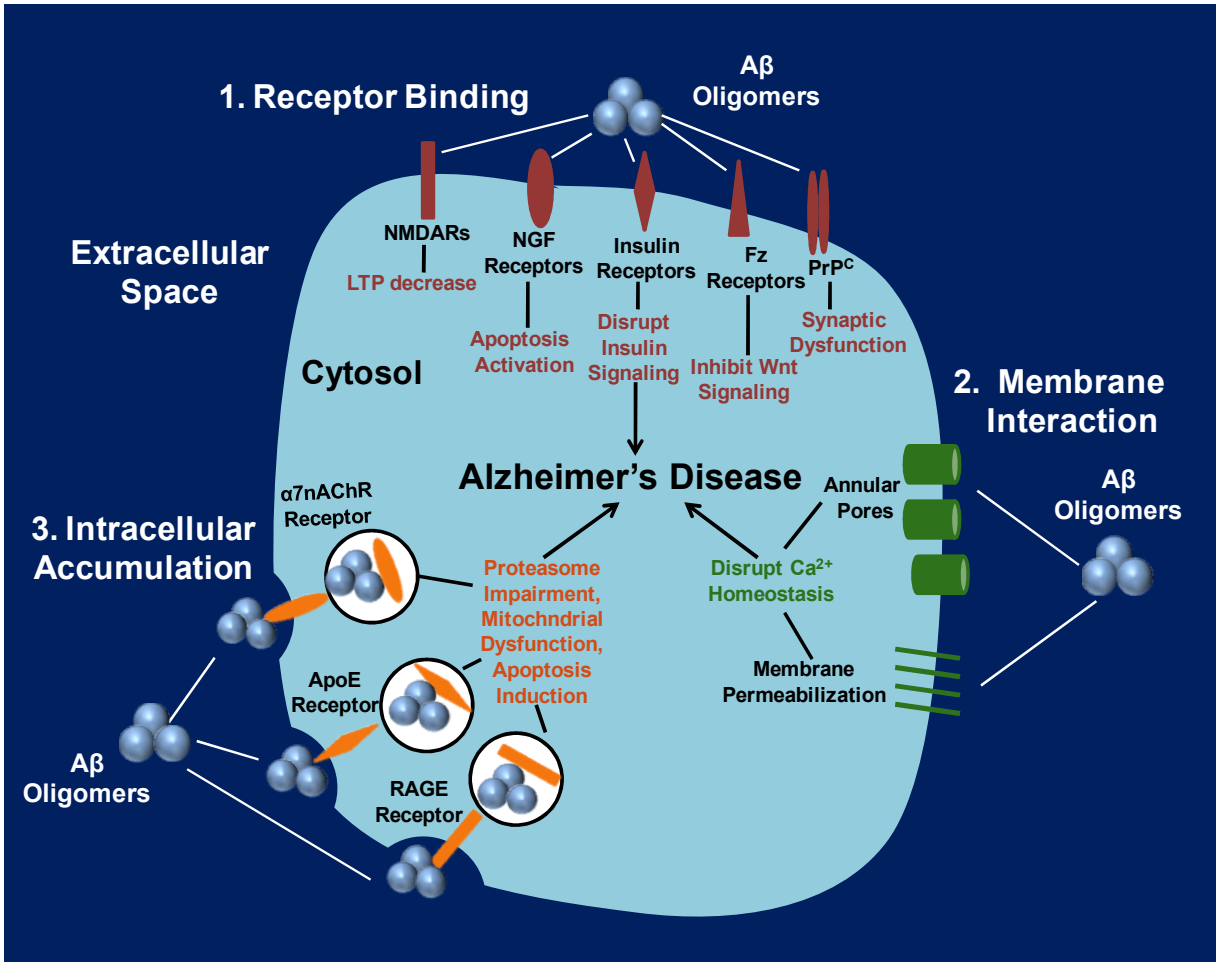

Figure 1.12: Mechanisms of toxicity induced by Aβ oligomers. (1) Aβ oligomers can bind to multiple receptors with the high affinity that triggers a downstream signaling cascade. (2) Aβ oligomers can interact with membrane and form annular pores or ion channels, which further result in disruption of calcium homeostasis. (3) Aβ oligomers can be secreted into the cell through multiple receptors, get accumulated inside the cell and leads to proteasomal impairment, mitochondrial dysfunction, and cell death. NMDARs = N-methyl-D-aspartate receptors; NGF = Nerve growth factor; Fz = Frizzled; PrP^C = Cellular prion protein; α7nAChR = α7 nicotinic acetylcholine receptor; ApoE = Apolipoprotein E; RAGE = Receptor for advanced glycation end products.

encephalopathy in animals (114). Binding of PrP^C to Aβ oligomers activate Fyn kinase, which further phosphorylates the GluN2B subunit of NMDARs and leads to the loss of cell surface

NMDARs. Also, Aβ oligomers-induced activation of Fyn kinase leads to tau phosphorylation. Thus, the binding of PrP^C to Aβ oligomers triggers a downstream signaling cascade, which results in synaptic impairments (115). However, some studies reported that PrP^C does bind to Aβ oligomers, but PrP^C does not mediate the toxic effects caused by Aβ oligomers (116, 117). This discrepancy could arise due to the use of different Aβ oligomers that vary in conformation, size, morphology, and cytotoxicity. In addition to being PrP^C as a "bad receptor" for Aβ oligomers, PrP^C also plays the role of "good receptor" in AD. The postulated protective functions of PrP^C are as follows. PrP^C could potentially decrease Aβ peptide formation by inhibiting the β-secretase cleavage of APP, exosomal PrP^C reduces the toxic effects by accelerating Aβ aggregation, and N1, the main physiological cleavage fragment of PrP suppresses Aβ oligomers toxicity in mice. Thus, PrP^C plays a dual role in AD (115).

1.10.2 Cell membrane-mediated toxicity

The integrity of the cell membrane is very crucial for the cell viability as the cell membrane regulates the exchange of materials between the extracellular and intracellular compartments. Various neurodegenerative amyloid disorders like Parkinson's disease and AD have long been associated with the increase in the cell permeability and the intracellular concentrationof calcium ions (109). One of the mechanisms of neurodegeneration caused by Aβ is through the amyloid pores formation. According to the amyloid channel hypothesis, soluble Aβ oligomers insert directly into the lipid bilayers, form calcium-permeable channels, and disrupt the calcium homeostasis (118). In 1993, Prof Pollard's group demonstrated that the synthetic Aβ peptide inserts into the artificial lipid bilayer and form cation-selective channels (119). Disruption of calcium-ion homeostasis by Aβ channels on the neuronal membranes may promote tau phosphorylation and free radical formation that further accelerates neurodegeneration (120, 121). These Aβ pore-like structures have also been shown in AD human brain tissue (122). A growing body of evidence suggests an increase in the conductance of lipid bilayers by Aβ oligomers, but these membranes do not exhibit pore-like structures(123, 124). In contrast to the amyloid pore hypothesis, the authors proposed that the rise in conductance and ion permeability by Aβ oligomers occurs by spreading out the lipid headgroups, which further causes thinning of the lipid membrane and reduces the membrane permeability barrier (109). The membrane permeability by Aβ oligomers is because of the defects in lipid bilayers, not due to the amyloid

pores. The rise in membrane conductance could result in membrane depolarization, which can affect cell signaling and cause defects in the cytosolic ion homeostasis (125).

1.10.3 Toxicity by intracellular accumulation

Mounting evidence suggested that Aβ accumulates not only in the extracellular space but also in the intracellular space. Aβ is produced wherever APP, β-secretases, and γ-secretases are present, and these are localized in various compartments of the cell (109). Other than the generation of Aβ intracellular, the extracellular Aβ can be secreted back into the cell and internalized through various receptors. Studies have shown that the receptors including α7 nicotinic acetylcholine receptor (α7nAChR) (126), apolipoprotein E (apoE) receptors which is a member of the low-density lipoprotein (LDL) receptor family (127), and the receptor for advanced glycation end products (RAGE) bind to Aβ (128). This facilitates the cellular uptake and intracellular accumulation of Aβ. The intracellular Aβ has been shown to cause proteasomal inhibition (129), induce apoptosis (130), mitochondrial dysfunction (131), and lysosomal damage (132).

1.11 Thesis motivation and perspective

Alzheimer's disease (AD) is an age-related neurodegenerative brain disorder that involves a decline in cognitive functions such as language, behavioral changes, and motor difficulties, and ultimately leads to death. AD is characterized by the accumulation of extracellular amyloid plaques of amyloid-β (Aβ) peptide and the intracellular neurofibrillary tangles of tau protein. Soluble oligomers of Aβ peptide are known to be the potent neurotoxic species that cause synaptic dysfunction and inhibit long-term potentiation. Therefore, it is of significant interest to understand how these soluble oligomers of Aβ cause toxicity.

This thesis aims at dissecting the underlying molecular mechanisms of toxicity govern by conformationally distinct soluble Aβ oligomers. In order to characterize the structural attributes of various soluble oligomers, two conformation-specific antibodies, the anti-amyloid fibril antibody (OC) and anti-amyloid oligomer antibody (A11) that recognize mutually exclusive structural epitopes of fibrillar and prefibrillar oligomers have been generated. Using a wide range of biophysical and biochemical techniques including dynamic light scattering (DLS), size-exclusion chromatography (SEC), atomic force microscopy (AFM), dot-blot assay and SDS-PAGE, we prepared and characterized the conformationally distinct soluble Aβ oligomers

(Chapter 2). Soluble Aβ oligomers are known to bind to the prion protein (PrP), a cell-surface receptor and mediate their downstream cellular toxicity. In chapter 3, we demonstrate the mechanism of heterotypic interaction between the conformationally distinct Aβ oligomers and PrP using steady-state fluorescence, SEC, pull-down assay, and the cytotoxicity assay. Soluble Aβ oligomers are known to interact with the cell membrane and form amyloid pores in the membrane. In chapter 4, we shed light on the behavior of the conformationally distinct Aβ oligomers in the membrane environment. I believe this thesis will improve our current understanding of the structurally different Aβ oligomers and provide insights for designing the therapeutic agents to combat Alzheimer's disease.

1.12 References:

1. Fact Sheet. (2019) Alzheimer's Disease : Facts & Figures. *BrightFocus Foundation*

2. Kern, A., and Behl, C. (2009) The unsolved relationship of brain aging and late-onset Alzheimer disease. *Biochim. Biophys. Acta - Gen. Subj.* **1790**, 1124–1132

3. Stelzmann, R. A., Schnitzlein, H. N., and Murtagh, F. R. (1995) An English translation of Alzheimer's 1907 Paper , " Über eine eigenartige Erkankung der Hirnrinde ." *Clinical Anatomy*. **1**, 429–431

4. Bondi, M. W., Edmonds, E. C., and Salmon, D. P. (2017) Alzheimer's Disease : Past, Present , and Future. *J. Int. Neuropsych. Soc.* **23**, 818-831

5. Femminella, G. D., Thayanandan, T., Calsolaro, V., Komici, K., Rengo, G., Corbi, G., and Ferrara, N. (2018) Imaging and molecular mechanisms of Alzheimer's disease: A review. *Int. J. Mol. Sci.* **19**, 3702

6. Serrano-Pozo, A., Frosch, M. P., Masliah, E., and Hyman, B. T. (2011) Neuropathological Alterations in Alzheimer Disease. *Cold Spring Harb. Perspect. Med.* **1**, 1–23

7. Braak, H., Alafuzoff, I., Arzberger, T., Kretzschmar, H., and Tredici, K. D. (2006) Staging of Alzheimer disease-associated neurofibrillary pathology using paraffin sections and immunocytochemistry. *Acta Neuropathol.* **112**, 389–404

8. Thal, D. R., Rüb, U., Orantes, M., and Braak, H. (2002) Phases of Aß-deposition in the human brain and its relevance for the development of AD. *Neurology.* **58**, 1791-1800

9. Hardy J. and Allosp D. (1991) Amyloid deposition as the central event in the etiology of Alzheimer's disease. *Trends Pharmacol Sci.* **12**, 383-388

10. Hardy, J. A., and Higgins, G. A. (1992) Alzheimer's Disease : The Amyloid Cascade Hypothesis. *Science.* **256**, 184-185

11. Ricciarelli, R., and Fedele, E. (2017) The Amyloid Cascade Hypothesis in Alzheimer's Disease : It's Time to Change Our Mind. *Curr. Neuropharmacol.* **15**, 926-935

12. Dawkins, E., and Small, D. H. (2014) Insights into the physiological function of the β-amyloid precursor protein: beyond Alzheimer's disease. *J. Neurochem.* **129**, 756–769

13. Muller-hill, H., and Beyreuther, K. (1989) MOLECULAR BIOLOGY OF ALZHEIMER'S DISEASE. *Annu. Rev. Biochem.* **58**, 287-307

14. De Silva, H. A. R., Jen, A., Wickenden, C., Jen, L. S., Wilkinson, S. L., and Patel, A. J. (1997) Cell-specific expression of β-amyloid precursor protein isoform mRNAs and proteins in neurons and astrocytes. *Mol. Brain Res.* **47**, 147–156

15. Kang, J., Lemaire, H. G., Unterbeck, A., Salbaum, J. M., Masters, C. L., Grzeschik, K. H., Multhaup, G., Beyreuther, K., and Müller-Hill, B. (1987) The precursor of Alzheimer's disease amyloid A4 protein resembles a cell-surface receptor. *Nature*. **325**, 733–736

16. Gupta, S., Banerjee, P., Laferla, F. M., and Selkoe, D. J. (2010) Alzheimer's Disease : Genes , Proteins , and Therapy. *Physiol. Rev.* **81**, 741–766

17. Bhattacharya, R., Barren, C., and Kovacs, D. M. (2013) Palmitoylation of Amyloid Precursor Protein Regulates Amyloidogenic Processing in Lipid Rafts. *J. Neurosci.* **33**, 11169–11183

18. Haass, C., Koo, E. H., Mellon, A., Hung, A. Y., and Selkoe, D. J. (1992) Targeting of cell-surface β-amyloid precursor protein to lysosomes: Alternative processing into amyloid-

bearing fragments. *Nature*. **357**, 500–503

19. Yamazaki, T., Koo, E. H., and Selkoe, D. J. (1996) Trafficking of cell-surface amyloid-β protein precursor: II. Endocytosis, recycling, and lysosomal targeting detected by immunolocalization. *J. Cell Sci.* **109**, 999–1008

20. Haass, C., Kaether, C., Thinakaran, G., and Sisodia, S. (2012) Trafficking and proteolytic processing of APP. *Cold Spring Harb. Perspect. Med.* **2**, 1–26

21. Chow, V. W., Mattson, M. P., Wong, P. C., and Gleichmann, M. (2010) An overview of APP processing enzymes and products. *Neuromolecular Med.* **12**, 1–12

22. Lazarov, O., and Demars, M. P. (2012) All in the family: How the APPs regulate neurogenesis. *Front. Neurosci.* **6**, 1–21

23. Asai, M., Hattori, C., Szabó, B., Sasagawa, N., Maruyama, K., Tanuma, S. I., and Ishiura, S. (2003) Putative function of ADAM9, ADAM10, and ADAM17 as APP α-secretase. *Biochem. Biophys. Res. Commun.* **301**, 231–235

24. Tanabe, C., Hotoda, N., Sasagawa, N., Sehara-Fujisawa, A., Maruyama, K., and Ishiura, S. (2007) ADAM19 is tightly associated with constitutive Alzheimer's disease APP α-secretase in A172 cells. *Biochem. Biophys. Res. Commun.* **352**, 111–117

25. Strooper, B. De, and Annaert, W. (1997) Proteolytic processing and cell biological functions of the amyloid precursor. *J. Cell Sci.* **113**, 1857–1870

26. Skovronsky, D. M., Moore, D. B., Milla, M. E., Doms, R. W., and Lee, V. M. Y. (2000) Protein kinase C-dependent α-secretase competes with β-secretase for cleavage of amyloid-β precursor protein in the trans-Golgi network. *J. Biol. Chem.* **275**, 2568–2575

27. Mattson, M. P., Cheng, B., Culwell, A. R., Esch, F. S., Lieberburg, I., and Rydel, R. E. (1993) Evidence for excitoprotective and intraneuronal calcium-regulating roles for secreted forms of the β-amyloid precursor protein. *Neuron*. **10**, 243–254

28. Furukawa, K., Barger, S. W., Blalock, E. M., and Mattson, M. P. (1996) Activation of K+

channels and suppression of neuronal activity by secreted β-amyloid-precursor protein. *Nature*. **379**, 74–78

29. Wolfe, M. S. (2008) Inhibition and Modulation of γ-Secretase for Alzheimer's Disease. *Neurotherapeutics*. **5**, 391–398

30. Li, H., Wolfe, M. S., and Selkoe, D. J. (2009) Toward Structural Elucidation of the γ-Secretase Complex. *Structure*. **17**, 326–334

31. Huse, J. T., Liu, K., Pijak, D. S., Carlin, D., Lee, V. M. Y., and Doms, R. W. (2002) β-secretase processing in the trans-Golgi network preferentially generates truncated amyloid species that accumulate in Alzheimer's disease brain. *J. Biol. Chem.* **277**, 16278–16284

32. Nikolaev, A., McLaughlin, T., O'Leary, D. D. M., and Tessier-Lavigne, M. (2009) APP binds DR6 to trigger axon pruning and neuron death via distinct caspases. *Nature*. **457**, 981–989

33. Haass, C., and Selkoe, D. J. (2007) Soluble protein oligomers in neurodegeneration: Lessons from the Alzheimer's amyloid β-peptide. *Nat. Rev. Mol. Cell Biol.* **8**, 101–112

34. Cupers, P., Orlans, I., Craessaerts, K., Annaert, W., and De Strooper, B. (2001) The amyloid precursor protein (APP)-cytoplasmic fragment generated by γ-secretase is rapidly degraded but distributes partially in a nuclear fraction of neurones in culture. *J. Neurochem.* **78**, 1168–1178

35. Fiore, F., Zambrano, N., Minopoli, G., Donini, V., Duilio, A., and Russo, T. (1995) The regions of the Fe65 protein homologous to the phosphotyrosine interaction/phosphotyrosine binding domain of Shc bind the intracellular domain of the Alzheimer's amyloid precursor protein. *J. Biol. Chem.* **270**, 30853–30856

36. Cao, X., and Sudhof, T. C. (2001) A Transcriptively Active Complex of APP with Fe65 and Histone Acetyltransferase Tip60. *Science.* **293**, 115-120

37. Checler, F., Sunyach, C., Pardossi-Piquard, R., Sevalle, J., Vincent, B., Kawarai, T., Girardot, N., George-Hyslop, P. S., and da Costa, C. (2007) The γ/ε-Secretase-Derived

APP Intracellular Domain Fragments Regulate p53. *Curr. Alzheimer Res.* **4**, 423–426

38. Kim, H., Kim, E., Lee, J., Park, C. H., Kim, S., Seo, J., Chang, K., Yu, E., Jeong, S., Chong, Y. H., and Suh, Y. (2003) C-terminal fragments of amyloid precursor protein exert neurotoxicity by inducing glycogen synthase kinase-3β expression. *FASEB J.* **17**, 1951-1953

39. Belyaev, N. D., Nalivaeva, N. N., Makova, N. Z., and Turner, A. J. (2009) Neprilysin gene expression requires binding of the amyloid precursor protein intracellular domain to its promoter: Implications for Alzheimer disease. *EMBO Rep.* **10**, 94–100

40. Murphy, M. P., and Levine, H. (2010) Alzheimer's Disease and the Amyloid-β Peptide. *J. Alzheimer's. Dis.* **19**, 311–323

41. Larner, A. J., and Doran, M. (2009) Genotype-Phenotype Relationships of Presenilin-1 Mutations in Alzheimer's Disease : An Update. *J. Alzheimer's. Dis.* **17**, 259–265

42. Hass, C., Schlossmacher, M. G., Hung, A., Vigo-pelfreyt, C., Mellon, A., Ostaszewski, B. L., Lieberburgt, I., Koo, E. H., Schenkt, D., Teplow, D. B., and Selkoe, D. J. (1992) Amyloid β-peptide is produced by cultured cells during normal metabolism. *Nature* **359**, 322–325

43. Giuffrida, M. L., Caraci, F., Pignataro, B., Cataldo, S., Bona, P. De, Bruno, V., Molinaro, G., Pappalardo, G., Messina, A., Palmigiano, A., Garozzo, D., Nicoletti, F., Rizzarelli, E., and Copani, A. (2009) β-Amyloid Monomers Are Neuroprotective. *J. Neurosci.* **29**, 10582–10587

44. Pearson, H. A., and Peers, C. (2006) Physiological roles for amyloid β peptides. *J. Physiol.* **575**, 5–10

45. Barrow, C. J., and Zagorski, M. G. (1991) Solution Structures of β Peptide and Its Constituent Fragments: Relation to Amyloid Deposition. *Science.* **253**, 179–182

46. Zhang, S., Iwata, K., Lachenmann, M. J., Peng, J. W., Li, S., Stimson, E. R., Lu, Y. A., Felix, A. M., Maggio, J. E., and Lee, J. P. (2000) The Alzheimer's Peptide Aβ Adopts a

Collapsed Coil Structure in Water. *J. Struct. Biol.* **130**, 130–141

47. Chen, G. F., Xu, T. H., Yan, Y., Zhou, Y. R., Jiang, Y., Melcher, K., and Xu, H. E. (2017) Amyloid beta: Structure, biology and structure-based therapeutic development. *Acta Pharmacol. Sin.* **38**, 1205–1235

48. Finder, V. H., and Glockshuber, R. (2007) Amyloid-β aggregation. *Neurodegener. Dis.* **4**, 13–27

49. Cohen, S. I. A., Linse, S., Luheshi, L. M., Hellstrand, E., White, D. A., Rajah, L., Otzen, D. E., Vendruscolo, M., Dobson, C. M., and Knowles, T. P. J. (2013) Proliferation of amyloid-β42 aggregates occurs through a secondary nucleation mechanism. *Proc. Natl. Acad. Sci. U. S. A.* **110**, 9758–9763

50. Ohm, T. G., Müller, H., Braak, H., and Bohl, J. (1995) Close-meshed prevalence rates of different stages as a tool to uncover the rate of Alzheimer's disease-related neurofibrillary changes. *Neuroscience*. **64**, 209–217

51. Kirschner, D. A., Inouye, H., Duffy, L. K., Sinclair, A., Lind, M., and Selkoe, D. J. (1987) Synthetic peptide homologous to beta protein from Alzheimer disease forms amyloid-like fibrils in vitro. *Proc. Natl. Acad. Sci. U. S. A.* **84**, 6953–6957

52. Rambaran, R. N., and Serpell, L. C. (2008) Amyloid fibrils: abnormal protein assembly. *Prion*. **2**, 112–117

53. Goldsbury, C., Kistler, J., Aebi, U., Arvinte, T., and Cooper, G. J. . (1999) Watching Amyloid Fibrils Grow By Time-Lapse Atomic Force Microscopy. *J. Mol. Biol.* **285**, 33–39

54. Serpell, L. C., Sunde, M., Benson, M. D., Tennent, G. A., Pepys, M. B., and Fraser, P. E. (2000) The Protofilament Substructure of Amyloid Fibrils. *J. Mol. Biol.* **300**, 1033–1039

55. Fraser, P. E., Serpell, L. C., Pepys, M. B., Bartlam, M., Blake, C. C. ., and Sunde, M. (2002) Common core structure of amyloid fibrils by synchrotron X-ray diffraction. *J. Mol. Biol.* **273**, 729–739

56. Makin, O. S., Sikorski, P., and Serpell, L. C. (2006) Diffraction to study protein and peptide assemblies. *Curr. Opin. Chem. Biol.* **10**, 417–422

57. Eisenberg, D. S., and Sawaya, M. R. (2017) Structural Studies of Amyloid Proteins at the Molecular Level. *Annu. Rev. Biochem.* **86**, 69-95

58. Nettleton, E. J., Bouchard, M., Robinson, C. V, Dobson, C. M., and Saibil, H. R. (2002) The protofilament structure of insulin amyloid fibrils. *Proc. Natl. Acad. Sci. U. S. A.* **99,** 9196-9201

59. Jime, Â. L., Tennent, G., Pepys, M., and Saibil, H. R. (2001) Structural Diversity of ex vivo Amyloid Fibrils Studied by Cryo-electron Microscopy. *J. Mol. Biol.* **311**, 241-247

60. Sachse, C., Xu, C., Wieligmann, K., Diekmann, S., Grigorieff, N., and Fändrich, M. (2006) Quaternary Structure of a Mature Amyloid Fibril from Alzheimer's Aβ (1-40) Peptide. *J. Mol. Biol.* **1**, 347–354

61. Serpell, L. C. (2000) Alzheimer's amyloid fibrils : structure and assembly. *Biochim. Biophys. Acta - Mol. Basis Dis.* **1502**, 16–30

62. Fändrich, M., Meinhardt, J., and Grigorieff, N. (2009) Structural polymorphism of Alzheimer Aβ and other amyloid fibrils. *Prion*. **3**, 89–93

63. Fandrich, M., Nystrom, S., Nilsson, K. P. R., Bockmann, A., LeVine III, H., and Hammarstrom, P. (2019) Amyloid fibril polymorphism - a challenge for molecular imaging and therapy. *J. Intern Med.* **283**, 218–237

64. Lansbury, P. T., Costa, P. R., Griffiths, J. M., Simon, E. J., Auger, M., Halverson, K., Kocisko, D. A., Hendsch, Z. S., Ashburn, T. T., Spencer, R. G. S., Tidor, B., and Griffin, R. G. (1995) Structural model for the β-amyloid fibril based on interstrand alignment of an anti-parallel-sheet comprising a C-terminal peptide. *Nature.* **2**, 990-998

65. Benzinger, T. L. S., Gregory, D. M., Burkoth, T. S., Miller-Auer, H., Lynn, D. G., Botto, R. E., and Meredith, S. C. (1998) Propagating structure of Alzheimer's β-amyloid$_{(10-35)}$ is parallel β-sheet with residues in exact register. *Proc. Natl. Acad. Sci. U. S. A.* **95**, 13407–

13412

66. Tycko, R. (2011) Solid-State NMR Studies of Amyloid Fibril Structure. *Annu. Rev. Phys. Chem.* **62**, 279–299

67. Tycko, R. (2015) Amyloid Polymorphism: Structural Basis and Neurobiological Relevance. *Neuron*. **86**, 632–645

68. Paravastu, A. K., Leapman, R. D., Yau, W. M., and Tycko, R. (2008) Molecular structural basis for polymorphism in Alzheimer's β-amyloid fibrils. *Proc. Natl. Acad. Sci. U. S. A.* **105**, 18349–18354

69. Petkova, A. T., Yau, W. M., and Tycko, R. (2006) Experimental constraints on quaternary structure in Alzheimer's β-amyloid fibrils. *Biochemistry*. **45**, 498–512

70. Lu, J. X., Qiang, W., Yau, W. M., Schwieters, C. D., Meredith, S. C., and Tycko, R. (2013) Molecular Structure of β-Amyloid Fibrils in Alzheimer's Disease Brain Tissue. *Cell*. **154**, 1257-1268

71. Qiang, W., Yau, W. M., Luo, Y., Mattson, M. P., and Tycko, R. (2012) Antiparallel β-sheet architecture in Iowa-mutant β-amyloid fibrils. *Proc. Natl. Acad. Sci. U. S. A.* **109**, 4443–4448

72. Xiao, Y., Ma, B., McElheny, D., Parthasarathy, S., Long, F., Hoshi, M., Nussinov, R., and Ishii, Y. (2015) Aβ(1-42) fibril structure illuminates self-recognition and replication of amyloid in Alzheimer's disease. *Nat. Struct. Mol. Biol.* **22**, 499–505

73. Wälti, M. A., Ravotti, F., Arai, H., Glabe, C. G., Wall, J. S., Böckmann, A., Güntert, P., Meier, B. H., and Riek, R. (2016) Atomic-resolution structure of a disease-relevant Aβ(1-42) amyloid fibril. *Proc. Natl. Acad. Sci. U. S. A.* **113**, E4976–E4984

74. Wetzel, R., Shivaprasad, S., and Williams, A. D. (2008) Plasticity of amyloid fibrils. *Biochemistry* **46**, 1–10

75. Walsh, D. M., and Selkoe, D. J. (2007) Aβ oligomers - A decade of discovery. *J.*

Neurochem. **101**, 1172–1184

76. Viola, K. L., Klein, W. L., and Cline, E. N. (2018) The Amyloid-β Oligomer Hypothesis : Beginning of the Third Decade. *J. Alzheimer's Dis.* **64**, S567-S610

77. Lambert, M. P., Barlow, A. K., Chromy, B. A., Edwards, C., Freed, R., Liosatos, M., Morgan, T. E., Rozovsky, I., Trommer, B., Viola, K. L., Wals, P., Zhang, C., Finch, C. E., Kraft, G. A., and Klein, W. L. (1998) Diffusible , nonfibrillar ligands derived from $A\beta_{1-42}$ are potent central nervous system neurotoxins. *Proc. Natl. Acad. Sci.U. S. A.* **95**, 6448–6453

78. Mclean, C. A., Cherny, R. A., Fraser, F. W., Fuller, S. J., Smith, M. J., Beyreuther, K., Bush, A. I., and Masters, C. L. (1999) Soluble Pool of Aβ Amyloid as a Determinant of Severity of Neurodegeneration in Alzheimer's Disease. *Ann. Neurol.* **46**, 860-866

79. Lue, L., Kuo, Y., Roher, A. E., Brachova, L., Shen, Y., Sue, L., Beach, T., Kurth, J. H., Rydel, R. E., and Rogers, J. (1999) Soluble Amyloid-β Peptide Concentration as a Predictor of Synaptic Change in Alzheimer's Disease. *Am. J. Pathol.* **155**, 853–862

80. Näsuland, J., Haroutunian, V., Mohs, R., Davis, K. L., Davies, P., Greengard, P., and Buxbaum, J. D. (2015) Correlation Between Elevated Levels of Amyloid-β Peptide in the Brain and Cognitive Decline. *JAMA* **283**, 1571–1577

81. Brorsson, A., Bolognesi, B., Tartaglia, G. G., Shammas, S. L., Favrin, G., Watson, I., Lomas, D. A., Chiti, F., Vendruscolo, M., Dobson, C. M., Crowther, D. C., and Luheshi, L. M. (2010) Intrinsic Determinants of Neurotoxic Aggregate Formation by the Amyloid-β Peptide. *Biophys J.* **98**, 1677–1684

82. Rushworth, J. V, and Hooper, N. M. (2011) Lipid Rafts : Linking Alzheimer's Amyloid-β Production, Aggregation, and Toxicity at Neuronal Membranes. *Int. J. Alzheimer's Dis.* **2011**, 1-14

83. Kuo, Y., Emmerling, M. R., Vigo-pelfrey, C., Kasunic, T. C., Kirkpatrick, J. B., Murdoch, G. H., Ball, M. J., and Roher, A. E. (1996) Water-soluble Aβ (N-40 , N-42) Oligomers in Normal and Alzheimer Disease Brains *. *J. Biol. Chem.* **271**, 4077–4081

84. Walsh, D. M., Lomakin, A., Benedek, G. B., Condron, M. M., and Teplow, D. B. (1997) Amyloid-β Protein Fibrillogenesis. *J. Biol. Chem.* **272**, 22364–22372

85. Bitan, G. A. L., Fradinger, E. A., Spring, S. M., and Teplow, D. B. (2005) Neurotoxic protein oligomers — what you see is not always what you get. *Amyloid* **12**, 88–95

86. Stine, W. B., Jungbauer, L., Yu, C., and Ladu, M. J. (2013) Preparing Synthetic Aβ in Different Aggregation States. *Methods Mol. Biol.* **670**, 13-32

87. Larson, M. E., and Lesné, S. E. (2012) Soluble Aβ oligomer production and toxicity. *J. Neurochem.* **120**, 125–139

88. Marina, G. B., Kirkitadze, D., Lomakin, A., Vollers, S. S., Benedek, G. B., and Teplow, D. B. (2003) Amyloid β-protein (Aβ) assembly: Aβ40 and Aβ42 oligomerize through distinct pathways. *Proc. Natl. Acad. Sci. U. S. A.* **100**, 330–335

89. Rosensweig, C., Ono, K., Murakami, K., Lowenstein, D. K., Bitan, G., and Teplow, D. B., (2012) Preparation of Stable Amyloid β-Protein Oligomers of Defined Assembly Order. *Methods Mol. Biol.* **849**, 1–11

90. Podlisny, M. B., Ostaszewski, B. L., Squazzo, S. L., Koo, E. H., Rydell, R. E., Teplow, D. B., and Selkoe, D. J. (1995) Aggregation of secreted amyloid β-protein into sodium dodecyl sulfate- stable oligomers in cell culture. *J. Biol. Chem.* **270**, 9564–9570

91. Lesné, S., Ming, T. K., Kotilinek, L., Kayed, R., Glabe, C. G., Yang, A., Gallagher, M., and Ashe, K. H. (2006) A specific amyloid-β protein assembly in the brain impairs memory. *Nature*. **440**, 352–357

92. Shankar, G. M., Bloodgood, B. L., Townsend, M., Walsh, D. M., Selkoe, D. J., and Sabatini, B. L. (2007) Natural oligomers of the Alzheimer amyloid-β protein induce reversible synapse loss by modulating an NMDA-type glutamate receptor-dependent signaling pathway. *J. Neurosci.* **27**, 2866–2875

93. Cheng, I. H., Scearce-levie, K., Legleiter, J., Palop, J. J., Gerstein, H., Bien-ly, N., and Lesne, S. (2007) Accelerating Amyloid-β Fibrillization Reduces Oligomer Levels and

Functional Deficits in Alzheimer Disease Mouse Models *. *J. Biol. Chem.* **282**, 23818–23828

94. Bernstein, S. L., Dupuis, N. F., Lazo, N. D., Wyttenbach, T., Condron, M. M., Bitan, G., Teplow, D. B., Shea, J., Ruotolo, B. T., Robinson, C. V, and Bowers, M. T. (2009) Amyloid-β protein oligomerization and the importance of tetramers and dodecamers in the aetiology of Alzheimer ' s disease. *Nature Chemistry* **1**, 1–6

95. Lacor, P. N., Buniel, M. C., Chang, L., Fernandez, S. J., Gong, Y., Viola, K. L., Lambert, M. P., Velasco, P. T., Bigio, E. H., Finch, C. E., Krafft, G. A., and Klein, W. L. (2004) Synaptic Targeting by Alzheimer's-Related Amyloid-β Oligomers. *J. Neurosci*. **24**, 10191–10200

96. Chang, L., Bakhos, L., Wang, Z., Venton, D. L., and Klein, W. L. (2003) ALZHEIMER'S THERAPEUTICS : Anti-Amyloid Femtomole Immunodetection of Synthetic and Endogenous Amyloid-β Oligomers and Its Application to Alzheimer's Disease Drug Candidate Screening. *J. Mol. Neurosci*. **20**, 305–313

97. Gong, Y., Chang, L., Viola, K. L., Lacor, P. N., Lambert, M. P., Finch, C. E., Krafft, G. A., and Klein, W. L. (2003) Alzheimer's disease-affected brain : Presence of oligomeric Aβ ligands (ADDLs) suggests a molecular basis for reversible memory loss. *Proc. Natl. Acad. Sci. U. S. A.* **100**, 10417–10422

98. Laurén, J., Gimbel, D. A., Nygaard, H. B., Gilbert, J. W., and Strittmatter, S. M. (2009) Cellular prion protein mediates impairment of synaptic plasticity by amyloid-β oligomers. *Nature*. **457**, 1128–1132

99. Barghorn, S., Nimmrich, V., Striebinger, A., Krantz, C., Keller, P., Janson, B., Bahr, M., Schmidt, M., Bitner, R. S., Harlan, J., Barlow, E., Ebert, U., and Hillen, H. (2005) Globular amyloid β-peptide$_{1-42}$ oligomer - a homogenous and stable neuropathological protein in Alzheimer ' s disease. *J. Neurochem.* **95**, 834-847

100. Gellermann, G. P., Byrnes, H., Striebinger, A., Ullrich, K., Mueller, R., Hillen, H., and Barghorn, S. (2008) Aβ -globulomers are formed independently of the fibril pathway.

Neurobiol. Dis. **30**, 212–220

101. Nimmrich, V., Grimm, C., Draguhn, A., Barghorn, S., Lehmann, A., Schoemaker, H., Hillen, H., Gross, G., Ebert, U., and Bruehl, C. (2008) Amyloid β Oligomers ($A\beta_{1-42}$ Globulomer) Suppress Spontaneous Synaptic Activity by Inhibition of P/Q-Type Calcium Currents. *J. Neurosci*. **28**, 788–797

102. Lashuel, H. A., Hartley, D. M., Petre, B. M., Wall, J. S., Simon, M. N., Walz, T., and Lansbury, P. T. (2003) Mixtures of wild-type and a pathogenic (E22G) form of Aβ40 in vitro accumulate protofibrils, including amyloid pores. *J. Mol. Biol.* **332**, 795–808

103. Kayed, R., Pensalfini, A., Margol, L., Sokolov, Y., Sarsoza, F., Head, E., Hall, J., and Glabe, C. (2009) Annular protofibrils area structurally and functionally distinct type of amyloid oligomer. *J. Biol. Chem.* **284**, 4230–4237

104. Glabe, C. G. (2008) Structural classification of toxic amyloid oligomers. *J. Biol. Chem.* **283**, 29639–29643

105. Kayed, R., Head, E., Thompson, J. L., McIntire, T. M., Milton, S. C., Cotman, C. W., and Glabel, C. G. (2003) Common structure of soluble amyloid oligomers implies common mechanism of pathogenesis. *Science.* **300**, 486–489

106. Kayed, R., Head, E., Sarsoza, F., Saing, T., Cotman, C. W., Necula, M., Margol, L., Wu, J., Breydo, L., Thompson, J. L., Rasool, S., Gurlo, T., Butler, P., and Glabe, C. G. (2007) Fibril specific, conformation dependent antibodies recognize a generic epitope common to amyloid fibrils and fibrillar oligomers that is absent in prefibrillar oligomers. *Mol. Neurodegener.* **2**, 1–11

107. Chimon, S., Shaibat, M. A., Jones, C. R., Calero, D. C., Aizezi, B., and Ishii, Y. (2007) Evidence of fibril-like β-sheet structures in a neurotoxic amyloid intermediate of Alzheimer's β-amyloid. *Nat. Struct. Mol. Biol.* **14**, 1157–1164

108. Laganowsky, A., Liu, C., Sawaya, M. R., Whitelegge, J. P., Park, J., Zhao, M., Pensalfini, A., Soriaga, A. B., Landau, M., Teng, P. K., Cascio, D., Glabe, C., and Eisenberg, D. (2012) Atomic view of a toxic amyloid small oligomer. *Science.* **335**, 1228–1231

109. Kayed, R., and Lasagna-reeves, C. A. (2013) Molecular Mechanisms of Amyloid Oligomers Toxicity. *J. Alzheimer's Dis.* **33**, S67-78

110. Rönicke, R., Mikhaylova, M., Rönicke, S., Meinhardt, J., Schröder, U. H., Fändrich, M., Reiser, G., Kreutz, M. R., and Reymann, K. G. (2011) Early neuronal dysfunction by amyloid-β oligomers depends on activation of NR2B-containing NMDA receptors. *Neurobiol. Aging.* **32**, 2219–2228

111. Yamamoto, N., Matsubara, E., Maeda, S., Minagawa, H., Takashima, A., Michikawa, M., and Yanagisawa, K. (2007) A Ganglioside-induced Toxic Soluble Aβ Assembly ITS ENHANCED FORMATION FROM Aβ BEARING THE ARCTIC MUTATION *. *J. Biol. Chem.* **282**, 2646–2655

112. Magdesian, M. H., Carvalho, M. M. V. F., Mendes, F. A., Saraiva, L. M., Juliano, M. A., and Juliano, L. (2008) Amyloid-β Binds to the Extracellular Cysteine-rich Domain of Frizzled and Inhibits Wnt /β Catenin Signaling *. *J. Biol. Chem.* **283**, 9359–9368

113. Zhao, W., and Alkon, D. L. (2001) Role of insulin and insulin receptor in learning and memory. *Mol. Cell. Endocrinol*. **177**, 125–134

114. Prusiner, S. B. (1998) Prions. *Proc. Natl. Acad. Sci.* **95**, 13363–13383

115. Jarosz-Griffiths, H. H., Noble, E., Rushworth, J. V., and Hooper, N. M. (2016) Amyloid-β receptors: The good, the bad, and the prion protein. *J. Biol. Chem.* **291**, 3174–3183

116. Cissé, M., Sanchez, P. E., Kim, D. H., Ho, K., Yu, G. Q., and Mucke, L. (2011) Ablation of cellular prion protein does not ameliorate abnormal neural network activity or cognitive dysfunction in the J20 line of human amyloid precursor protein transgenic mice. *J. Neurosci.* **31**, 10427–10431

117. Nicoll, A. J., Panico, S., Freir, D. B., Wright, D., Terry, C., Risse, E., Herron, C. E., Malley, T. O., Wadsworth, J. D. F., Farrow, M. A., Walsh, D. M., Saibil, H. R., and Collinge, J. (2013) Amyloid-β nanotubes are associated with prion protein-dependent synaptotoxicity. *Nat. Commun.* **4**, 1-9

118. Lashuel, H. A., Hartley, D., Petre, B. M., Walz, T., and Lansbury, P. T. (2002) Neurodegenerative disease: Amyloid pores from pathogenic mutations. *Nature*. **418**, 291-292

119. Arispe, N., Rojas, E., and Pollard, H. B. (1993) Alzheimer disease amyloid β protein forms calcium channels in bilayer membranes: Blockade by tromethamine and aluminium. *Proc. Natl. Acad. Sci. U. S. A.* **90**, 567–571

120. Yatin, S. M., Aksenova, M., Aksenov, M., Markesbery, W. R., Aulick, T., and Allan Butterfield, D. (1998) Temporal relations among amyloid β-peptide-induced free-radical oxidative stress, neuronal toxicity, and neuronal defensive responses. *J. Mol. Neurosci.* **11**, 183–197

121. Takashima, A., Noguchi, K., Sato, K., Hoshino, T., and Imahori, K. (1993) tau Protein kinase I is essential for amyloid β-protein-induced neurotoxicity. *Proc. Natl. Acad. Sci. U. S. A.* **90**, 7789–7793

122. Lasagna-Reeves, C. A., Glabe, C. G., and Kayed, R. (2011) Amyloid-β annular protofibrils evade fibrillar fate in Alzheimer disease brain. *J. Biol. Chem.* **286**, 22122–22130

123. Demuro, A., Mina, E., Kayed, R., Milton, S. C., Parker, I., and Glabe, C. G. (2005) Calcium dysregulation and membrane disruption as a ubiquitous neurotoxic mechanism of soluble amyloid oligomers. *J. Biol. Chem.* **280**, 17294–17300

124. Kayed, R., Sokolov, Y., Edmonds, B., McIntire, T. M., Milton, S. C., Hall, J. E., and Glabe, C. G. (2004) Permeabilization of lipid bilayers is a common conformation-dependent activity of soluble amyloid oligomers in protein misfolding diseases. *J. Biol. Chem.* **279**, 46363–46366

125. Mattson, M. P., Barger, S. W., Cheng, B., Lieberburg, I., Smith-Swintosky, V. L., and Rydel, R. E. (1993) β-Amyloid precursor protein metabolites and loss of neuronal Ca^{2+} homeostasis in Alzheimer's disease. *Trends Neurosci.* **16**, 409-414

126. Wang, H.-Y., Lee, D. H. S., D'Andrea, M. R., Peterson, P. A., Shank, R. P., and Reitz, A.

B. (2000) β-Amyloid$_{1–42}$ Binds to α7 Nicotinic Acetylcholine Receptor with High Affinity . *J. Biol. Chem.* **275**, 5626–5632

127. Bu, G., Cam, J., and Zerbinatti, C. (2006) LRP in amyloid-β production and metabolism. *Ann. N. Y. Acad. Sci.* **1086**, 35–53

128. Deane, R., Yan, S. Du, Submamaryan, R. K., LaRue, B., Jovanovic, S., Hogg, E., Welch, D., Manness, L., Lin, C., Yu, J., Zhu, H., Ghiso, J., Frangione, B., Stern, A., Schmidt, A. M., Armstrong, D. L., Arnold, B., Liliensiek, B., Nawroth, P., Hofman, F., Kindy, M., Stern, D., and Zlokovic, B. (2003) RAGE mediates amyloid-β peptide transport across the blood-brain barrier and accumulation in brain. *Nat. Med.* **9**, 907–913

129. Tseng, B. P., Green, K. N., Chan, J. L., Blurton-Jones, M., and LaFerla, F. M. (2008) Aβ inhibits the proteasome and enhances amyloid and tau accumulation. *Neurobiol. Aging*. **29**, 1607–1618

130. Chui, D. H., Dobo, E., Makifuchi, T., Akiyama, H., Kawakatsu, S., Petit, A., Checler, F., Araki, W., Takahashi, K., and Tabira, T. (2001) Apoptotic neurons in Alzheimer's disease frequently show intracellular Aβ42 labeling. *J. Alzheimer's Dis.* **3**, 231–239

131. Manczak, M., Anekonda, T. S., Henson, E., Park, B. S., Quinn, J., and Reddy, P. H. (2006) Mitochondria are a direct site of Aβ accumulation in Alzheimer's disease neurons: Implications for free radical generation and oxidative damage in disease progression. *Hum. Mol. Genet.* **15**, 1437–1449

132. Chafekar, S. M., Baas, F., and Scheper, W. (2008) Oligomer-specific Aβ toxicity in cell models is mediated by selective uptake. *Biochim. Biophys. Acta - Mol. Basis Dis.* **1782**, 523–531

Structural Classification of Amyloid-β Oligomers

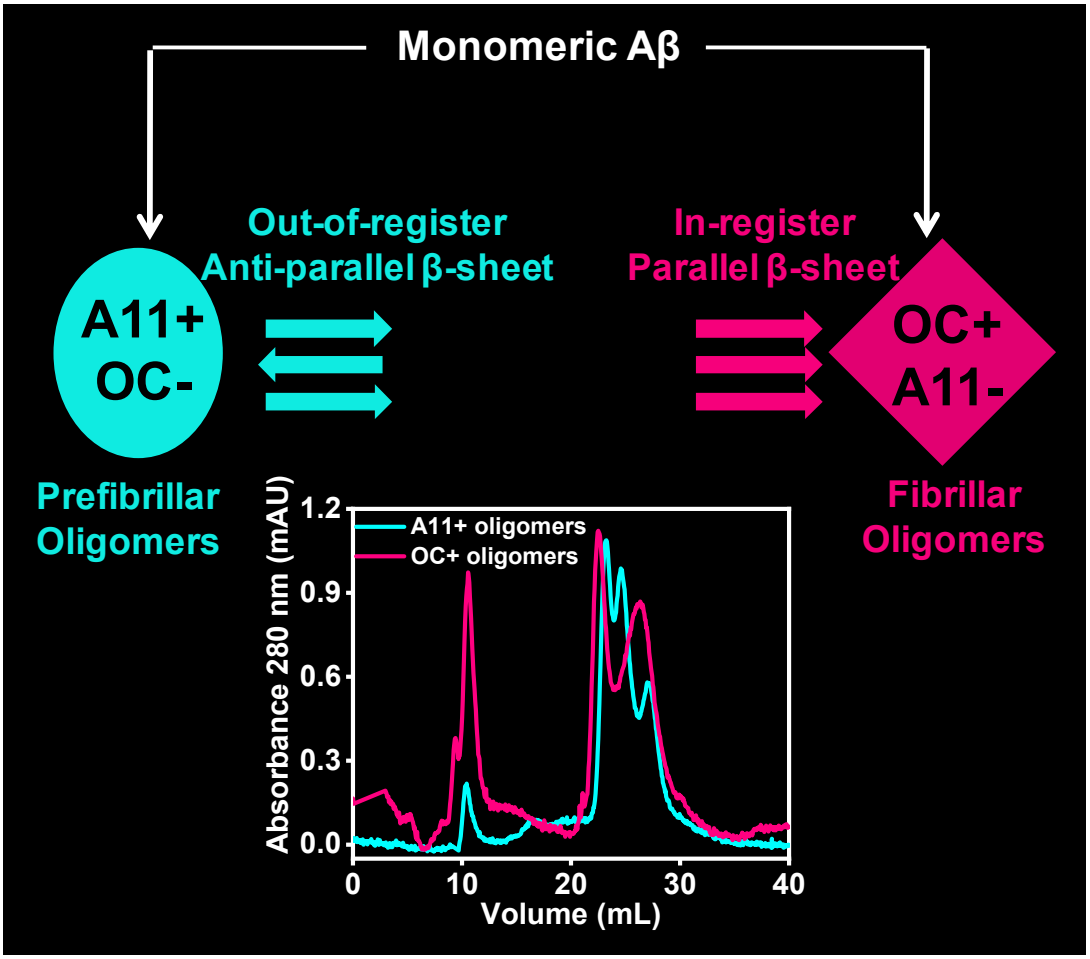

The work described in chapter 2 has been published in *ACS Chemical Neuroscience*.

Reference: Madhu, P., and Mukhopadhyay, S. *ACS Chem. Neurosci.* **2020**, 11, 86-98.

2.1 Introduction

Alzheimer's disease (AD) is an age-related devastating neurodegenerative brain disorder characterized by memory impairments and cognitive deficits (1). A pathological characteristic of AD is the accumulation of extracellular fibrillar deposits of amyloid-β (Aβ) peptide known as amyloid plaques (2). Cleavage of amyloid precursor protein (APP) by β- and γ-secretases produces Aβ peptides of 39-43 in length among which Aβ40 is the most abundant (3). The familial AD (FAD) mutations correlate well with the increased production of Aβ42 in senile plaques (4). Persuasive evidence suggests that AD pathogenesis is characterized by the elevated concentration of soluble Aβ42 oligomers rather than the insoluble amyloid plaque load, and therefore, soluble Aβ oligomers are considered to be the primary toxic species (5–8). Soluble Aβ oligomers block hippocampal long-term potentiation and cause synaptic dysfunction by interfering with the convoluted system of receptors and downstream signaling pathways (8). The cytotoxicity of Aβ42 does not depend only on the aggregate morphotype but also depends on the cell morphotype. The Aβ42 aggregates in the neurons are more toxic than the glial cells (9). An array of soluble Aβ aggregates exists such as prefibrillar oligomers, dodecamers, globulomers, Aβ-derived diffusible ligands (ADDLs), amylospheroids, protofibrils, and so forth. The oligomers vary in size, morphology, toxicity, and methods of preparation that raises the question of structural determinants among different oligomer preparations. The varied pathogenesis exhibited by the oligomer distributions of FAD mutants is proposed to arise due to distinct oligomer structures (10).

In order to characterize the structural attributes of various soluble Aβ oligomers, conformation-dependent antibodies have been generated. These conformation-specific antibodies recognize the generic conformational epitopes present in distinct aggregation states. Two conformation-specific antibodies, the anti-amyloid fibril antibody (OC), and anti-amyloid oligomer antibody (A11) that recognize mutually exclusive structural epitopes of fibrillar and prefibrillar oligomers, respectively, have been reported (11–14). These antibodies identify distinct structural epitopes on a spectrum of amyloid-forming proteins in addition to Aβ (15–17). OC antibody has been shown to identify the in-register parallel β-sheet packing in fibrillar oligomers, whereas, A11 antibody detects out-of-register anti-parallel β-sheet structure arrangements in prefibrillar oligomers (18, 19). These two conformationally distinct Aβ oligomers have been found in the

brains of transgenic mice and AD patients and are also generated *in vitro* (12). In this work, we have prepared the conformationally distinct, prefibrillar (A11-positive) and fibrillar Aβ oligomers (OC-positive), and characterized the Aβ oligomers using a wide array of biophysical and biochemical techniques.

2.2 Experimental section

2.2.1 Materials

Sodium phosphate dibasic, Sodium hydroxide, Sodium chloride, and 1,1,1,3,3,3-Hexafluoro-2-propanol (HFIP) were procured from Sigma (St. Louis, MO, USA). Bovine serum albumin, and Potassium chloride were purchased from HiMedia. A11, anti-amyloid oligomer antibody, OC, anti-amyloid fibril antibody, HRP-conjugated goat-anti-rabbit antibody, and Nitrocellulose membrane, 0.45 μ, were purchased from Merck. Antibody 6E10 (anti-β-amyloid (1-16)) was purchased from Biolegend. HRP-conjugated rabbit-anti-mouse antibody and Enhanced chemiluminescence (ECL) kit from Thermofisher scientific. Beta-Amyloid (42) was procured from Anaspec (USA).

2.2.2 Preparation of monomeric Aβ42 (mAβ)

mAβ was prepared as described previously (20). Briefly, lyophilized Aβ42 powder was weighed and dissolved in 100 mM NaOH to prepare a stock of 2 mM Aβ. The sample was sonicated three times using bath sonicator with an interval of 15 minutes (frequency 37 kHz, power 100 %, 1 minute, pulse mode). Then the sample was diluted in phosphate-buffered saline (PBS), pH 7.4, 0.02 % NaN3 to a concentration of 45 μM followed by further bath sonication for a minute. The sample was aliquoted, snap-frozen in liquid N2, and stored at -80 0C. At the time of experiments, samples were removed from the freezer and incubated on ice. Dynamic light scattering measurements confirmed that this preparation yielded mAβ42 (Figure 2c), and the hydrodynamic radius was ~ 1 nm that is consistent with monomeric Aβ.

2.2.3 Preparation of conformationally distinct Aβ42 oligomers

The A11-positive Aβ42 oligomers were prepared as described previously with slight modifications (20, 21). The mAβ as mentioned in the above section (before keeping at -80 ^{0}C)

was incubated at 25 ^{0}C. The A11-positive oligomers are found to be formed after 3 days and are stable up to 5 days. The OC-positive Aβ oligomers were prepared from the peptide film as described previously (22). The peptide film was prepared by dissolving Aβ peptide in 1,1,1,3,3,3-Hexafluoro-2-propanol (HFIP) to a concentration of 1 mg/mL and left to stand for 2 h followed by solvent evaporation on a SCANVAC (Bionics Asia). The peptide film was dissolved in 50 mM NaOH to a concentration of 1 mg/mL. The sample was sonicated three times and diluted in PBS buffer, pH 7.4, 0.02 % NaN3 to a concentration of 45 μM. The solution was centrifuged at 22,000 X g for 30 minutes to discard any fibrillar material and discarded the pelleted fraction (5 % of the volume).The supernatant was incubated for 3 days at 25 ^{0}C. FAM-labeled OC- and A11-positive Aβ oligomers were prepared by mixing 2 % of N-terminal FAM-labeled Aβ42 peptide with unlabeled Aβ peptide.

2.2.4 Dot-blot assay

The 0th day aliquots and aliquots after 3 days from both oligomeric preparations were spotted (2 μL) on nitrocellulose membrane. The blots were blocked in 3 % BSA in PBST (0.05 % Tween-20) for 1 h at room temperature. The membranes were probed with primary antibodies overnight at 4 ^{0}C (A11, 1:500; OC, 1:1000 and 6E10, 1:1000). The blots were washed six times with PBST and incubated with appropriate HRP-conjugated secondary antibodies for 1 h at room temperature. Then the blots were washed thrice and visualized using ECL kit.

2.2.5 Dynamic light scattering

The sizes of Aβ oligomers were measured using a Malvern Zetasizer Nano-ZS90 instrument. Samples were excited using a He-Ne laser (632 nm). All the buffers were filtered through 0.02 μ filters (Anatop 10 filter; Whatman).

2.2.7 AFM imaging

AFM images of Aβ oligomers were acquired using Innova atomic force microscopy (Bruker). Ten μL of the sample was deposited on freshly cleaved, and milli-Q water washed muscovite mica (Grade V-4 mica from SPI, PA). The sample was incubated on mica for 5 minutes, followed by five times washing with 100 μL of milli-Q water. The sample was dried under a

stream of nitrogen gas. Data was acquired using NanoDrive (v8.03) software. The images were processed and analyzed by using WSxM 8.0.51 (23).

2.2.8 Size-exclusion chromatography (SEC)

The samples of volume 500 µL were injected with a 500 µL loop on Superdex-200 column (manually packed), having column volume 30 mL. The samples were eluted with a flow rate of 0.3 mL/min using AKTA Prime FPLC system (G.E., Healthcare), and the absorbance was recorded at 280 nm. The column was calibrated with a volume of 150 µL of protein mix that was prepared by mixing six standard globular proteins at a concentration of 1 mg/mL each protein. The void volume was measured using blue dextran at a concentration of 1 mg/mL, volume 150 µL. The partition coefficient (K_{av}) of each protein was calculated from its measured elution volume, and the calibration curve was constructed between K_{av} and the logarithm of molecular weight (log M).

$$K_{av} = (V_E - V_O) / (V_C - V_O) \quad \text{--- (1)}$$

where, V_E, V_O, and V_C are elution volume, void volume and column volume, respectively.

2.3. Results

2.3.1 Structural characterization of Aβ oligomers by conformation-dependent antibodies

We prepared both prefibrillar (A11-positive) and fibrillar (OC-positive) Aβ oligomers using synthetic Aβ42 peptide and characterized them by the dot-blot assay. The dot-blot assay showed that the 0^{th} day aliquots of both reactions reacted weakly with anti-amyloid oligomer (A11) and anti-amyloid fibrillar (OC) antibodies but strongly reacted with the anti-Aβ 6E10 antibody. This observation indicated that the reactions started with monomeric Aβ (mAβ) (Figure 2.1). After three days, the aliquots under A11-positive oligomer forming condition were recognized by A11 antibody but not by OC and 6E10 antibodies. Whereas OC-positive oligomer forming condition yielded strong reactivity with OC and 6E10 antibodies but not against A11 antibody. This confirmed that both A11- and OC-positive Aβ oligomers had little or no cross-reactivities.

(a)

DAEFRHDSGYEVHHQKLVFFAEDVGSNKGAIIGLMVGGVVIA

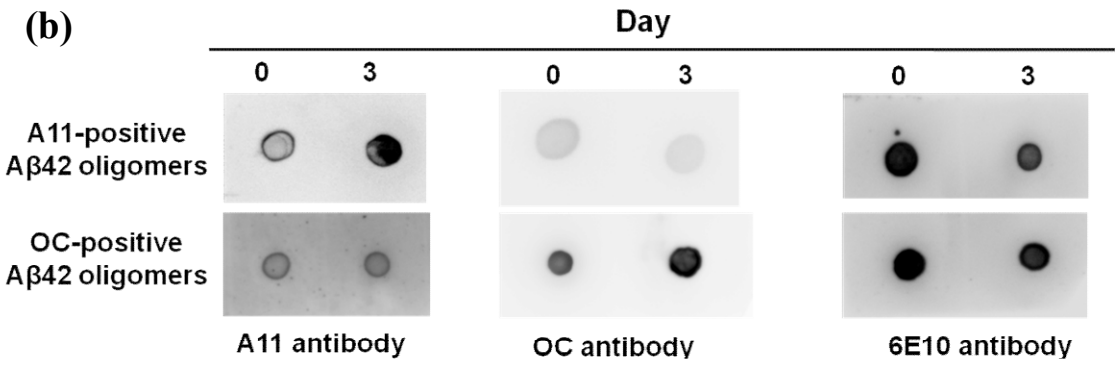

Figure 2.1: (a) The amino acid sequence of Aβ42. The negatively and positively charged amino acids are shown in red and blue, respectively. (b) Structural characterization of conformationally distinct Aβ oligomers by dot-blot assay. Samples from the 0^{th} day and after 3 days were spotted on nitrocellulose membrane from the respective oligomer preparations and dot-blotted with the respective antibodies.

2.3.2 Size estimation of conformationally distinct Aβ oligomers

We further characterized the structurally distinct Aβ oligomers on the basis of sizes by utilizing atomic force microscopy (AFM), dynamic light scattering (DLS), and size-exclusion chromatography (SEC). AFM imaging of Aβ oligomers revealed that both species appeared as spherical particles of similar sizes, in the range of 5-20 nm with no fibrillar aggregates (Figure 2.2a). Our dynamic light scattering measurements showed that the hydrodynamic diameter of mAβ as ~ 2 nm, which is in line with a previous report (24). The OC- and A11-positive oligomers exhibited hydrodynamic diameters of 50 nm and 40 nm, respectively (Figure 2.2b). The number % area under the peak for both OC- and A11-positive oligomers is ~ 99 %, which suggests that most of Aβ are in the aggregated state. Additionally, we characterized these oligomeric preparations using the size-exclusion chromatography (SEC). We calibrated the superdex G-200 column, volume 30 mL, using a mixture of six standard globular proteins (Figure 2.2c & 2.2d). Using the calibration curve, we estimated the different-sized Aβ oligomeric species (Figure 2.2e). Since oligomers might not be globular in shape, the actual sizes of the

oligomers might be different from the estimated sizes of the oligomeric species. These results corroborated our light scattering data and revealed the presence of a larger fraction of higher-order species in OC-positive Aβ oligomers compared to A11-positive Aβ oligomers.

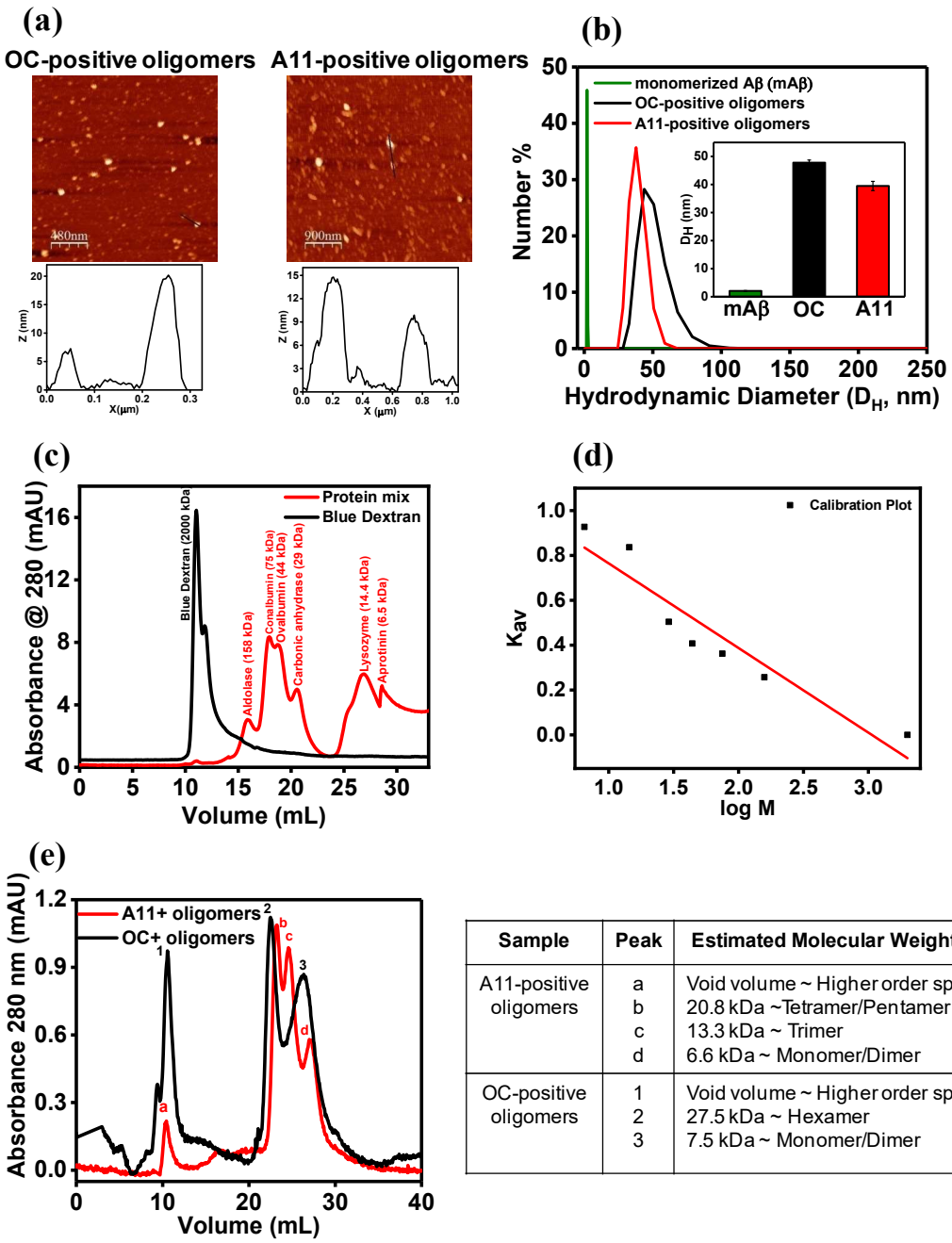

Sample	Peak	Estimated Molecular Weight (kDa)
A11-positive oligomers	a b c d	Void volume ~ Higher order species 20.8 kDa ~Tetramer/Pentamer 13.3 kDa ~ Trimer 6.6 kDa ~ Monomer/Dimer
OC-positive oligomers	1 2 3	Void volume ~ Higher order species 27.5 kDa ~ Hexamer 7.5 kDa ~ Monomer/Dimer

Figure 2.2: Size estimation of structurally distinct Aβ oligomers. (a) AFM images of OC- and A11-positive Aβ oligomers with their respective height profiles. (b) Size distribution by dynamic light scattering measurements of mAβ (olive), OC- (black) and A11-positive Aβ oligomers (red)

and the inset shows the bar plot of the hydrodynamic diameter of Aβ oligomers, (n = 3, the data is presented as mean ± S.D.). P*** < 0.0001 compared to the mAβ (One-Way ANOVA test). (c) SEC data of a mixture of six standard globular proteins (red) and blue dextran (black) (d) Calibration curve constructed from the SEC data of protein mix (adjusted $R^2 = 0.87$). (e) SEC data of OC- (black) and A11-positive Aβ oligomers (red) and the analysis of chromatograms.

2.4 Summary

In this study, we have prepared and characterized the two conformationally distinct Aβ oligomers using an array of biophysical and biochemical tools. Our study suggests that the two types, prefibrillar (A11-positive) and fibrillar (OC-positive) Aβ oligomers are structurally distinct and consist of the varied size distribution of oligomeric species. We further study the mechanism of toxicity caused by these Aβ oligomeric preparations in the forthcoming chapters.

2.5 References

1. Selkoe, D. J. (2002) Alzheimer's Disease Is a Synaptic Failure. *Science.* **298**, 789–791

2. Hardy, J., and Selkoe, D. J. (2002) The Amyloid Hypothesis of Alzheimer's Disease: Progress and Problems on the Road to Therapeutics. *Science.* **297**, 353–356

3. Wärmländer, S., Tiiman, A., Abelein, A., Luo, J., Jarvet, J., Söderberg, K. L., Danielsson, J., and Gräslund, A. (2013) Biophysical studies of the amyloid β-peptide: Interactions with metal ions and small molecules. *ChemBioChem*. **14**, 1692–1704

4. Younkin, S. G. (1998) The role of Aβ42 in Alzheimer's disease. *J. Physiol.* **92**, 289-292

5. Small, D. H., Mok, S. S., and Bornstein, J. C. (2001) Alzheimer's disease and Aβ toxicity: from top to bottom. *Nat. Rev. Neurosci.* **2**, 595–598

6. Lesné, S., Ming, T. K., Kotilinek, L., Kayed, R., Glabe, C. G., Yang, A., Gallagher, M., and Ashe, K. H. (2006) A specific amyloid-β protein assembly in the brain impairs memory. *Nature*. **440**, 352–357

7. Walsh, D. M., and Selkoe, D. J. (2007) Aβ oligomers - A decade of discovery. *J.*

Neurochem. **101**, 1172–1184

8. Haass, C., and Selkoe, D. J. (2007) Soluble protein oligomers in neurodegeneration: Lessons from the Alzheimer's amyloid β-peptide. *Nat. Rev. Mol. Cell Biol.* **8**, 101–112

9. Jonson, M., Nyström, S., Sandberg, A., Carlback, M., Michno, W., Hanrieder, J., Starkenberg, A., Nilsson, K. P. R., Thor, S., and Hammarström, P. (2018) Aggregated Aβ1-42 Is Selectively Toxic for Neurons, Whereas Glial Cells Produce Mature Fibrils with Low Toxicity in Drosophila. *Cell Chem. Biol.* **25**, 595-610.

10. Gessel, M. M., Bernstein, S., Kemper, M., Teplow, D. B., and Bowers, M. T. (2012) Familial Alzheimers disease mutations differentially alter amyloid β-protein oligomerization. *ACS Chem. Neurosci.* **3**, 909–918

11. Kayed, R., Head, E., Sarsoza, F., Saing, T., Cotman, C. W., Necula, M., Margol, L., Wu, J., Breydo, L., Thompson, J. L., Rasool, S., Gurlo, T., Butler, P., and Glabe, C. G. (2007) Fibril specific, conformation dependent antibodies recognize a generic epitope common to amyloid fibrils and fibrillar oligomers that is absent in prefibrillar oligomers. *Mol. Neurodegener.* **2**, 1–11

12. Glabe, C. G. (2008) Structural classification of toxic amyloid oligomers. *J. Biol. Chem.* **283**, 29639–29643

13. Wu, J. W., Breydo, L., Isas, J. M., Lee, J., Kuznetsov, Y. G., Langen, R., and Glabe, C. (2010) Fibrillar oligomers nucleate the oligomerization of monomeric amyloid β but do not seed fibril formation. *J. Biol. Chem.* **285**, 6071–6079

14. Breydo, L., Kurouski, D., Rasool, S., Milton, S., Wu, J. W., Uversky, V. N., Lednev, I. K., and Glabe, C. G. (2016) Structural differences between amyloid beta oligomers. *Biochem. Biophys. Res. Commun.* **477**, 700–705

15. Kayed, R., Head, E., Thompson, J. L., McIntire, T. M., Milton, S. C., Cotman, C. W., and Glabel, C. G. (2003) Common structure of soluble amyloid oligomers implies common mechanism of pathogenesis. *Science.* **300**, 486–489

16. Krishnan, R., Goodman, J. L., Mukhopadhyay, S., Pacheco, C. D., Lemke, E. A., Deniz, A. A., and Lindquist, S. (2012) Conserved features of intermediates in amyloid assembly determine their benign or toxic states. *Proc. Natl. Acad. Sci. U. S. A.* **109**, 11172–11177

17. Wang, X., Smith, D. R., Jones, J. W., and Chapman, M. R. (2007) In vitro polymerization of a functional Escherichia coli amyloid protein. *J. Biol. Chem.* **282**, 3713–3719

18. Laganowsky, A., Liu, C., Sawaya, M. R., Whitelegge, J. P., Park, J., Zhao, M., Pensalfini, A., Soriaga, A. B., Landau, M., Teng, P. K., Cascio, D., Glabe, C., and Eisenberg, D. (2012) Atomic view of a toxic amyloid small oligomer. *Science.* **335**, 1228–1231

19. Liu, C., Zhao, M., Jiang, L., Cheng, P., Park, J., Sawaya, M. R., and Pensal, A. (2012) Out-of-register β -sheets suggest a pathway to toxic amyloid aggregates. *Proc. Natl. Acad. Sci. U. S. A.* **109***, 20913-20918*

20. Necula, M., Kayed, R., Milton, S., and Glabe, C. G. (2007) Small molecule inhibitors of aggregation indicate that amyloid-β oligomerization and fibrillization pathways are independent and distinct. *J. Biol. Chem.* **282**, 10311–10324

21. Teplow, D. B. (2006) Preparation of Amyloid β-Protein for Structural and Functional Studies. *Methods Enzymol.* **413**, 20–33

22. Ladiwala, A. R. A., Litt, J., Kane, R. S., Aucoin, D. S., Smith, S. O., Ranjan, S., Davis, J., Van Nostrand, W. E., and Tessier, P. M. (2012) Conformational differences between two amyloid-β oligomers of similar size and dissimilar toxicity. *J. Biol. Chem.* **287**, 24765–24773

23. Horcas, I., Fernández, R., Gómez-Rodríguez, J. M., Colchero, J., Gómez-Herrero, J., and Baro, A. M. (2007) WSXM: A software for scanning probe microscopy and a tool for nanotechnology. *Rev. Sci. Instrum.* **78**, 013705

24. Nag, S., Sarkar, B., Bandyopadhyay, A., Sahoo, B., Sreenivasan, V. K. A., Kombrabail, M., Muralidharan, C., and Maiti, S. (2011) Nature of the amyloid-β monomer and the monomer-oligomer equilibrium. *J. Biol. Chem.* **286**, 13827–13833

Preferential Recruitment of Conformationally Distinct Amyloid-β Oligomers by the Human Prion Protein

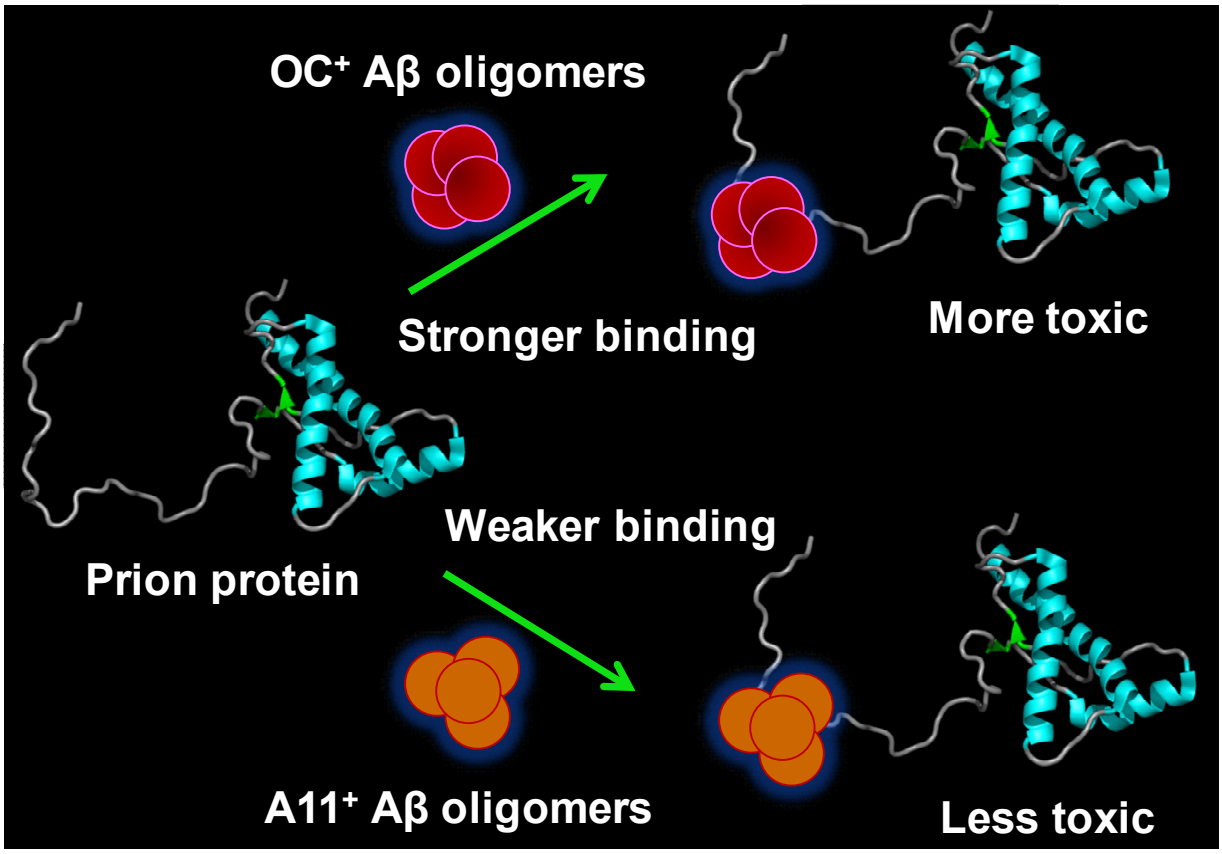

The work described in chapter 3 has been published in *ACS Chemical Neuroscience*.

Reference: Madhu, P., and Mukhopadhyay, S. *ACS Chem. Neurosci.* **2020,** 11, 86-98.

3.1 Introduction

Amyloid-β (Aβ) peptide, a small peptide that is found in the extracellular deposits of Alzheimer's disease (AD). AD is an age-related brain disorder that is characterized by memory impairments and cognitive deficits (1). A growing body of evidence suggests that the soluble Aβ oligomers inhibit long-term potentiation and are more potent neurotoxins than the insoluble amyloid plaques (2–5). A wide variety of soluble Aβ oligomers exists, such as protofibrils, prefibrillar oligomers, globulomers, amylospheroids, dodecamers, and so on, which vary in preparation methods, toxicity, size, and morphology. In order to study the structural aspects of oligomers, two conformation-specific antibodies have been produced which recognize two classes of oligomers that are present in the brain of AD patients, produced *in vitro*, and amyloid precursor protein (APP) transgenic mice (6–9). These two antibodies identify mutually exclusive structural epitopes independent of the amino acid sequence on a range of amyloid-forming proteins, including Aβ (10–12). The anti-amyloid fibril antibody (OC) detects fibrillar oligomers having an in-register parallel β-sheet structure, and the anti-amyloid oligomer antibody (A11) identifies prefibrillar oligomers having out-of-register anti-parallel β-sheet packing (13, 14). However, the mechanism by which these oligomers exert their toxic effects is not clearly understood.

A body of evidence indicates that the interaction of a variety of cell-surface receptors with Aβ oligomers can trigger a downstream signaling cascade that leads to cellular toxicity. These studies suggested that the prion protein (PrP) is one of the high-affinity binding receptors for Aβ oligomers, and this binding event inhibits long-term potentiation (15–19). Human PrP is a membrane-anchored protein that undergoes misfolding into the scrapie prion, which is a disease-related amyloid-forming isoform (20). The conversion of PrP to the scrapie prion can be catalyzed by the RNA molecules that bind to the N-terminal region of PrP (21). The binding of Aβ oligomers to PrP results in dendritic spine loss and alters synaptic function by the activation of Fyn kinase which further phosphorylates the GluN2B subunit of N-methyl-D-aspartate receptors (NMDARs) and also leads to tau phosphorylation (22, 23). The other studies have indicated that cognitive deficit induced by Aβ oligomers is independent of PrP (24–27). Distinct Aβ oligomeric species can potentially have different roles in mediating cellular toxicity. Therefore, it is important to study the interaction of PrP with conformationally distinct Aβ oligomers that are of interest to understand the molecular basis of cellular toxicity.

In this work, we aimed at investigating the heterotypic assembly of conformationally distinct, prefibrillar (A11-positive) and fibrillar Aβ42 oligomers (OC-positive) with human PrP. Using site-specific fluorescence polarization studies, we first show that the intrinsically disordered N-terminal segment of PrP forms critical electrostatic interactions with Aβ42 oligomers (Figure 3.1). Our studies revealed that PrP interacts more strongly with OC-positive Aβ42 oligomers in comparison to A11-positive oligomers, and this interaction leads to the increase in cellular toxicity. Our results support the notion that the binding of OC-positive Aβ42 oligomers to PrP is the potentially druggable target for AD treatment.

(a)

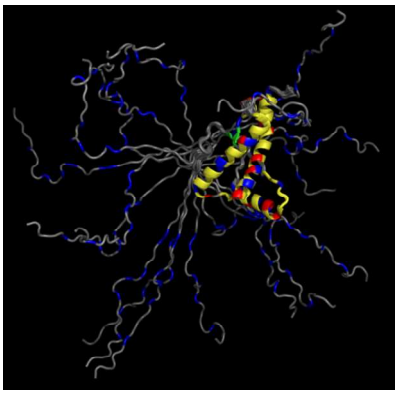

(b)

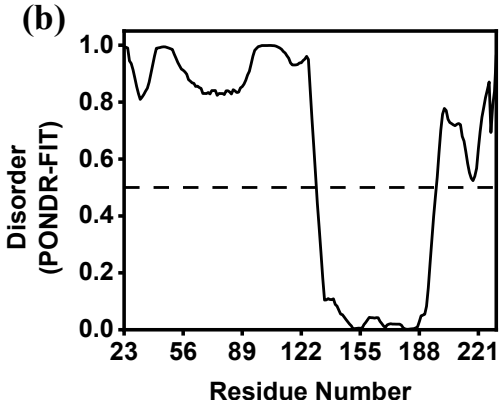

(c)

KKRPKPGGWN TGGSRYPGQG SPGGNRYPPQ GGGGWGQPHG GGWGQPHGGG
WGQPHGGGWG QPHGGGWGQG GGTHSQWNKP SKPKTNMKHM AGAAAAGAVV
GGLGGYMLGS AMSRPIIHFG SDYEDRYYRE NMHRYPNQVY YRPMDEYSNQ
NNFVHDCVNI TIKQHTVTTT TKGENFTETD VKMMERVVEQ MCITQYERES
QAYYQRGSS

(d)

DAEFRHDSGYEVHHQKLVFFAEDVGSNKGAIIGLMVGGVVIA

Figure 3.1: (a) The overlay of all twenty models that are deduced from the NMR structure of human PrP (90-231) (PDB ID: 2LSB) generated using PyMol (Version 1.8, Schrödinger, LLC, New York, NY). The positively and negatively charged amino acids are shown in blue and red, respectively. (b) PONDR plot determining the disorder/order in PrP (23-231) sequence (generated from http://www.pondr.com/) and plotted using origin. (c) The amino acid sequence of human PrP (23-231). The residues chosen for single-Cys mutations are shown as underscored. (d) The amino acid sequence of Aβ42.

3.2 Experimental section

3.2.1 Materials

Sodium phosphate monobasic, Sodium phosphate dibasic, L-Glutathione reduced, and 2-Mercaptoethanol were procured from Sigma (St. Louis, MO, USA). Tris base was purchased from HiMedia. Guanidinium hydrochloride and Urea were procured from Amresco. Isopropyl-β-thiogalactopyranoside (IPTG) and antibiotics (Ampicillin, Kanamycin,and Chloramphenicol) were obtained from Gold Biocom (USA). IAEDANS(5-((((2-Iodoacetyl)amino)ethyl)amino)Napthalene-1-Sulphonic acid) and Fluorescein-5-Maleimide from Invitrogen. Beta-Amyloid (42) and FAM-labeled, Beta-Amyloid (1-42) were procured from Anaspec (USA). Ni-NTA resin was purchased from Qiagen, Glutathione beads were obtained from Sigma and PD-10 and G-200 obtained from GE Healthcare Life Sciences (USA).

3.2.2 Mutagenesis, expression, purification, and labeling

His-tagged recombinant human prion protein (23-231) cloned in the pRSET-B plasmid was transformed into E. coli strain BL21(DE3) pLysS. Human prion protein (90-231) cloned in pQE-30 was expressed in SG13009[pREP4]. Single cysteine mutants of PrP (23-231) (W31C, W99C, A120C, and S230C) were created by site-directed mutagenesis. The N-terminal truncated construct PrP (112-231) was created by using the two primers flanking the PrP (112-231) with Nhe1 and EcoR1 restriction sites and cloned the PCR fragment into pRSET-B. Single cysteine mutant, A120C of truncated PrP (112-231) was also created using site-directed mutagenesis. The glutathione-S-transferase (GST)-tagged PrP (23-231) was constructed by using the two primers flanking PrP having N-terminal his-tag with EcoR1 and XhoI restriction sites that enabled us to clone the PCR product into pGEX-4T3.The primers sequences used for mutagenesis are given in Table 3.1 and verified by sequencing. Wild-type and variants of PrP were overexpressed by inducing with 1 mM Isopropyl-beta-D-thiogalactopyranoside (IPTG). Cell pellet of wild-type PrP was lysed by sonication in lysis buffer containing 6 M GdmCl, 10 mM Tris, 100 mM sodium phosphate and 10 mM reduced glutathione buffer pH 8.0. The lysate was centrifugedand the supernatant was loaded on Ni-NTA resin. Protein was purified on Ni-NTA resin via stepwise oxidation followed by elution under the native condition in 10 mM Tris, 100 mM sodium

phosphate, 500 mM imidazole pH 5.8 as described previously (28, 29) and refolded on PD-10 column in 5 mM phosphate buffer pH 6.5.

Table 3.1: **Primers used for site-directed mutagenesis**

Constructs	Primer	Sequence (5' to 3')
W31C PrP	Forward	GAAGCCTGGAGGATGTAACACTGGG
	Reverse	CCCAGTGTTACATCCTCCAGGCTTC
W99C PrP	Forward	CCCACAGTCAGTGTAACAAGCCGAG
	Reverse	CTCGGCTTGTTACACTGACTGTGGG
A120C PrP	Forward	GCAGCAGCTGGGTGTGTGGTGGGGGGC
	Reverse	GCCCCCCACCACACACCCAGCTGCTGC
S230C PrP	Forward	CCAGAGAGGATGCTCCTGAGAATTCG
	Reverse	CGAATTCTC AGGAGCATCCTCTCTGG
PrP (112-231)	Forward	AAAAGCTAGCATGGCTGGTGCTGCAGCAGC
	Reverse	GCTTCGAATTCTCAGGACGATCCTC
GST-PrP (23-231)	Forward	CCCGAATTCAATGCGGGGTTCTCATCATC
	Reverse	GGGCTCGAGTCAGGACGATCCTCTCTGG

Single cysteine PrP mutants, PrP (90-231), A120C PrP (112-231), and GST-tagged PrP were purified under denaturing conditions (using 8 M urea) on Ni-NTA column as described previously (30). The W99C PrP mutant was prone to form disulfide cross-linked dimer and therefore was passed through size exclusion chromatography, superdex-200 (column volume 120 mL) under denaturing condition after elution from Ni-NTA column to remove higher order species. For labeling cysteine mutants with IAEDANS, a 200 mM stock of dye was prepared in DMSO and added to the protein in 10 equivalents. The labeling reaction was carried out at pH 8 under denaturing conditions for 1 hr. A ten-fold molar excess of dye was further added to the reaction and was incubated for an hour. PD-10 column was used for removal of the free dye and refolding of protein in 5 mM sodium phosphate pH 6.5 buffer. The Cys-99 mutant of PrP was labeled with fluorescein-5-maleimide by preparing a 20 mM stock of dye in DMSO. Protein was

labeled with fluorescein-5-maleimide at pH 7.0 under denaturing conditions in a similar way as of IAEDANS. The protein was subjected to PD-10 column for free dye removal and refolding of protein.

3.2.3 Preparation of amyloid-derived diffusible ligands (ADDLs)

ADDLs are small diffusible oligomers, which have been shown to inhibit long-term potentiation (LTP) by binding to the PrP^C (15). The ADDLs were prepared as described previously (6, 31). Briefly, Aβ peptide film was prepared using HFIP, and the film was dissolved in anhydrous DMSO at 5 mM Aβ concentration. Diluted the sample into cold phenol red-free Ham's F-12 medium without L-glutamine (Caisson Labs) at 80 μM concentration and the solution was incubated at 4 ^{0}C for 24 h.

3.2.4 Preparation of Aβ fibrils

The A11-positive Aβ oligomers formed after 5 days of reaction were diluted to 10 μM in 5 mM sodium phosphate pH 6.5 buffer and incubated at 25 ^{0}C for further 5 days.

3.2.5 AFM imaging

AFM images of Aβ oligomers in the presence of PrP were acquired using Innova atomic force microscopy (Bruker). Twenty μL of sample was added on freshly cleaved, and filtered-water (0.2 μ filter) washed mica (Grade V-4 mica from SPI, PA). Incubated the sample on mica for 10 minutes followed by washing with 100 μL of filtered water. Dried the sample using a gentle stream of nitrogen gas and acquired the images using NanoDrive (v8.03) software. The images were processed using WSxM 8.0 (32).

3.2.6 CD experiments

The CD spectra of 5 μM protein were recorded on an Applied Photophysics Chirascan CD spectrophotometer using a 2 mm path length quartz cell in 5 mM sodium phosphate pH 6.5. The spectra were blank subtracted and smoothened using Pro data software. The spectra were plotted using Origin 8.5 software.

3.2.7 Steady-state fluorescence

Steady-state fluorescence experiments were carried out on a Fluormax-4 (Horiba Jobin Yvon, NJ). All the experiments were carried out in 5 mM sodium phosphate buffer, pH 6.5. For AEDANS fluorescence experiments, the PrP concentration was 1μM. The residue-specific interaction, electrostatic interaction, and FRET experiments were performed in 1:2 ratio of PrP:Aβ. AEDANS fluorescence was monitored using 340 nm excitation wavelength,and steady-state fluorescence anisotropy was measured at 495 nm. The steady-state fluorescence anisotropy is given by the following relationship:

$$r_{ss} = (I_{\parallel} - I_{\perp}G) / (I_{\parallel} + 2I_{\perp}G) \quad \text{--- (1)}$$

Where, $I_{\parallel}$ and $I_{\perp}$are the parallel and perpendicular fluorescence intensities respectively, with respect to the excitation polarizer. The perpendicular components were always corrected using a G-factor. Tryptophan fluorescence anisotropy was measured at 345 nm by using a 295-nm excitation wavelength. For tryptophan fluorescence, PrP (90-231) concentration was 5μM and varied the concentration of Aβ oligomers.

For FRET measurements, 2 μM of FAM-labeled Aβ oligomers (acceptor) were added into 1 μMAEDANS labeled PrP (donor), and the samples were excited at 340 nm. Spectra were recorded in the range of 440-600 nm and corrected with respect to the direct excitation of FAM-labeled Aβ oligomers with unlabeled PrP at 340 nm. The FRET efficiency was calculated using the following relationship (33):

$$E = 1\text{-}F_{DA}/F_D \quad \text{--- (2)}$$

Quenching experiment was performed using 100 nM of fluorescein-5-maleimide labeled at position 99 of PrP with the varied concentration of Aβ oligomers,and the fluorescence was monitored at 520 nm using 485 nm excitation wavelength. The fluorescence quenching was calculated as:

$$\Delta F = (F_0\text{-}F) \quad \text{--- (3)}$$

Where F_0 is the fluorescence intensity in the absence of Aβ oligomers and F is the measured fluorescence intensity in the presence of Aβ oligomers. The extent of quenching is the ratio of $\Delta F/F_0$ that is related to the amount of bound PrP. The ratio of $\Delta F/F_0$ was plotted against the Aβ concentration to obtain the binding isotherms. Since the experiments were setup with the PrP concentration in nM, which is the range of the dissociation constant, K_d, the binding isotherms were fitted by a quadratic equationusing Origin 8.5 software. We assumed a bimolecular interaction (1:1 model) and estimated the K_d with respect to the monomer equivalents as described previously (34, 35). The binding relationship is given as follows:

$$P + A\beta \longrightarrow P\text{-}A\beta \quad \text{--- (4)}$$

$$K_d = [P]_{free}\,[A\beta]_{free} / [P\text{-}A\beta] \quad \text{--- (5)}$$

$$[P]_{free} = [P] - [P\text{-}A\beta] \quad \text{--- (6)}$$

$$[A\beta]_{free} = [A\beta] - [P\text{-}A\beta] \quad \text{--- (7)}$$

$$[P\text{-}A\beta] = (\Delta F/F_0)\,[P] \quad \text{--- (8)}$$

$$\Delta F/F_0 = 0.5\,[1 + [A\beta]/[P] + K_d/[P] - ((1 + [A\beta]/[P] + K_d/[P])^2 - 4[A\beta]/[P])^{1/2}] \quad \text{--- (9)}$$

where $[P]_{free}$ is the free concentration of PrP, $[A\beta]_{free}$ is the free concentration of Aβ, [P-Aβ] is the bound PrP concentration, [Aβ] is the total concentration of Aβ oligomers with respect to monomer, [P] is the total PrP concentration (100 nM), and K_d is the dissociation constant.

For the ThT fluorescence experiment, the samples were mixed with 10 μM of ThT and incubated at room temperature. The concentrations of Aβ and PrP were 10 μM and 5 μM, respectively. The samples were excited at 440 nm, and the spectra were recorded in the range of 460-560 nm.

3.2.8 Stopped-flow fluorescence measurements

The stopped-flow fluorescence kinetic data were acquired on Chirascan spectrometer (Applied Photophysics, UK) connected to stopped-flow apparatus (SF.3; Applied Photophysics) as reported previously (36). Fluorescein-5-maleimide labeled at position 99 of PrP was rapidly mixed with Aβ oligomers in 1:10 ratio. The final concentration of PrP and Aβ oligomers were

100 nM and 200 nM respectively. The dead-time of mixing was ~ 5 ms. Samples were excited at 485 nm and fluorescence was recorded by using 495 nm long-pass filter. Fluorescein-5-maleimide labeled PrP was mixed with 5 mM sodium phosphate buffer, pH 6.5 to obtain the baseline signal. The kinetic traces were acquired for 10 s with 1,000 data points and averaged over multiple datasets. Data were fit biexponentially in Origin.

3.2.9 Size-exclusion chromatography (SEC)

Samples of PrP (8 μM) with Aβ oligomers in 1:4 ratio with a volume of 500 μL were incubated for 4 h before injecting onto the column. Samples were injected with a 500 μL loop on Superdex-200 column (manually packed, column volume 30 mL) and eluted with a flow rate of 0.3 mL/min.

3.2.10 Pull-down assay

Refolded GST-tagged PrP and the cell lysate of empty vector overexpressing GST were mixed with Aβ oligomers in binding buffer (5 mM sodium phosphate pH 8.0, 0.1 % tween-20)and rotated for 4 h at 4 ^{0}C. Ten μL of glutathione agarose beads were added onto the samples and rotated the samples for another 4 h at 4 ^{0}C. The tubes were spun at 1000 X g for 1 min. The supernatant was discarded. Beads were washed twice with 0.5 mL of binding buffer and resuspended in 20 μL of 2X loading buffer. Aβ oligomers were also mixed with 2X loading buffer. The samples were boiled at 95 0C and loaded the samples on NuPAGE 4-12 % Bis-Tris gel and analyzed using silver-staining.

3.2.11 Cytotoxicity assays

HeLa cells were maintained in Dulbecco's modified Eagle's medium supplemented with 10% FBS, penicillin/streptomycin and nonessential amino acids at 37 °C in 5% CO_2 as described previously (30). For cytotoxicity assay, cells were plated in a 96-well plate at a seeding density of 10,000 cells in 100 μL of media per well. After 1 day, cells were treated with 0.5 μM of PrP, 1 μM of Aβ oligomers, with and without PrP and their respective buffers as control. Cells were incubated for 24 h at 37 °C followed by addition of 3-(4,5-dimethylthiazol-2-yl)-2,5-diphenyl tetrazolium bromide (MTT) to a concentration of 0.5 mg/mL in each well. Cells were further incubated for 4 h at 37 °C and the insoluble formazan was solubilized in 200 μL of dimethyl

sulfoxide. The solubilized formazan was quantified spectrophotometrically at 490 nm in Multiskan Go (Thermoscientific). The experiment was repeated three times in triplicate.

3.2.12 Statistical analysis

All the experiments were repeated three times and the data were shown as mean ± standard deviation from three independent measurements. The statistical analysis on the fluorescence anisotropy data of PrP with Aβ oligomers was performed by carrying out One-Way ANOVA test and reported the p-value. The fluorescence quenching data of PrP with Aβ oligomers were fitted using non-linear curve fitting and the adjusted R^2 was reported. We have performed the student's t-test on the cytotoxicity assay and reported the p-value. All the data analysis and data plotting were performed using Origin 9.6.

3.3 Results

3.3.1 Site-specific interaction of human PrP with conformationally distinct Aβ oligomers

In order to characterize the heterotypic assembly of Aβ42 oligomers and PrP in a site-specific manner, we incorporated single cysteines at various residue positions (31, 99, 120, and 230) encompassing the distinct regions of PrP involving the N-terminal region, the middle region, and

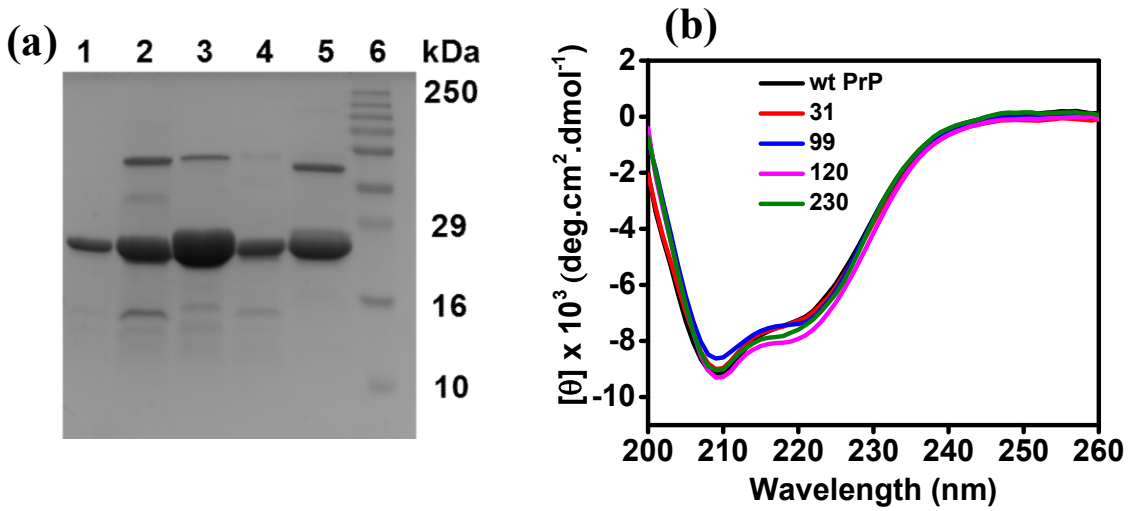

Figure 3.2: (a) 15 % SDS-PAGE of purified wt (lane 1), 31C (lane 2), 99C (lane 3), 120C (lane 4), 230C PrP (lane 5) and Marker (lane 6). (b) Far-UV CD spectra of wild-type and cysteine mutants of PrP in their native states.

the C-terminal end. All the single-cysteine mutants are in the disordered region of PrP which is indicated by the NMR structure and the PONDR plot (Figure 3.1a & 3.1b) (37, 38). The residue positions 31, 99, 120, and 230 were chosen based on the previous reports (Figure 3.1c) (30, 39). These single-cysteine mutants enabled us to covalently label the protein with an environment-sensitive thiol-reactive fluorescent dye, such as IAEDANS (5-((((2-Iodoacetyl)amino)ethyl)amino)Napthalene-1-Sulphonic acid). Our circular dichroism (CD) results showed that the labeling of single-cysteine mutants with IAEDANS did not perturb the native structure of PrP (Figure 3.2).

In order to gain region-specific information about the binding of Aβ oligomers to PrP, we monitored steady-state fluorescence anisotropy of AEDANS labeled PrP. Steady-state fluorescence anisotropy reports the rotational mobility around the residue position (33). Binding of two macromolecules would result in the increase in the anisotropy due to the enhanced rotational constraint at a given region of the protein containing the fluorophore. To trace the rise

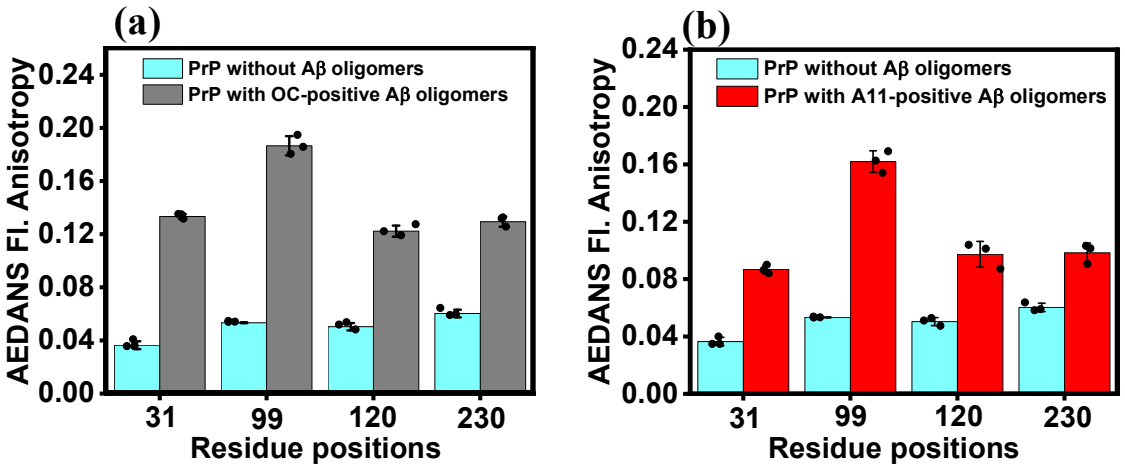

Figure 3.3: Site-specific binding of PrP to Aβ oligomers. Steady-state fluorescence anisotropy of 1 μM AEDANS labeled PrP without (cyan) and with 2 μM of (a) OC- (gray) and (b) A11-positive Aβ oligomers (red). The scatter plots represent the data obtained from each independent experiment, and the bar plots show the mean ± standard deviation (n = 3). P*** < 0.0001 compared to the PrP anisotropy without Aβ oligomers (One-Way ANOVA test).

in rotational constraints upon binding, we performed AEDANS fluorescence anisotropy measurements for all of the PrP constructs with and without Aβ42 oligomers (Figure 3.3a &

3.3b). The concentration of Aβ oligomers is according to its monomer equivalent. In the free form, anisotropy was low for all residue positions (0.03 - 0.05). A sharp rise in the fluorescence anisotropy in the presence of Aβ oligomers revealed that both OC- and A11-positive Aβ oligomers bind to PrP. The conformational mobility map depicted in Figure 3.3a & 3.3b shows that the region around residue 99 of PrP interacts more closely with both types of Aβ oligomers than the other regions of PrP. The low anisotropy values at positions 31, 120, and 230 were suggestive of a higher degree of flexibility as compared to position 99 with A11-positive Aβ oligomers. A comparatively higher anisotropy at position 31 as opposed to 120 and 230 suggests a higher rotational constraint to the position 31 upon binding to OC-positive Aβ oligomers.

3.3.2 Intrinsically disordered N-terminal of PrP participate in binding

Previous reports have shown that the C-terminal of PrP does not participate in binding to Aβ oligomers. In order to verify that we deleted the N-terminal region (residues 23 to 111) and created a single-cysteine mutation at residue position 120 in the truncated PrP (112-231). We monitored the steady-state fluorescence anisotropy of AEDANS labeled at position 120, and there was no significant increase in the anisotropy value in the presence of both the Aβ oligomers

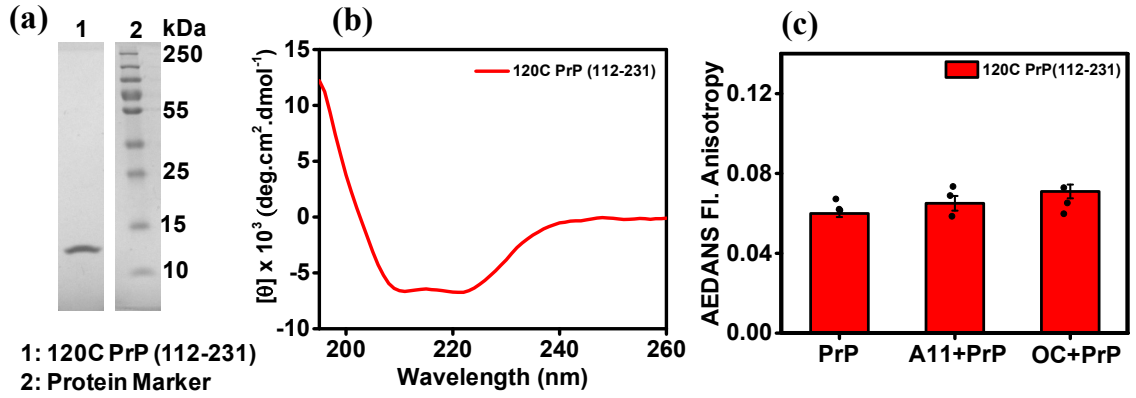

Figure 3.4: (a) 12 % SDS-PAGE of purified 120C PrP (112-231). (b) Far-UV CD spectra of 120C PrP (112-231). (c) Steady-state fluorescence anisotropy of 1 µM AEDANS labeled 120C PrP (112-231) without and with 2 µM Aβ oligomers. The scatter plot represents the data obtained from each independent experiment and the bar plot shows the mean ± standard deviation (n = 3).

(Figure 3.4). These results confirmed that the regions comprising residues 31 and 99 in PrP participate in binding to Aβ oligomers, which is in line with the previous reports that indicated two putative binding sites (15, 16, 18). However, the extent of binding of Aβ oligomers in these two regions of PrP is not known. Therefore, we next studied the interaction of Aβ oligomers at these two putative binding sites of PrP.

3.3.3 Region encompassing residue 99 of PrP is the primary binding site for Aβ oligomers

We asked the question: Do these two regions near residues 31 and 99 in PrP differ in their binding to Aβ oligomers? In order to determine the extent of binding, we set out to perform the titration of Aβ oligomers into AEDANS labeled at residue positions 31and 99 of PrP by varying the amount of Aβ at a fixed concentration of PrP. A saturation at a lower Aβ concentration range would indicate a stronger binding to the specific site of PrP. We carried out the AEDANS fluorescence anisotropy measurements and observed a rise in the anisotropy as a function of Aβ concentration (Figure 3.5a & 3.5b). Since the oligomeric mixture contains mAβ, we verified that the increase in anisotropy upon addition of Aβ oligomers is due to the PrP-binding with Aβ oligomers, and not with mAβ. We performed AEDANS fluorescence anisotropy measurements (position 99 of PrP) as a function of mAβ concentration. No significant increase in the anisotropy in the presence of mAβ as compared to the oligomers suggested that mAβ does not bind to PrP (Figure 3.5c). These findings are in accordance with the previous studies indicating Aβ oligomers are the key binding partners of PrP (15, 16). The site-specific anisotropy map revealed that the binding of both OC- and A11-positive Aβ oligomers to residue position 99 of PrP was saturated at a lower concentration as compared to position 31 of PrP which suggested that the region comprising residue 99 serves as the primary binding site. In order to further validate our results, we employed intermolecular fluorescence resonance energy transfer (FRET) measurements. For this experiment, we prepared OC- and A11-positive Aβ42 oligomers derived from carboxyfluorescein (FAM)-labeled Aβ42. We then monitored intermolecular FRET between AEDANS (donor) labeled at positions 31, 99, 120, and 230 of PrP and N-terminal FAM-labeled (acceptor) Aβ oligomers. The FRET efficiency represents the intermolecular proximity between the donor and the acceptor and would be high if they are proximal in the heterotypic assembly. The A11-positive Aβ oligomers showed ~ 10 % FRET with residue 31, 120, and 230 of PrP but exhibited ~ 20 % FRET efficiency with residue 99 of PrP indicating that

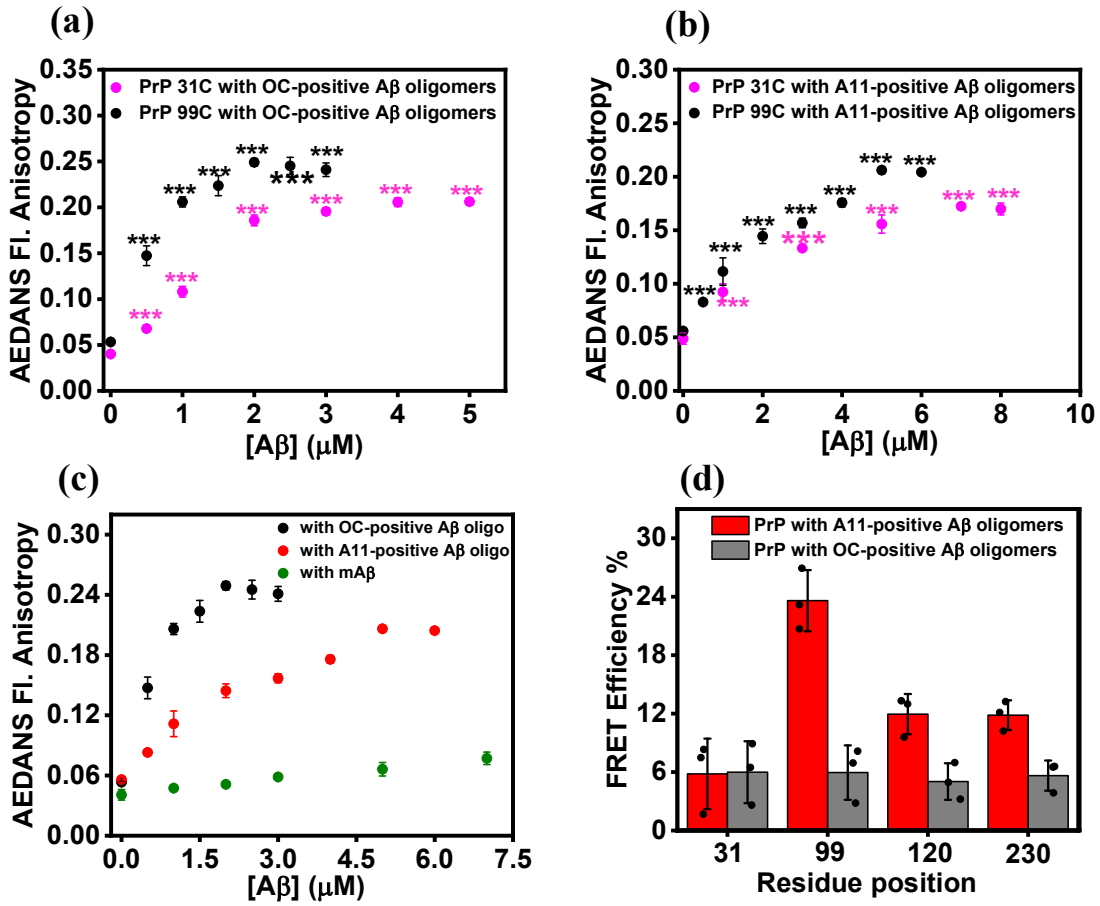

Figure 3.5: Titration of 1 μM AEDANS labeled at positions 31 (magenta) and 99 of PrP (black) with varying concentrations of (a) OC- and (b) A11-positive Aβ oligomers. The scatter plots represent the mean ± standard deviation (n = 3). P*** < 0.0001 relative to the PrP anisotropy without Aβ oligomers at all the data points (One-Way ANOVA test). (c) Titration of 1μM AEDANS labeled at position 99 of PrP with monomeric Aβ (olive), OC- (black) and A11-positive Aβ oligomers (red) by steady-state AEDANS fluorescence anisotropy measurements. The scatter plot represents the mean from three independent measurements with the standard deviation (n = 3). (d) Plot of PrP-Aβ oligomers FRET efficiency of 1 μM AEDANS-labeled (donor) PrP at different residues with 2 μM of FAM-5-labeled (acceptor) OC- (gray) and A11-positive Aβ oligomers (red). The scatter plots represent the data obtained from each independent experiment, and the bar plot shows the mean ± standard deviation (n = 3).

the region near residue 99 is closer to A11-positive Aβ oligomerss. On the contrary, the OC-positive Aβ oligomers exhibit ~ 5 % FRET with all residue positions 31, 99, 120, and 230

(Figure 3.5d). This is an interesting observation. We speculate that the N-terminal part of Aβ in OC-positive Aβ oligomers is far from the binding site of PrP. Taken together, our data revealed that the primary binding region for the interaction of Aβ oligomers and PrP is the region encompassing residue 99 in PrP. Next, we investigated the mode of interaction between Aβ oligomers and PrP in the heterotypic assembly.

3.3.4 Electrostatic interaction is involved in PrP-Aβ binding

A closer look at the amino acid sequence revealed that the preeminent binding region of PrP contains a large number of positively charged residues (Figure 3.1c). Therefore, we postulated that the interaction between PrP and Aβ oligomers could be primarily driven by electrostatic interactions. In order to verify this, we monitored AEDANS fluorescence at the primary binding region of PrP in the presence of OC- and A11-positive Aβ oligomers as a function of ionic strength by varying the salt concentration. We observed a decrease in the fluorescence anisotropy

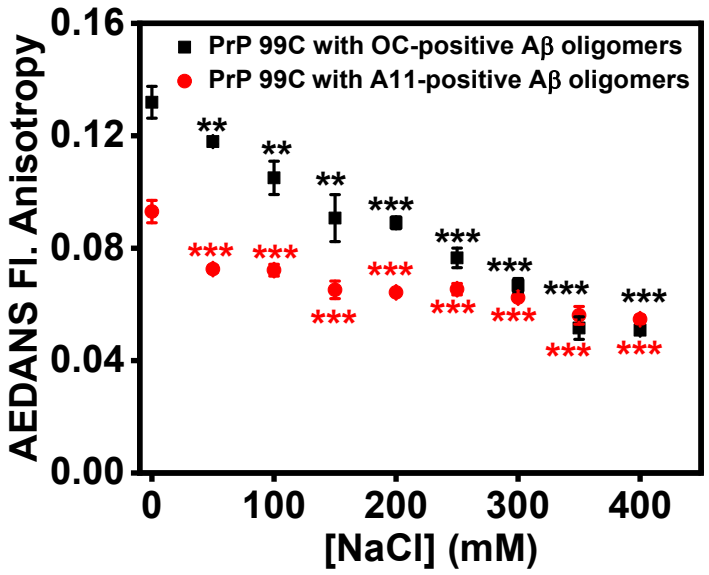

Figure 3.6: Steady-state fluorescence anisotropy of 1 μM AEDANS labeled residue 99 of PrP with 2 μM of Aβ oligomers in the presence of different concentrations of salt. The scatter plots represent the mean ± standard deviation (n = 3). P** < 0.01, P*** < 0.0001 compared to the anisotropy without salt (One-Way ANOVA test).

and a red-shift with increasing concentration of salt for both OC- and A11-positive Aβ oligomers (Figure 3.6). The result showed that the interaction is weaker at higher ionic strength, suggesting that the electrostatic interaction plays a crucial role in the heterotypic assembly of PrP and Aβ oligomers. Next, we asked the question: which type of Aβ oligomer preferentially binds to PrP.

3.3.5 Binding of PrP (90-231) to Aβ oligomers

In order to decipher the role of conformationally distinct oligomers in the PrP-Aβ interaction, we compared the AEDANS fluorescence anisotropy data at residue position 99 of PrP with both OC- and A11-positive Aβ oligomers. The fluorescence anisotropy was saturated at a lower concentration of OC-positive Aβ oligomers in contrast to A11-positive Aβ oligomers with the primary binding region of PrP (Figure 3.5c). Also, we examined the binding between Aβ oligomers and a truncated fragment of human prion, PrP (90-231) that contains the preeminent binding region of Aβ oligomers. We took the advantage of a single tryptophan at residue position 99 present in PrP (90-231) and performed the titration of mAβ and Aβ oligomers into PrP (90-231) (Figure 3.7). We monitored tryptophan fluorescence anisotropy by varying the amount of Aβ at a fixed concentration of PrP (90-231). As expected, mAβ did not show much increase in anisotropy as opposed to Aβ oligomers. Results from both the PrP constructs, the truncated and the full-length PrP, exhibited a lower saturation concentration for OC-positive oligomers indicating a higher binding affinity in comparison to A11-positive Aβ oligomers.

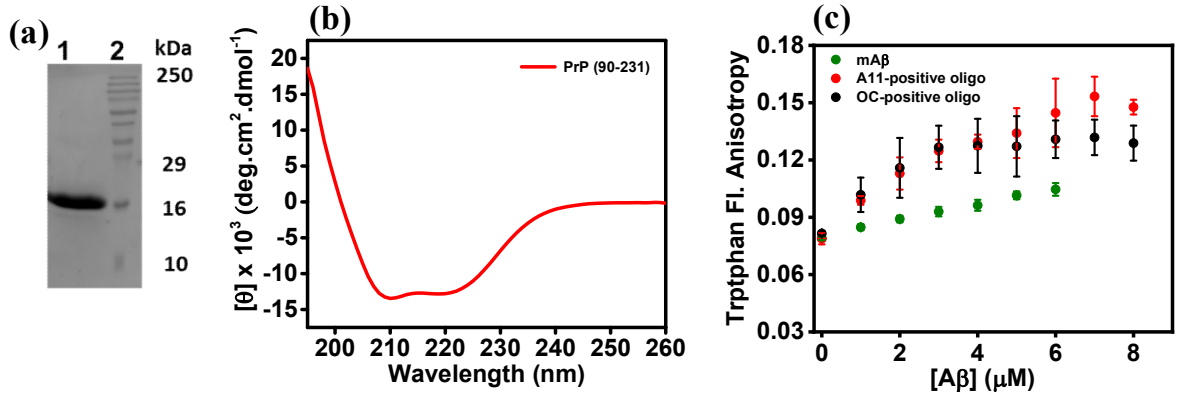

Figure 3.7: (a) 15 % SDS-PAGE of purified PrP (90-231). (b) Far-UV CD spectra of PrP (90-231). (c) Titration of 5 μM PrP (90-231) with the varied concentrations of OC- (grey) and A11-positive Aβ oligomers (red) by steady-state tryptophan fluorescence anisotropy measurements.

3.3.6 Preferential recruitment of OC-positive Aβ oligomers by PrP

Next, we intended to quantify the binding interaction of two different types of Aβ oligomers with PrP. Previous studies have shown that the binding of Aβ oligomers and PrP occurred in the nanomolar range (15, 16, 40). In order to estimate the apparent dissociation constant (K_d), the concentration of PrP should be below the K_d or in the range of K_d. The micromolar concentration of proteins essential for AEDANS fluorescence experiments pose a bottleneck in the estimation of binding affinities that are in the nanomolar range. This is because all of the added Aβ is binding to PrP to the point where PrP is saturated that lead to no free Aβ and we cannot measure the binding affinity from the AEDANS fluorescence experiment. To measure the binding affinities, we labeled residue 99 of PrP with fluorescein-5-maleimide, which is a thiol-reactive fluorescent probe and yields fluorescence at a much lower (nanomolar) concentration because of high quantum yield of fluorescein. The fluorescence spectra of 100 nM labeled PrP were recorded with and without Aβ oligomers. We observed fluorescence quenching of PrP labeled with fluorescein upon addition of OC- and A11-positive Aβ oligomers (Figure 3.8a & 3.8b).

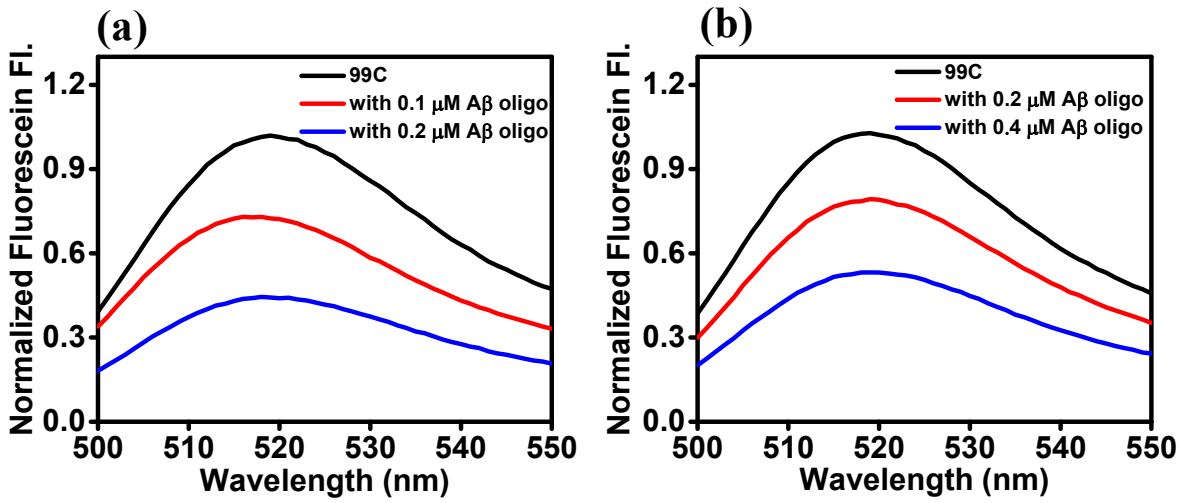

Figure 3.8: Fluorescence spectra of 100 nM fluorescein-5-maleimide labeled residue 99 of PrP without and with different concentrations of (a) OC- and (b) A11-positive Aβ oligomers.

The observed fluorescence quenching was likely due to the presence of aromatic amino acids such as tyrosine and phenylalanine present in Aβ. The extent of fluorescence quenching is related to the extent of interaction between PrP and Aβ oligomers. In order to determine the

extent of quenching, we performed a titration experiment and determined the binding parameter, K_d. We performed the titration of Aβ oligomers into PrP labeled at position 99 and monitored the changes in the fluorescence intensity as a function of Aβ concentration. These titration experiments yielded apparent dissociation constants (K_d). The OC-positive Aβ oligomers exhibited a strong binding with PrP (K_d ~17 nM), whereas, the A11-positive Aβ oligomers showed a much weaker binding (K_d ~ 500 nM) (Figure 3.9a & 3.9b).

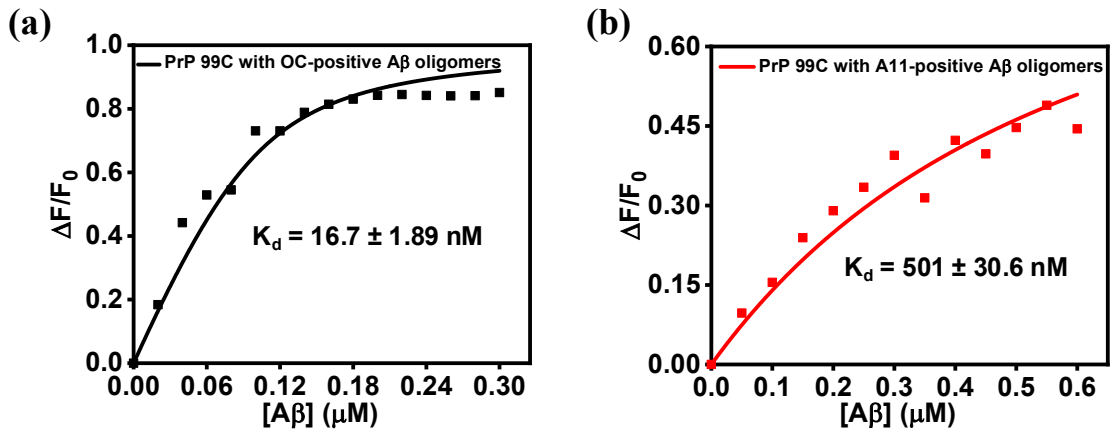

Figure 3.9: Determination of binding affinity between conformationally distinct Aβ oligomers and PrP. Fluorescence quenching plots of 100 nM fluorescein-5-maleimide labeled PrP at residue position 99 with varying concentrations of (a) OC- (black) and (b) A11-positive Aβ oligomers (red). The scatter plots represent one of the data set from three independent experiments, and all the three data sets were fitted using the binding equation 6 (adjusted R^2 = 0.93 for A11-positive oligomers, adjusted R^2 = 0.95 for OC-positive oligomers). The dissociation constants, K_d is calculated from each experiment and represented as mean ± standard deviation (n = 3).

In order to further validate our results, we prepared Aβ-derived diffusible ligands (ADDLs) that have previously been shown to be OC-positive. We further confirmed that these ADDLs are OC-positive and performed the titration of ADDLs into fluorescein-5-maleimide labeled PrP at position 99 (Figure 3.10a and 3.10b). The binding trend of ADDLs with PrP was similar to OC-positive oligomers. Taken together, our equilibrium studies indicated that the OC-positive Aβ oligomers bind more strongly with PrP compared to A11-positive Aβ oligomers.

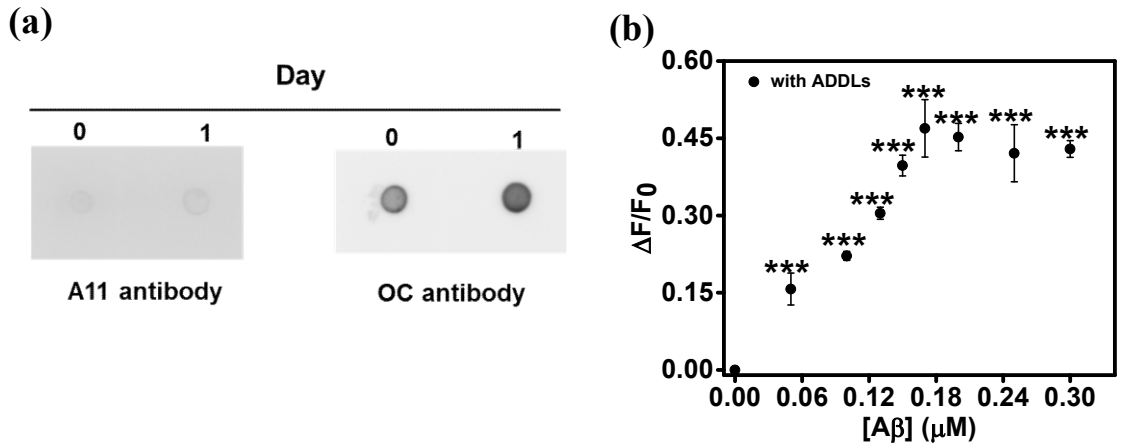

Figure 3.10: (a) Samples from 0th day and after 1st day were spotted on nitrocellulose membrane from the ADDLs preparations and dot-blotted with the respective antibodies. (b) Fluorescence quenching plot of 100 nM fluorescein-5-maleimide labeled PrP at residue position 99 with varying concentrations of ADDLs (black). The scatter plot represents the mean ± standard deviation (n = 3). P*** < 0.0001 compared to PrP without ADDLs (One-Way ANOVA test).

Next, we aimed at investigating the binding kinetics of PrP and Aβ oligomers using stopped-flow fluorescence measurements. Our stopped-flow experiment revealed that the fluorescein-5-maleimide labeled at position 99 of PrP upon rapid mixing with OC-positive Aβ oligomers exhibited a fast decrease in the fluorescence intensity, whereas, A11-positive Aβ oligomers showed no such decrease in the time range of 5s (Figure 3.11). The decrease in fluorescein-5-maleimide fluorescence upon rapid mixing with OC-positive Aβ oligomers displayed typical biexponential decay kinetics, indicating stepwise binding events. Therefore, both our kinetic- and equilibrium data suggested that OC-positive Aβ oligomers exhibit much higher binding affinity compared to A11-positive Aβ oligomers and that the conformation of Aβ oligomers plays a critical role in Aβ-PrP heterotypic assembly.

3.3.7 Role of size-distribution of Aβ oligomers in PrP-Aβ binding

Next, in order to discern the role of conformation and size-distribution of Aβ oligomers in PrP-binding, we performed the glutathione S-transferase (GST) pull-down assay between GST-fused PrP and Aβ oligomers to detect the sizes of the Aβ oligomers that bind to PrP (Figure 3.12a).We used an empty vector overexpressing GST as a negative control. Our results showed the presence

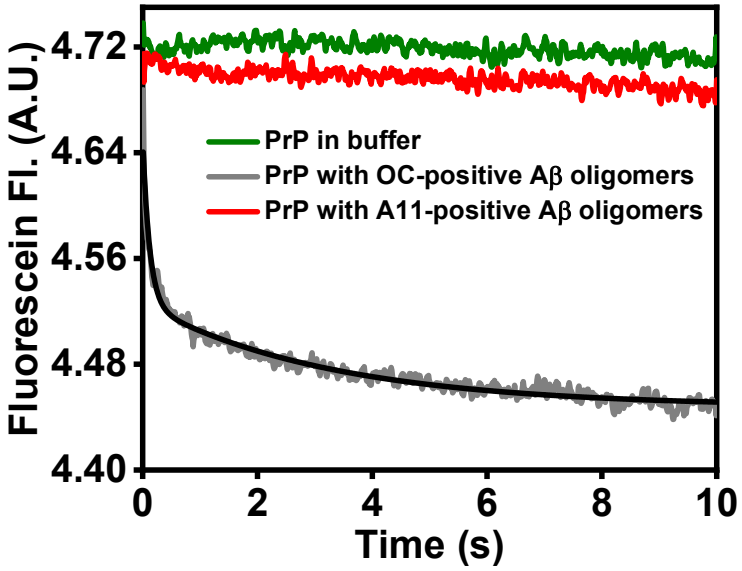

Figure: 3.11: Stopped-flow fluorescence kinetics of fluorescein-5-maleimide labeled residue 99 of PrP without (olive) and with OC- (grey) and A11-positive Aβ oligomers (red).

of Aβ with GST-fused PrP on the SDS-PAGE, confirming the interaction of Aβ oligomers with PrP. However, we observed the bands corresponding to the monomeric Aβ, instead of Aβ oligomers, on the SDS-PAGE. This could be due to the SDS-induced disaggregation of oligomers in the presence of the loading dye. Our pull-down assays were unable to distinguish the sizes of the Aβ oligomers that bind to PrP. Therefore, we next performed the SEC assays to detect the PrP-Aβ oligomer complexes. The chromatogram showed that free PrP eluted at avolume ~ 26 mL (Figure 3.12b). The A11- and OC-positive Aβ oligomers, when mixed with PrP, exhibited two similar peaks, which are at ~ 21.2 mL and ~ 26 mL. The peak at ~ 26 mL could be due to free PrP or unbound Aβ oligomers while the peak at ~ 21.2 mL is unique to all the control samples of unbound PrP, A11- and OC-positive oligomers (Figure 3.12b). The molecular weight of the bound species from this peak could not be analyzed as the expected position of PrP is different from the observed position, which could be due to the interaction of PrP with the column matrix. The same peak observed for both types of Aβ oligomers with PrP indicated that the similar sizes of Aβ oligomers in both the conformations are likely to interact with PrP. We would like to note that a peak at the void volume (~ 11 mL) for PrP with OC-positive oligomers indicated the presence of higher order species. These higher order species

could be due to unbound OC-positive oligomers or PrP bound higher order oligomeric species. Taken together, our findings revealed that the similar sizes of the Aβ oligomeric species are capable of interacting with PrP.

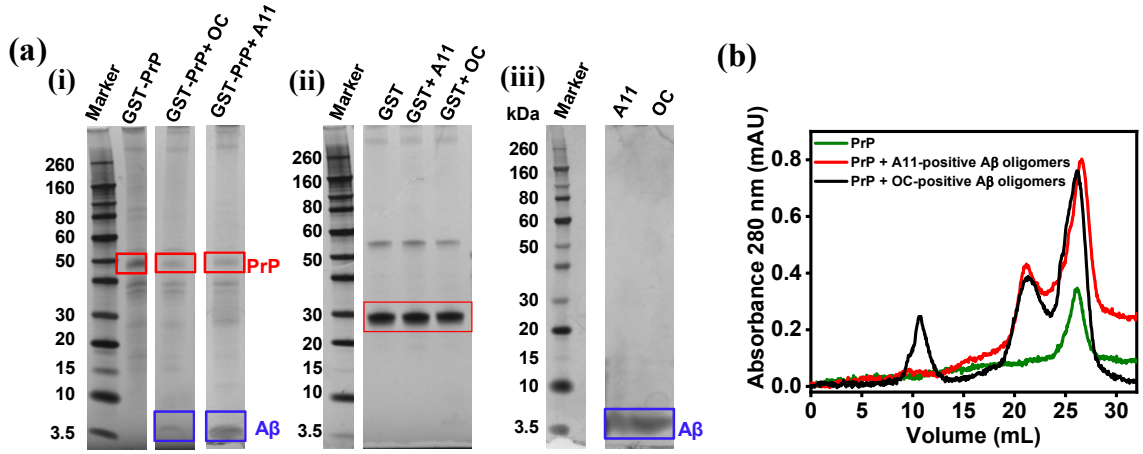

Figure 3.12: (a) GST pull-down assays showing the interaction of Aβ oligomers with PrP: (i) GST-fused PrP and (ii) empty vector expressing GST with A11- and OC-positive oligomers. (iii) A11- and OC-positive oligomers without PrP. In the presence of the loading dye, both types of Aβ-oligomers appear as monomeric Aβ on the gradient SDS-PAGE due to SDS-induced monomerization of oligomers. (b) SEC chromatograms of PrP (olive), PrP with OC-(black), and A11-positive oligomers (red).

3.3.8 Aggregation state of PrP-Aβ complex

We next asked the question: What happens to the aggregation state of Aβ oligomers in the presence of PrP. In order to study that we monitored thioflavin T (ThT) fluorescence, a well-known amyloid marker, of mixtures of Aβ oligomers and PrP and compared with the ThT fluorescence of Aβ fibrils. We observed that there is little or no increase in the ThT-fluorescence of Aβ oligomers in the presence of PrP, even after10 days (Figure 3.13a). Additionally, AFM images showed the presence of oligomers and/or amorphous aggregates (Figure 3.13b). These results indicated that the heterotypic complexes of PrP and Aβ oligomers are unlikely to convert into typical amyloid fibrils and are in line with a previous report (18).

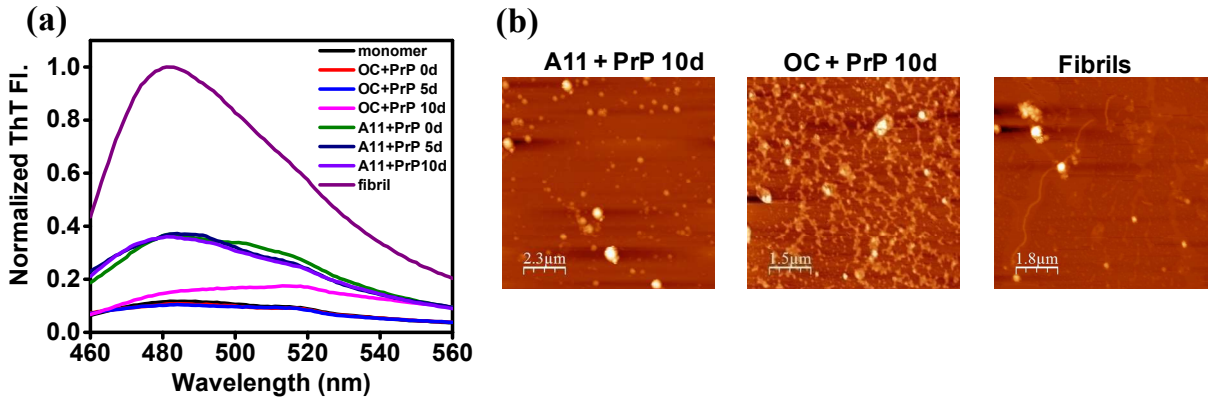

Figure 3.13: (a) ThT fluorescence spectra of 10 µM Aβ in the monomeric and fibrillar forms and 10 µM Aβ oligomers in the presence of 5 µM PrP at different incubation times. (b) AFM images of Aβ fibrils and Aβ oligomers in the presence of PrP after 10 days.

3.3.9 Effect of PrP on the cytotoxicity of conformationally distinct Aβ oligomers

We next asked the following questions: Do these conformationally distinct Aβ oligomers differ in cytotoxicity? And how does their toxicity alter in the presence of PrP? In order to quantify the cytotoxic effect, we performed the MTT assay that is a well-known colorimetric cell-based assay used to determine the cell viability and the cytotoxic effect. HeLa cells were exogenously challenged with native PrP, OC- and A11-positive Aβ oligomers, both with and without PrP. Both conformationally distinct Aβ oligomers exhibited cytotoxicity, and as expected, PrP was innocuous (Figure 3.14). We observed that OC-positive Aβ oligomers resulted in the death of ~ 47% cells while A11-positive Aβ oligomers caused ~ 60% cell death, which indicated that A11-positive oligomers are more cytotoxic than OC-positive oligomers. The OC-positive oligomers in the presence of PrP resulted in the death of ~ 62% cells. On the contrary, A11-positive oligomers exhibited nearly the same toxic effects with and without PrP. Our data suggested that OC-positive Aβ oligomers exhibit more pronounced toxicity upon binding to PrP, whereas, the toxicity exerted by A11-positive Aβ oligomers is independent of binding to PrP.

3.4 Discussion

AD is a clinicopathological syndrome where people suffer from cognitive deficits and memory impairments that are mainly caused by Aβ oligomers. Previous studies have identified PrP as one

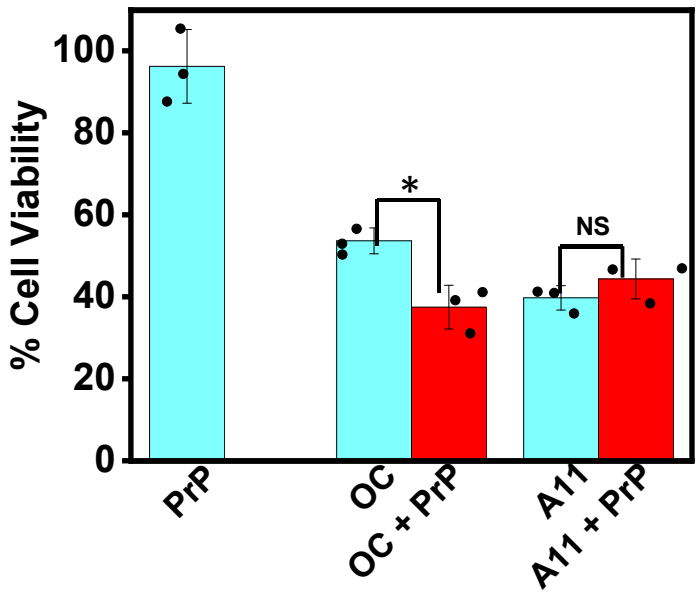

Figure 3.14: Toxic effects of Aβ oligomers with and without PrP on HeLa cells. MTT assay showing significant reduction in cell viability upon treatment of cells with Aβ oligomers in the presence and absence of PrP. The experiment is repeated three times in triplicate, and the mean value of each experiment is represented in the scatter plot. The bar plot shows the mean ± standard deviation (n = 3). NS indicates no significant difference in MTT reduction between cells treated with A11-positive Aβ oligomers in the presence and absence of PrP. For OC-positive Aβ oligomers with and without PrP: *P < 0.025 (Student's t-test).

of the binding receptors, so-called a "bad receptor" of Aβ oligomers. It is not clear whether the role of PrP in AD is protective or lethal (41, 42). The postulated protective roles of PrP are as follows. PrP could potentially decrease Aβ peptide formation by inhibiting the β-secretase cleavage of APP, exosomal PrP reduces the toxic effects by accelerating Aβ aggregation, and N1, the main physiological cleavage fragment of PrP suppresses Aβ oligomers toxicity in mice (18, 43, 44). However, a growing body of evidence suggested that PrP mediates Aβ oligomer-induced synaptic dysfunction. Some studies reported that ablation of PrP does not ameliorate the toxicity caused by Aβ oligomers (15, 19, 25, 27). This discrepancy could arise due to the use of different Aβ oligomers that vary in conformation, size, morphology, and cytotoxicity. The notion that Aβ oligomers exist in predominantly two distinct conformations, A11- and OC-positive

oligomers, emerged from the classification of amyloid oligomers (7). The intriguing role of toxicity mediated by binding of Aβ oligomers to PrP has potentially major implications in AD and provides an amenable therapeutic target. Our studies demonstrated that the preferential binding of conformationally distinct OC-positive Aβ oligomers to PrP can mediate PrP-dependent Aβ cytotoxicity.

Previous studies have indicated PrP has two putative binding sites for Aβ oligomers (15, 16). These sites are located around 23-27 and 95-105. Our results clearly showed that the preeminent binding determinant for the interaction of PrP and Aβ oligomers is the region harboring residue 99 that lies in segment 95-105. We speculate that both binding regions are important for interaction, but the region near residue 99 in PrP plays a crucial role in recruiting Aβ oligomers. This intrinsically disordered region of PrP contains a number of positively charged residues that are involved in electrostatic interaction with the negatively charged residues of Aβ. We believe that electrostatic interactions, in conjunction with the conformational rearrangements of the flexible N-terminal domain of PrP (18), are crucial for the recruitment of Aβ oligomers.

It is believed that the conformation of Aβ oligomer is paramount in PrP binding and mediating the neuronal toxicity (17). We were able to discern the binding affinities of different conformationally distinct oligomers with PrP and identify the oligomeric species having PrP-dependent cytotoxicity. By using an array of biophysical tools, we analyzed the binding affinities of Aβ oligomers to PrP. These data indicated that OC-positive Aβ oligomers bind more strongly to PrP compared to A11-positive Aβ oligomers. Additionally, our results show that the kinetics of interaction of PrP with OC-positive Aβ oligomers is much faster than that of A11-positive oligomers (Figure 3.11). The stopped-flow kinetics exhibited a biphasic profile that might potentially indicate the presence of separable steps of binding-induced conformational changes of PrP. Our SEC chromatograms showed similar profiles of PrP-Aβ oligomers, indicating that similar Aβ oligomeric species bind to PrP (Figure 3.12b). The analysis of SEC chromatograms of two types of Aβ oligomers indicated that the common species among the two preparations is the (lower order) dimeric Aβ (Figure 2.2e, Chapter 2). Previous studies also showed that the lower order oligomers display a strong binding affinity with PrP, and the dimeric Aβ has the highest binding affinity (30, 45). Our data together with the previous reports suggested that the interaction of Aβ oligomers with PrP might be dominated by the dimeric Aβ species. A recent

report has shown that the Aβ dimer can adopt a variety of structures that includes parallel, antiparallel, extended, and compact structure (46). So, the difference in binding among two preparations could be due to the difference in conformation of dimeric Aβ. Other than conformation, the two Aβ oligomeric preparations differ in the presence of a larger fraction of higher order oligomers in OC-positive oligomers as compared to the A11-positive oligomers. Therefore, the preferential binding of OC-positive Aβ oligomers to PrP might be due to the different conformations adopted by the dimeric Aβ among the two preparations or the binding of higher order oligomers to PrP which leads to more number of bound species in OC-positive oligomers.

Our cytotoxicity assay suggested that A11-positive Aβ oligomers are more cytotoxic in comparison to OC-positive Aβ oligomers, which is in accordance with the earlier report (47). The OC-positive oligomers became highly toxic in the presence of PrP. Our cytotoxicity results are in close agreement with a previous study performed in neuronal cell lines (17). However, we would like to point out that the increase in toxicity could also be due to an alteration in the distribution of oligomeric species upon binding to PrP. Our intermolecular FRET experiments also provided important insights into the architecture of the heterotypic assembly of PrP and Aβ oligomers. Despite stronger binding, we were unable to detect any significant energy transfer between OC-positive oligomers and PrP. This could be due to the following reason. OC-positive oligomers have been shown to possess an in-register parallel β-sheet organization. The interaction of PrP with such a parallel in-register Aβ assembly is expected to position the acceptor label at the N-terminal end of Aβ peptide at a distal location from the donor at 99 of PrP. On the contrary, the A11-positive oligomers that are known to contain anti-parallel β-sheet arrangements will have an alternate proximal and distal separation between the donor and the acceptor. Therefore, despite having a much weaker association between A11-positive oligomer and PrP, the assembly exhibits intermolecular energy transfer.

We propose a model as depicted in Figure 3.15 that summarizes our findings. The association between the principle binding region of PrP and Aβ oligomers is driven by the electrostatic interaction and that PrP serves as a receptor to mediate the deleterious effects of OC-positive Aβ oligomers. Previous results have indicated that the OC-positive fibrillar Aβ oligomers are highly abundant *in vitro* and have a spatiotemporal relationship with amyloid plaques in the brain of

transgenic mice (47, 48). The observation that OC-positive Aβ oligomers show high binding affinity to PrP and their occurrence in high concentration around the amyloid plaques is intriguing. This could potentially result in a substantial amount of PrP-bound OC-positive oligomers in the AD brain. Additionally, we found that these PrP-bound Aβ oligomers are highly detrimental that is consistent with *in vivo* studies (17). A recent study provided evidence that remodeling of OC-positive Aβ oligomers by using polyphenolic compounds, such as (-)-epigallocatechin gallate and resveratrol, obliterate the binding of Aβ oligomers to PrP and hence, reduces the downstream toxicity.

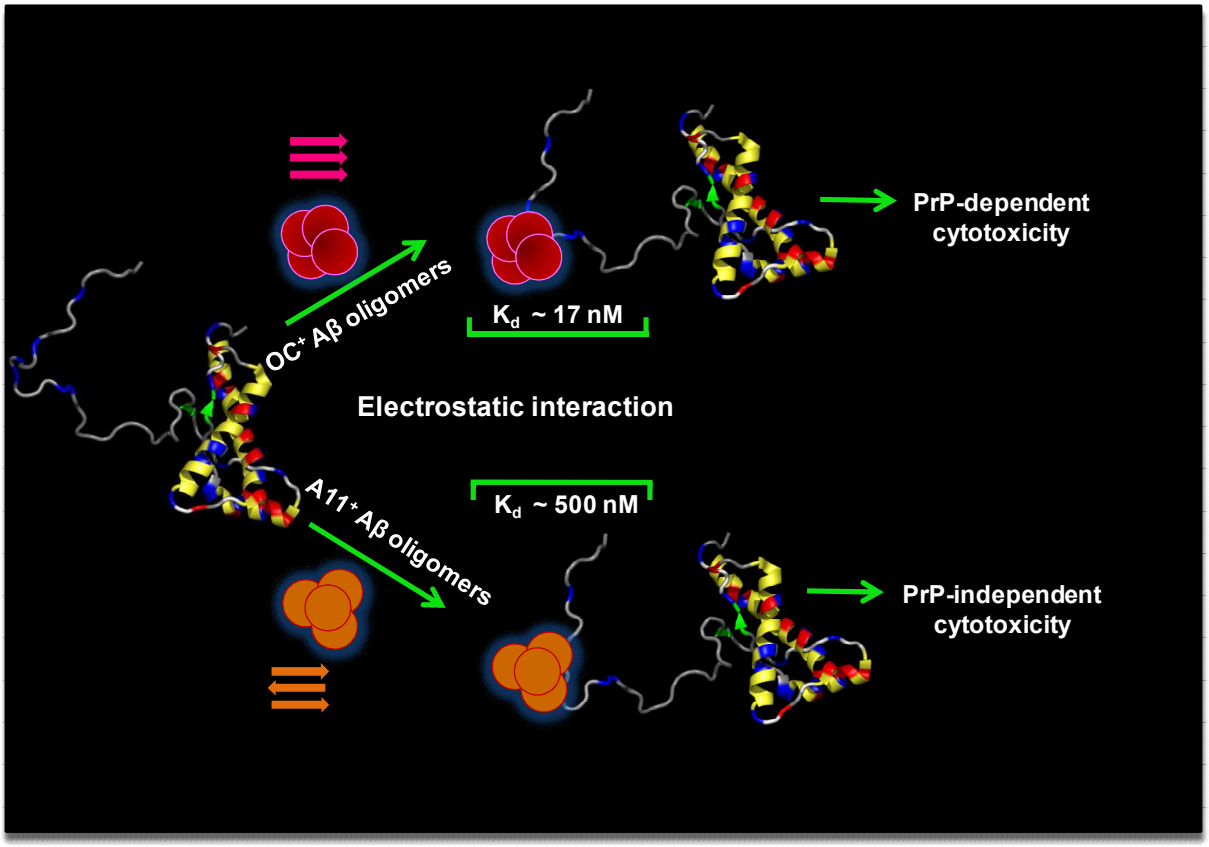

Figure 3.15: Proposed model for the interaction between conformationally distinct Aβ oligomers and PrP.

Previous studies have shown that the low molecular weight heparin (LMWHep) acts as therapeutic for the misfolding of PrP (49, 50). The binding of LMWHep to PrP occurs via the octapeptide repeat region of PrP leads to the transient aggregation state that shows a similar fold like native PrP with a less flexible N-terminal domain. This PrP-LMWHep complex inhibits the

RNA catalyzed the conversion of PrP to the scrapie form of PrP. Since both the Aβ oligomers and RNA have similar binding sites (N-terminal domain) to PrP (21), we hypothesize that the binding of LMWHep to PrP might also act as therapeutic potential for the interaction between PrP and Aβ oligomers and prevent the PrP mediated toxic effects of Aβ oligomers. Taken together, our current work along with the previous observations suggest that therapeutic strategies targeting the interaction between PrP and Aβ oligomers might reduce the lethal role of PrP and might play a pivotal role in anti-Alzheimer's therapeutics.

3.5 References

1. Selkoe, D. J. (2002) Alzheimer's Disease Is a Synaptic Failure. *Science.* **298**, 789–791

2. Small, D. H., Mok, S. S., and Bornstein, J. C. (2001) Alzheimer's disease and Abeta toxicity: from top to bottom. *Nat. Rev. Neurosci.* **2**, 595–598

3. Lesné, S., Ming, T. K., Kotilinek, L., Kayed, R., Glabe, C. G., Yang, A., Gallagher, M., and Ashe, K. H. (2006) A specific amyloid-β protein assembly in the brain impairs memory. *Nature*. **440**, 352–357

4. Walsh, D. M., and Selkoe, D. J. (2007) Aβ oligomers - A decade of discovery. *J. Neurochem.* **101**, 1172–1184

5. Haass, C., and Selkoe, D. J. (2007) Soluble protein oligomers in neurodegeneration: Lessons from the Alzheimer's amyloid β-peptide. *Nat. Rev. Mol. Cell Biol.* **8**, 101–112

6. Kayed, R., Head, E., Sarsoza, F., Saing, T., Cotman, C. W., Necula, M., Margol, L., Wu, J., Breydo, L., Thompson, J. L., Rasool, S., Gurlo, T., Butler, P., and Glabe, C. G. (2007) Fibril specific, conformation dependent antibodies recognize a generic epitope common to amyloid fibrils and fibrillar oligomers that is absent in prefibrillar oligomers. *Mol. Neurodegener.* **2**, 1–11

7. Glabe, C. G. (2008) Structural classification of toxic amyloid oligomers. *J. Biol. Chem.* **283**, 29639–29643

8. Wu, J. W., Breydo, L., Isas, J. M., Lee, J., Kuznetsov, Y. G., Langen, R., and Glabe, C.

(2010) Fibrillar oligomers nucleate the oligomerization of monomeric amyloid β but do not seed fibril formation. *J. Biol. Chem.* **285**, 6071–6079

9. Breydo, L., Kurouski, D., Rasool, S., Milton, S., Wu, J. W., Uversky, V. N., Lednev, I. K., and Glabe, C. G. (2016) Structural differences between amyloid beta oligomers. *Biochem. Biophys. Res. Commun.* **477**, 700–705

10. Kayed, R., Head, E., Thompson, J. L., McIntire, T. M., Milton, S. C., Cotman, C. W., and Glabel, C. G. (2003) Common structure of soluble amyloid oligomers implies common mechanism of pathogenesis. *Science.* **300**, 486–489

11. Krishnan, R., Goodman, J. L., Mukhopadhyay, S., Pacheco, C. D., Lemke, E. A., Deniz, A. A., and Lindquist, S. (2012) Conserved features of intermediates in amyloid assembly determine their benign or toxic states. *Proc. Natl. Acad. Sci. U. S. A*. **109**, 11172–11177

12. Wang, X., Smith, D. R., Jones, J. W., and Chapman, M. R. (2007) In vitro polymerization of a functional Escherichia coli amyloid protein. *J. Biol. Chem.* **282**, 3713–3719

13. Laganowsky, A., Liu, C., Sawaya, M. R., Whitelegge, J. P., Park, J., Zhao, M., Pensalfini, A., Soriaga, A. B., Landau, M., Teng, P. K., Cascio, D., Glabe, C., and Eisenberg, D. (2012) Atomic view of a toxic amyloid small oligomer. *Science.* **335**, 1228–1231

14. Liu, C., Zhao, M., Jiang, L., Cheng, P., Park, J., Sawaya, M. R., and Pensal, A. (2012) Out-of-register β -sheets suggest a pathway to toxic amyloid aggregates. *Proc. Natl. Acad. Sci. U. S. A*. **109**, 20913–20918

15. Laurén, J., Gimbel, D. A., Nygaard, H. B., Gilbert, J. W., and Strittmatter, S. M. (2009) Cellular prion protein mediates impairment of synaptic plasticity by amyloid-B oligomers. *Nature*. **457**, 1128–1132

16. Chen, S., Yadav, S. P., and Surewicz, W. K. (2010) Interaction between human prion protein and amyloid-β oligomers: Role of N-terminal residues. *J. Biol. Chem.* **285**, 26377–26383

17. Rushworth, J. V., Griffiths, H. H., Watt, N. T., and Hooper, N. M. (2013) Prion protein-

mediated toxicity of amyloid-β oligomers requires lipid rafts and the transmembrane LRP1. *J. Biol. Chem.* **288**, 8935–8951

18. Fluharty, B. R., Biasini, E., Stravalaci, M., Sclip, A., Diomede, L., Balducci, C., La Vitola, P., Messa, M., Colombo, L., Forloni, G., Borsello, T., Gobbi, M., and Harris, D. A. (2013) An N-terminal fragment of the prion protein binds to amyloid-β oligomers and inhibits their neurotoxicity in vivo. *J. Biol. Chem.* **288**, 7857–7866

19. Nicoll, A. J., Panico, S., Freir, D. B., Wright, D., Terry, C., Risse, E., Herron, C. E., Malley, T. O., Wadsworth, J. D. F., Farrow, M. A., Walsh, D. M., Saibil, H. R., and Collinge, J. (2013) Amyloid-β nanotubes are associated with prion protein-dependent synaptotoxicity. *Nat. Commun.* **4**, 2416

20. Prusiner, S. B. (1998) Prions. *Proc. Natl. Acad. Sci. U. S. A.* **95**, 13363–13383

21. Almeida, M. S., Silva, J. L., and Cordeiro, Y. (2008) Prion Protein Complexed to N2a Cellular RNAs through Its N-terminal Domain Forms Aggregates and Is Toxic to Murine. *J. Biol. Chem.* **283**, 19616–19625

22. Um, J. W., Nygaard, H. B., Heiss, J. K., Kostylev, M. A., Stagi, M., Vortmeyer, A., Wisniewski, T., Gunther, E. C., and Strittmatter, S. M. (2012) Alzheimer amyloid-Î 2 oligomer bound to postsynaptic prion protein activates Fyn to impair neurons. *Nat. Neurosci.* **15**, 1227–1235

23. Larson, M., Sherman, M. A., Amar, F., Nuvolone, M., Schneider, J. A., Bennett, D. A., Aguzzi, A., and Lesne, S. E. (2012) The Complex PrPc-Fyn Couples Human Oligomeric A with Pathological Tau Changes in Alzheimer's Disease. *J. Neurosci.* **32**, 16857–16871

24. Kessels, H. W., Nguyen, L. N., Nabavi, S., and Malinow, R. (2010) The prion protein as a receptor for amyloid-β. *Nature*. **466**, E3–E4

25. Balducci, C., Beeg, M., Stravalaci, M., Bastone, A., Sclip, A., Biasini, E., Tapella, L., Colombo, L., Manzoni, C., Borsello, T., Chiesa, R., Gobbi, M., Salmona, M., and Forloni, G. (2010) Synthetic amyloid- oligomers impair long-term memory independently of cellular prion protein. *Proc. Natl. Acad. Sci. U. S. A.* **107**, 2295–2300

26. Calella, A. M., Farinelli, M., Nuvolone, M., Mirante, O., Moos, R., Falsig, J., Mansuy, I. M., and Aguzzi, A. (2010) Prion protein and Aβ-related synaptic toxicity impairment. *EMBO Mol. Med.* **2**, 306–314

27. Cissé, M., Sanchez, P. E., Kim, D. H., Ho, K., Yu, G. Q., and Mucke, L. (2011) Ablation of cellular prion protein does not ameliorate abnormal neural network activity or cognitive dysfunction in the J20 line of human amyloid precursor protein transgenic mice. *J. Neurosci.* **31**, 10427–10431

28. Zahn, R., Von Schroetter, C., and Wüthrich, K. (1997) Human prion proteins expressed in Escherichia cell and purified by high-affinity column refolding. *FEBS Lett.* **417**, 400–404

29. Morillas, M., Swietnicki, W., Gambetti, P., and Surewicz, W. K. (1999) Membrane Environment Alters the Conformational Structure of the Recombinant Human Prion Protein. *J. Biol. Chem.* **274**, 36859–36865

30. Dalal, V., Arya, S., Bhattacharya, M., and Mukhopadhyay, S. (2015) Conformational Switching and Nanoscale Assembly of Human Prion Protein into Polymorphic Amyloids via Structurally Labile Oligomers. *Biochemistry*. **54**, 7505–7513

31. Lambert, M. P., Barlow, A. K., Chromy, B. A., Edwards, C., Freed, R., Liosatos, M., Morgan, T. E., Rozovsky, I., Trommer, B., Viola, K. L., Wals, P., Zhang, C., Finch, C. E., Kraft, G. A., and Klein, W. L. (1998) Diffusible , nonfibrillar ligands derived from $A\beta_{1-42}$ are potent central nervous system neurotoxins. *Proc. Natl. Acad. Sci.U. S. A.* **95**, 6448–6453

32. Horcas, I., Fernández, R., Gómez-Rodríguez, J. M., Colchero, J., Gómez-Herrero, J., and Baro, A. M. (2007) WSXM: A software for scanning probe microscopy and a tool for nanotechnology. *Rev. Sci. Instrum.* **78**, 013705

33. Lakowicz, J. R. (2006) Introduction to Fluorescence, *Principle of Fluorescence Spectroscopy,* Springer New York

34. Favicchio, R., Dragan, A. I., Kneale, G. G., and Read, C. M. (2009) Fluorescence spectroscopy and anisotropy in the analysis of DNA-Protein interactions. *Methods Mol.*

Biol. **543**, 589-611

35. Pollard, T. D. (2010) A Guide to Simple and Informative Binding Assays. *Mol. Biol. Cell*. **21**, 4061–4067

36. Bhattacharya, M., and Mukhopadhyay, S. (2012) Structural and dynamical insights into the molten-globule form of ovalbumin. *J. Phys. Chem. B*. **116**, 520–531

37. Xue, B., Dunbrack, R. L., Williams, R. W., Dunker, A. K., and Uversky, V. N. (2010) PONDR-FIT: A meta-predictor of intrinsically disordered amino acids. *Biochim. Biophys. Acta - Proteins Proteomics*. **1804**, 996–1010

38. Biljan, I., Giachin, G., Ilc, G., Zhukov, I., Plavec, J., and Legname, G. (2012) Structural basis for the protective effect of the human prion protein carrying the dominant-negative E219K polymorphism. *Biochem. J.* **446**, 243–251

39. Risse, E., Nicoll, A. J., Taylor, W. A., Wright, D., Badoni, M., Yang, X., Farrow, M. A., and Collinge, J. (2015) Identification of a compound that disrupts binding of amyloid-β to the prion protein using a novel fluorescencebased assay. *J. Biol. Chem.* **290**, 17020–17028

40. Ganzinger, K. A., Narayan, P., Qamar, S. S., Weimann, L., Ranasinghe, R. T., Aguzzi, A., Dobson, C. M., Mccoll, J., George-Hyslop, P. S., and Klenerman, D. (2014) Single-Molecule Imaging Reveals that Small Amyloid-β_{1-42} Oligomers Interact with the Cellular Prion Protein (PrP^{C}). *ChemBioChem.* **15**, 2515-2521

41. Jarosz-Griffiths, H. H., Noble, E., Rushworth, J. V., and Hooper, N. M. (2016) Amyloid-β receptors: The good, the bad, and the prion protein. *J. Biol. Chem.* **291**, 3174–3183

42. Purro, S. A., Nicoll, A. J., and Collinge, J. (2018) Prion Protein as a Toxic Acceptor of Amyloid-β Oligomers. *Biol. Psychiatry*. **83**, 358–368

43. Parkin, E. T., Watt, N. T., Hussain, I., Eckman, E. A., Eckman, C. B., Manson, J. C., Baybutt, H. N., Turner, A. J., and Hooper, N. M. (2007) Cellular prion protein regulates beta-secretase cleavage of the Alzheimer's amyloid precursor protein. *Proc. Natl. Acad. Sci. U. S. A.* **104**, 11062–11067

44. Falker, C., Hartmann, A., Guett, I., Dohler, F., Altmeppen, H., Betzel, C., Schubert, R., Thurm, D., Wegwitz, F., Joshi, P., Verderio, C., Krasemann, S., and Glatzel, M. (2016) Exosomal cellular prion protein drives fibrillization of amyloid beta and counteracts amyloid beta-mediated neurotoxicity. *J. Neurochem.* **137**, 88–100

45. Williams, T. L., Choi, J. K., Surewicz, K., and Surewicz, W. K. (2015) Soluble Prion Protein Binds Isolated Low Molecular Weight Amyloid-β Oligomers Causing Cytotoxicity Inhibition. *ACS Chem. Neurosci.* **6**, 1972–1980

46. Wei, G., Jewett, A., and Shea, J. E. (2010) Structural diversity of dimers of the Alzheimer's amyloid-β (25-35) peptide and polymorphism of the resulting fibrils. *Phys. Chem. Chem. Phys.* **12**, 3622–3329

47. Liu, P., Reed, M. N., Kotilinek, L. A., Grant, M. K. O., Forster, C. L., Qiang, W., Shapiro, S. L., Reichl, J. H., Chiang, A. C. A., Jankowsky, J. L., Wilmot, C. M., Cleary, J. P., Zahs, K. R., and Ashe, K. H. (2015) Quaternary Structure Defines a Large Class of Amyloid-β Oligomers Neutralized by Sequestration. *Cell Rep.* **11**, 1760–1771

48. Cohen, S. I. A., Linse, S., Luheshi, L. M., Hellstrand, E., White, D. A., Rajah, L., Otzen, D. E., Vendruscolo, M., Dobson, C. M., and Knowles, T. P. J. (2013) Proliferation of amyloid-β42 aggregates occurs through a secondary nucleation mechanism. *Proc. Natl. Acad. Sci. U. S. A.* **110**, 9758–9763

49. Vieira, T. C. R. G., Cordeiro, Y., Caughey, B., and Silva, J. L. (2014) Heparin binding confers prion stability and impairs its aggregation. *FASEB J.* **28**, 2667–2676

50. Vieira, T. C. R. G., Reynaldo, D. P., Gomes, M. P. B., Almeida, M. S., Cordeiro, Y., and Silva, J. L. (2011) Heparin binding by murine recombinant prion protein leads to transient aggregation and formation of rna-resistant species. *J. Am. Chem. Soc.* **133**, 334–344

Impact of Conformationally Distinct Alzheimer's Amyloid-β Oligomers on the Dynamics of Lipid Membrane Comprising Brain Total Lipid Extract

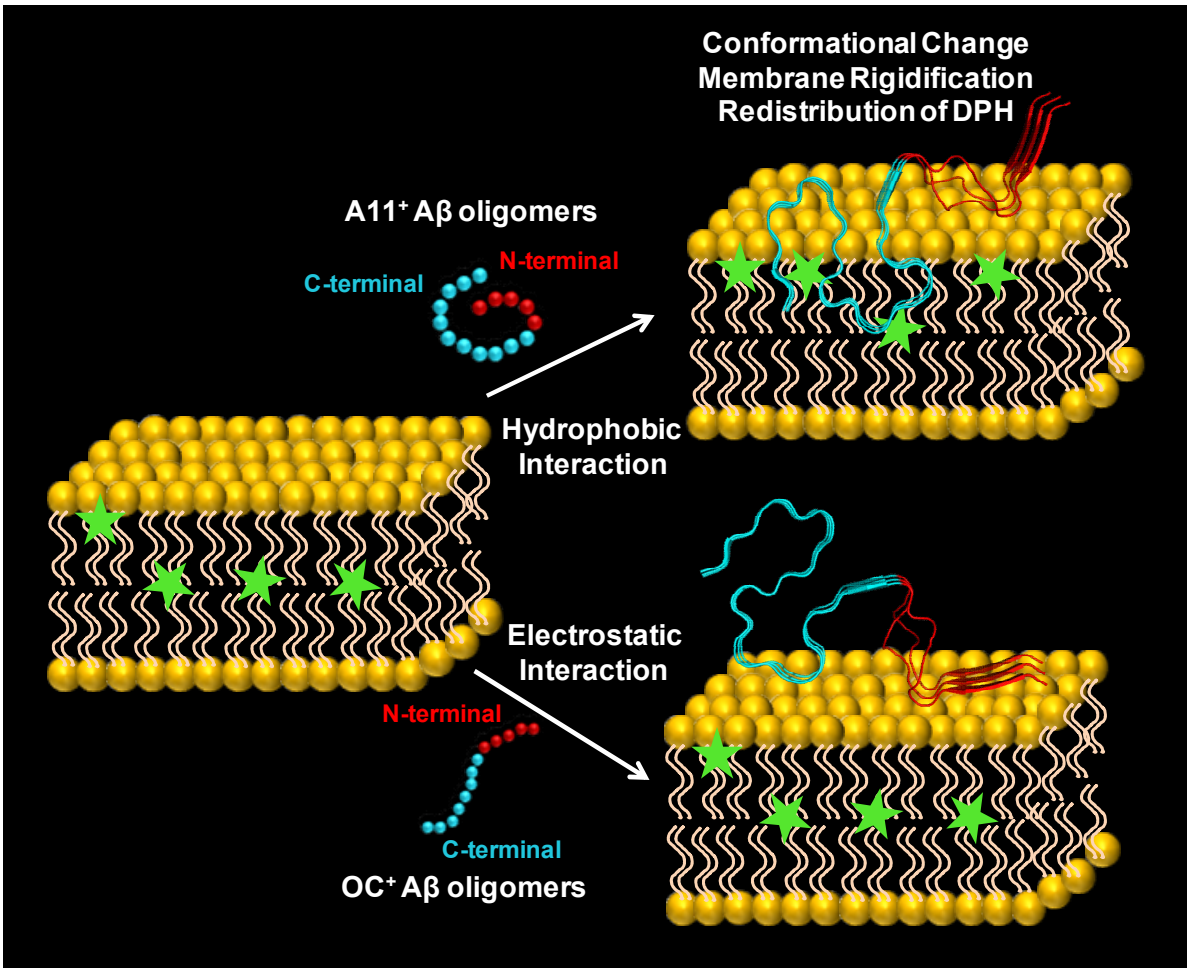

4.1 Introduction

Alzheimer's disease (AD) is a debilitating neurodegenerative disorder identified by the intracellular neurofibrillary tangles and the extracellular insoluble amyloid plaques. The amyloid cascade hypothesis, a widely accepted hypothesis for AD, states that the deposition of a small amphipathic amyloid-β peptide (Aβ), typically of 40 or 42 amino acid residues play a central role in AD. The progression of late-onset AD correlates with the elevated Aβ (1-42) level, indicating the less prevalent Aβ (1-42) is the primary neurotoxic form of Aβ peptide (1–3). Growing evidence suggests that the soluble oligomers of Aβ peptide inhibit long-term potentiation and are strongly associated with cognitive impairment (4–6). A plethora of studies have shown the existence of a variety of Aβ oligomers in AD brains, APP transgenic mice, in vivo, and in vitro. This multitude of soluble oligomers varies on the basis of morphology, size, toxicity, methods of preparations, which challenge the structural relationship among the different oligomeric species.7–9 In order to determine the structural relation between the various oligomers, two conformation-specific antibodies have been produced. These two conformation-specific antibodies identify the mutually exclusive conformational epitopes present in distinct oligomers. Two conformation-specific antibodies, anti-amyloid fibril (OC) and anti-amyloid oligomer (A11) antibodies detect the generic conformational epitopes of fibrillar and prefibrillar oligomers, respectively, on a range of amyloid-forming proteins (7–11). The OC and A11 antibodies recognize an in-register parallel β-sheet and out-of-register anti-parallel β-sheet structures, respectively (12, 13). However, how these two structurally distinct soluble Aβ oligomers cause synaptic dysfunction remains poorly understood.

Several studies have shown distinct pathways by which Aβ oligomers exhibit their neurotoxic effects in AD. This involves the interaction of Aβ oligomers with the cell membrane that results in the disruption of membrane integrity, and the binding of Aβ oligomers to various cell-surface receptors that trigger a downstream signaling cascade leading to cellular toxicity (14–16). Several mechanisms have been suggested for Aβ-induced membrane disruption (17–22). Primarily, Aβ oligomers have been found to puncture the cell membrane by the formation of ion-pore channels (23–26). The other proposed mechanism is the carpeting effect of Aβ, which causes an increase in the membrane conductance either by lowering the membrane dielectric barrier, thinning of the membrane, or spreading the lipid head groups (27–29). The precise

mechanism of Aβ-induced cell death is not defined yet, but studies support the notion that Aβ stimulates the influx of small ions, mainly Ca^{2+} ions, resulting in the membrane disruption (30). A body of evidence indicates that the membrane permeabilization depends on the conformational state of soluble Aβ oligomers (31, 32). Therefore, it is of paramount importance to understand the underlying mechanism of how two structurally distinct soluble Aβ oligomers impact membrane integrity. In this work, using brain total lipid extract (BTLE), we show that the A11-positive Aβ42 oligomers interact with the hydrophobic core of the lipid membrane via conformational change, leading to the membrane rigidification and the OC-positive Aβ42 oligomers interact with the lipid membrane in an electrostatic manner through the polar N-terminal of Aβ42 oligomers. Our studies revealed two different mechanisms by which two conformationally distinct Aβ42 oligomers interact with the lipid membrane and cause toxicity.

4.2 Experimental section

4.2.1 Materials

Sodium phosphate dibasic, Sodium chloride, Sodium hydroxide, Sodium azide, 4-(2-Hydroxyethyl)piperazine-1-ethanesulphonic acid (HEPES), Triton X-100, 1,6-Diphenyl-1,3,5-hexatriene (DPH), Bis[N,N-bis(carboxymethyl) aminomethyl] fluorescein (calcein), Dimethyl sulfoxide (DMSO), Chloroform and 1,1,1,3,3,3-Hexafluoro-2-propanol (HFIP) were procured from Sigma (St. Louis, MO, USA). Potassium chloride was purchased from HiMedia. Beta-Amyloid (42) and FAM-labeled, Beta-Amyloid (1-42) were obtained from Anaspec (USA). Chloroform solutions of 1-palmitoyl-2-oleoyl-sn-glycero-3-phosphoserine (POPS), 1-palmitoyl-2-oleoyl-sn-glycero-3-phosphocholine (POPC), and Brain total lipid extract (Porcine) were procured from Avanti Polar Lipids (Albaster, AL, USA).

4.2.2 Preparation of large unilamellar vesicles (LUVs)

Lipid vesicles were prepared using brain total lipid extract (BTLE), zwitterionic phospholipid, POPC, and a mixture of pure phospholipids, zwitterionic, POPC and anionic lipid, POPS in 3:1 molar ratio. The required volume of chloroform solutions of lipids was withdrawn using Hamilton syringe into a round bottom flask and dried the lipids under a gentle stream of nitrogen. To remove the residual traces of chloroform, the lipid film was further dried under vacuum for 3-4 h. After drying, hydration of the lipid film was carried out using PBS buffer, pH

7.4, for 1 h with intermittent vortexing to produce multilamellar vesicles. We subjected these multilamellar vesicles to 5 alternate freeze-thaw cycles using liquid nitrogen for freezing and dipped in hot water for thawing. To prepare LUVs, the resulting lipid vesicles were extruded through a polycarbonate filter of 100 nm pore size using the extrusion technique. The size of the LUVs was confirmed using dynamic light scattering (DLS) measurements on a Malvern Zetasizer Nano ZS90 instrument.

4.2.3 Steady-state fluorescence

All the steady-state fluorescence experiments were carried out on Fluormax-4 (Horiba Jobin Yvon, NJ) in PBS buffer, pH 7.4 using 10 X 1 mm fluorescence cuvette. The concentration of LUVs of BTLE was 76 μg. The concentrations of pure phospholipids, POPC, and the mixture of phospholipids (POPC:POPS in 3:1 ratio) were maintained at 100 μM. The samples of LUVs with Aβ oligomers were incubated for 2 h at room temperature. Steady-state fluorescence anisotropy (r_{ss}) was calculated using the following equation:

$$r_{ss} = \left(I_{\parallel} - I_{\perp}G\right) / \left(I_{\parallel} + 2I_{\perp}G\right) \ldots(1)$$

Here $I_{\parallel}$ and $I_{\perp}$ are the fluorescence intensities collected at 0° and 90° with respect to the excitation polarizer and $I_{\perp}$ was corrected using G-factor.

For DPH fluorescence experiments, 2 μM of DPH was added into the samples of lipid vesicles of BTLE containing different concentrations of Aβ oligomers. For the samples containing vesicles of POPC and mixture of phospholipids (POPC and POPS), DPH was used in 100:1 ratio of lipid:DPH. DPH fluorescence was monitored using excitation wavelength 355 nm, and the steady-state fluorescence anisotropy was measured at 425 nm.

For fluorescein fluorescence experiments, 76 μg of BTLE vesicles were added into 38 μg of FAM-labeled Aβ oligomers. The fluorescence was monitored by exciting the sample at 485 nm and the fluorescence spectra were recorded in the range of 500-600 nm. The steady-state fluorescence anisotropy was measured at 525 nm.

4.2.4 Time-resolved fluorescence measurements

The picosecond time-resolved fluorescence intensity decay and anisotropy decay measurements were carried out using time-correlated single-photon counting (TCSPC) setup (Horiba Jobin Yvon, NJ) as described previously (33, 34). The concentrations of lipid vesicles of BTLE and Aβ oligomers used for the sample preparation were 76 μg and 38 μg, respectively. For lipid vesicles of a mixture of pure phospholipids (POPC and POPS in 3:1 ratio), 100 μM of lipid vesicles were added into Aβ oligomers at 25:1 molar ratio of lipid:Aβ. The samples were incubated at room temperature for 2 h.

For DPH time-resolved fluorescence decays, the samples were excited using a 375-nm NanoLED picosecond laser diode. The instrument response function (IRF) was collected using a dilute solution of colloidal silica, and the full-width at half maximum (FWHM) was estimated to be ~ 260 ps. The emission wavelength was fixed at 425 nm, with a bandpass of 8 nm. The time-resolved DPH fluorescence intensity decays were measured at the magic angle of 54.7° with respect to the polarization of the incident light. The intensity decays were deconvoluted and analyzed with respect to IRF by using the following relationship:

$$I\,(t) = \alpha_1 e^{-t/\tau_1} + \alpha_2 e^{-t/\tau_2} \quad \ldots(2)$$

where, α_1 and α_2 represent the contributions associated with the two different lifetime components, τ_1 and τ_2, respectively. The typical parameters recovered from the analysis were shown in Table S2.

In order to perform the time-resolved anisotropy decay measurement of FAM-labeled Aβ oligomers, the samples were excited using a 485-nm NanoLED picosecond laser diode. FWHM was estimated to be ~ 275 ps. The emission wavelength was fixed at 525 nm with a bandpass of ~ 6 nm.

To carry out the time-resolved fluorescence anisotropy decay measurements for both DPH and FAM-labeled Aβ oligomers, the fluorescence intensities were collected at 0° [$I_{\parallel}(t)$] and 90° [$I_{\perp}(t)$] with respect to the geometric orientation of the excitation polarizer. The perpendicular component, $I_{\perp}(t)$, was corrected using G-factor. The anisotropy decays were analyzed by global

fitting of $I_{\parallel}(t)$ and $I_{\perp}(t)$ using the following equations, as described in our previous reports (33, 34).

$$I_{\parallel}(t) = I(t)[1 + 2r(t)]/3 \ldots(3)$$

$$I_{\perp}(t) = I(t)[1 - r(t)]/3 \ldots(4)$$

The time-resolved anisotropy decay, r(t) was characterized using the biexponential decay equation as follows:

$$r(t) = r_0 \left[\beta_{fast} e^{\left(-\frac{t}{\phi_{fast}}\right)} + \beta_{slow} e^{\left(-\frac{t}{\phi_{slow}}\right)}\right] \ldots(5)$$

where, r_0 represents the initial anisotropy. The anisotropy decay displayed two rotational correlation times, ϕ_{fast} and ϕ_{slow} and two associated amplitudes, β_{fast} and β_{slow}, respectively. ϕ_{fast} and ϕ_{slow} represent the local rotational mobility of the fluorophore and the overall global tumbling. The typical parameters recovered from the analysis of time-resolved fluorescence anisotropy decay of DPH and fluorescein were shown in Table S1 and Table S3.

In order to do the correct estimation of ϕ_{slow} that accounts for the slow diffusive dynamics of the DPH embedded vesicles, we varied ϕ_{slow} while keeping the shorter component, ϕ_{fast} fixed in our anisotropy decay analysis program. In each case, the goodness of fit was determined by reduced χ^2 values, the randomness of the residuals, and autocorrelation functions. In this way, we were able to assign ϕ_{slow} component as >175 ns, which allows us to extract the non-zero limiting anisotropy (r_∞). We calculated the membrane order parameter (S) by using the following equation (35):

$$S = \sqrt{\left(\frac{r_\infty}{r_o}\right)} \ldots(6)$$

4.2.5 Calcein release assay

For calcein release assay, we used 50 mM HEPES 5 mM NaCl buffer, pH 7.4 instead of PBS buffer (used in all the experiments) because of the very low solubility of calcein in PBS buffer. Calcein loaded vesicles were prepared as described above with slight modifications. The lipid film was hydrated in 50 mM HEPES 5 mM NaCl buffer containing 40 mM calcein. The resulting

suspension was subjected to freeze-thaw cycles followed by extruding the vesicles using a 100 nm polycarbonate filter. To separate free calcein from calcein-encapsulated LUVs, vesicles were loaded on Superdex G-75 (GE Healthcare) column. The eluted liposomal fractions were checked for the empty/leaky vesicles by monitoring the release of self-quenched calcein from the disruption of calcein-encapsulated vesicles. The fractions showing a significant increase in the calcein fluorescence upon addition of 3 % Triton X-100 were pooled together and used for the experiments. Calcein release was monitored using an excitation wavelength of 490 nm and an emission wavelength of 520 nm. The efficiency was calculated using the following equation:

$$Calcein\ release\ efficiency\ (\%) = [(F - F_0)/(F_{100} - F_0)] \times 100 \quad \ldots(7)$$

where, F is the observed fluorescence intensity upon addition of Aβ oligomers, F_0 is the initial fluorescence intensity of calcein-encapsulated vesicles, and F_{100} is the final fluorescence observed upon addition of 3 % Triton X-100. Calcein release efficiency of Aβ oligomers was reported after 4 h of the addition of 4 μM of Aβ oligomers into the vesicles.

4.2.6 Atomic force microscopy (AFM)

Thirty-eight μg of Aβ oligomers with and without the lipid vesicles of BTLE in a ratio of 2:1 of lipid:Aβ were incubated at room temperature for 24 h. After incubation, 20 μL of the samples were deposited on freshly cleaved and filtered milli-Q water-washed micas. The samples were incubated on mica for 5 minutes, followed by washing with 100 μL of filtered water twice. The samples were dried under a gentle stream of nitrogen and imaged on Innova atomic force microscopy (Bruker) using NanoDrive (v8.03) software. The images were processed using WSxM 5.0 Develop 8.3 (36).

4.3 Results

4.3.1 Dynamics of lipid membranes with Aβ oligomers using DPH

In order to investigate the interaction of Aβ oligomers with the lipid membrane, we initiated our studies by assessing the dynamical properties of the lipid membrane using the brain total lipid extract (BTLE), which is considered as the closest mimic of the neuronal membranes (37). We prepared the large unilamellar vesicles (LUVs) of size ~ 100 nm (Figure 4.1a). The two conformationally distinct Aβ oligomers have been prepared from synthetic Aβ42 peptide and

characterized using dot-blot assay by probing with A11 and OC antibodies as shown in our previous study (38). In order to examine the membrane microviscosity of the lipid bilayer, we utilized a well-known lipophilic fluorescent probe, 1,6-diphenyl-1,3,5-hexatriene (DPH). DPH anisotropy has been widely utilized to report the dynamics of the hydrophobic core of the lipid acyl chain regions of the membrane (39-41). We monitored the steady-state fluorescence

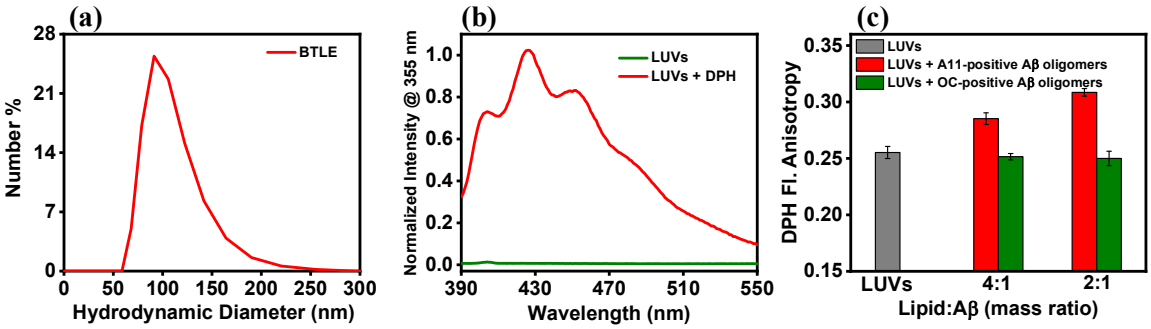

Figure 4.1. (a) Size distribution of lipid vesicles derived from BTLE by dynamic light scattering measurements (DLS). (b) Normalized spectra of 76 µg LUVs of BTLE with (red) and without DPH (olive) showing insignificant counts for LUVs without DPH. (c) Steady-state DPH fluorescence anisotropy of 76 µg of LUVs of BTLE without (grey) and with A11-(red) and OC-positive Aβ oligomers (olive) at different mass ratios of lipid:Aβ. The bar plot shows the mean ± standard deviation (n = 3).

anisotropy of DPH embedded LUVs at different ratios of lipid:Aβ. Since 60 % structural identity of lipids in BTLE is unknown (provided by Avanti Polar Lipids), we used a mass ratio of lipid:Aβ. In order to avoid the lipid-induced artifacts of scattering, we recorded the spectra of LUVs with and without DPH, which showed a very minimal scattering contribution from the lipid vesicles (Figure 4.1b). The DPH anisotropy of LUVs without Aβ oligomers was 0.24-0.25 (Figure 4.1c). Upon addition of A11-positive Aβ oligomers to DPH embedded LUVs, we observed a significant rise in the DPH fluorescence anisotropy, indicating a substantial rigidification of the membrane in the presence of A11-positive oligomers, corroborating with the previous study (42). In contrast, the lipid vesicles with OC-positive Aβ oligomers exhibited no considerable change in the DPH anisotropy (Figure 4.1c). This suggests that the different conformations of Aβ oligomers behave different in the lipid environment. We further verified our results using a mixture of pure phospholipids that mimic the mammalian membrane

composition, comprising 25 mol % of an anionic lipid, 1-palmitoyl-2-oleoyl-sn-glycero-3-phosphoserine (POPS) and 75 mol % of zwitterionic lipid, 1-palmitoyl-2-oleoyl-sn-glycero-3-phosphocholine (POPC). We prepared the LUVs (Figure 4.2a) and monitored the steady-state DPH fluorescence at varying ratios of lipid:Aβ (Figure 4.2b & 4.2c). With pure phospholipids also, we observed a substantial increase in the DPH fluorescence anisotropy in the presence of A11-positive Aβ oligomers (Figure 4.2c). Results from both the lipid vesicles, BTLE and the pure phospholipids, exhibited an increase in membrane microviscosity with the A11-positive Aβ oligomers as compared to the OC-positive Aβ oligomers. The steady-state fluorescence anisotropy, however, does not account for the different modes of rotational dynamics of DPH on the lipid membrane (33-35).

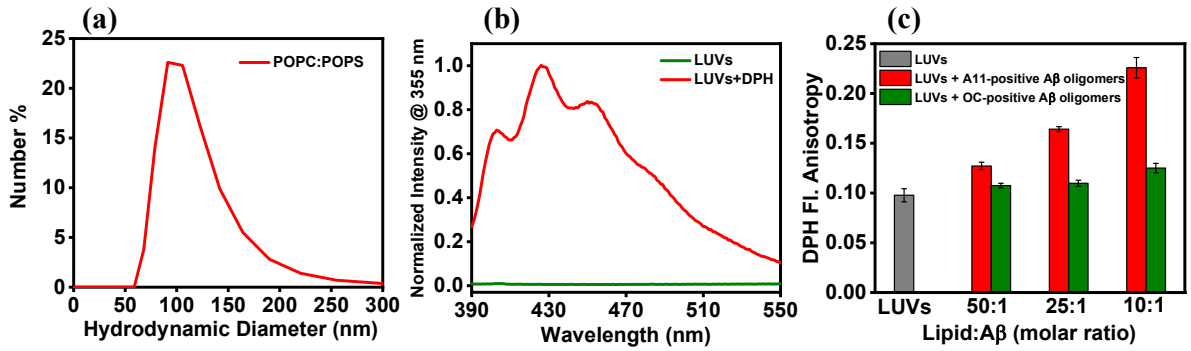

Figure 4.2. (a) Size distribution of lipid vesicles prepared from a mixture of phospholipids, POPC and POPS in 3:1 ratio by DLS. (b) Normalized spectra of 100 μM LUVs of POPC and POPS in 3:1 ratio with (red) and without DPH (olive) showing insignificant counts from LUVs without DPH. (c) Steady-state DPH fluorescence anisotropy of 100 μM LUVs of POPC and POPS in 3:1 ratio without (grey) and with A11-(red) and OC-positive Aβ oligomers (olive) at the varying ratio of LUV:Aβ (molar ratio). The bar plot shows the mean ± standard deviation (n = 3).

In order to discern the distinct dynamical motions of DPH in the vesicles, we carried out picosecond time-resolved fluorescence anisotropy decay measurements and monitored the fluorescence depolarization of DPH embedded LUVs of BTLE with and without Aβ oligomers. The time-resolved DPH fluorescence anisotropy decay profiles of LUVs exhibited typical biexponential depolarization kinetics revealing two well-defined rotational correlation times, a fast subnanosecond rotational correlation time (ϕ_{fast}) and a slow rotational correlation time (ϕ_{slow})

(Figure 4.3, Table 1). The subnanosecond component (ϕ_{fast} ~ 0.6 ns) corresponds to the wobbling-in-cone motion of DPH within the lipid vesicles (43, 44). In the presence of A11-positive Aβ oligomers, we observed a substantial rise in the value of ϕ_{fast} (~ 7 ns), indicating a drastic dampening in the local rotational motion of DPH in the lipid membrane. On the contrary, in the presence of OC-positive Aβ oligomers, we did not observe much dampening in the rotational dynamics of DPH (ϕ_{fast} ~ 1.5 ns). Our data analysis showed that ϕ_{slow} does not depolarize completely on the nanosecond timescale because of the slow rotational diffusion of the lipid vesicles, which allowed us to extract the non-zero limiting anisotropy (r_∞) with a rotational correlation time >175 ns (See Experimental section). Next, we calculated the lipid order parameter (S) from the r_∞ value using equation 6. We identified that addition of both the Aβ oligomers into the results in a slight increase in the membrane order. Lipid vesicles bound to the A11-positive oligomers displayed the highest membrane order (~ 0.87) as compared to the lipid vesicles without (~ 0.82) and with OC-positive oligomers (~ 0.84). Taken together, our DPH anisotropy data revealed that the incorporation of A11-positive Aβ oligomers into the vesicles restricts the local rotational diffusion of DPH and increases the membrane order, whereas the OC-positive Aβ oligomers do not show much interaction with the core of lipid membrane.

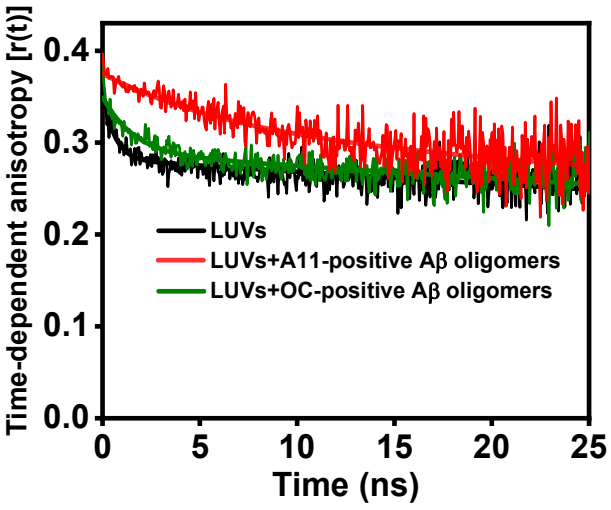

Figure 4.3 Time-resolved fluorescence anisotropy decay of DPH embedded LUVs without (black) and with A11-(red) and OC-positive Aβ oligomers (olive) at 2:1 ratio of lipid:Aβ. See the Experimental section for data analysis.

Table 1. Typical parameters recovered from the time-resolved DPH fluorescence anisotropy decay of LUVs of BTLE with and without Aβ oligomers

Sample	ϕ_{fast} (ns) (β_{fast})	ϕ_{slow} (ns) (β_{slow})	r_0	r_∞	S
LUVs	0.558±0.0281 (0.242±0.007)	>175 (0.758±0.007)	0.37	0.25	0.82
LUVs +A11-positive Aβ oligomers	7.62±1.98 (0.186±0.023)	>175 (0.814±0.023)	0.37	0.28	0.87
LUVs +OC-positive Aβ oligomers	1.52±0.176 (0.182±0.009)	>175 (0.818±0.009)	0.37	0.26	0.84

Since DPH is very sensitive to dielectric constant of the surrounding medium (45); therefore, we next asked how the microheterogeneous environment of the lipid membrane influences the location of DPH in the presence of Aβ oligomers. In order to investigate that, we measured the fluorescence intensity decays of DPH embedded vesicles and determined the lifetimes. The DPH lifetime intensity decays exhibited biexponential kinetics having two well-separated lifetimes, τ_1 and τ_2 (Figure 4.4a and equation 2 in the Experimental section). The shorter component, τ_1 reports the lifetime of DPH molecules near the membrane-water interface, and the longer component, τ_2 represents the lifetime of DPH in the hydrophobic core of the membrane (45). Our intensity decay analysis yielded τ_1 and τ_2 as ~ 5 ns and ~ 11 ns with their corresponding fractional contributions, α_1 and α_2, as ~ 10 % and 90 %, respectively, indicating a majority of DPH molecules in the non-aqueous interior of the membrane that corroborates with the previous report (45) (Table 2). Upon addition of A11-positive Aβ oligomers into the lipid vesicles, we obtained a drastic decrease in the fractional contribution, α_2 from ~ 90 to 30 % corresponding to the longer lifetime component (Figure 4.4b and Table 2), indicating the displacement of DPH molecules in the lipid membrane from the non-aqueous hydrophobic region to the membrane-water interface

in the presence of A11-positive Aβ oligomers. In contrast, the OC-positive oligomers did not exhibit any significant reduction in the fluorescence lifetime. We further verified our results using a mixture of pure phospholipids, POPC:POPS in 3:1 ratio. With pure phospholipids also, the α_2 value decreased markedly in the presence of A11-positive Aβ oligomers (Table 2). Our time-resolved fluorescence intensity data revealed that the addition of A11-positive Aβ oligomers into the lipid vesicles leads to a non-random equilibrium

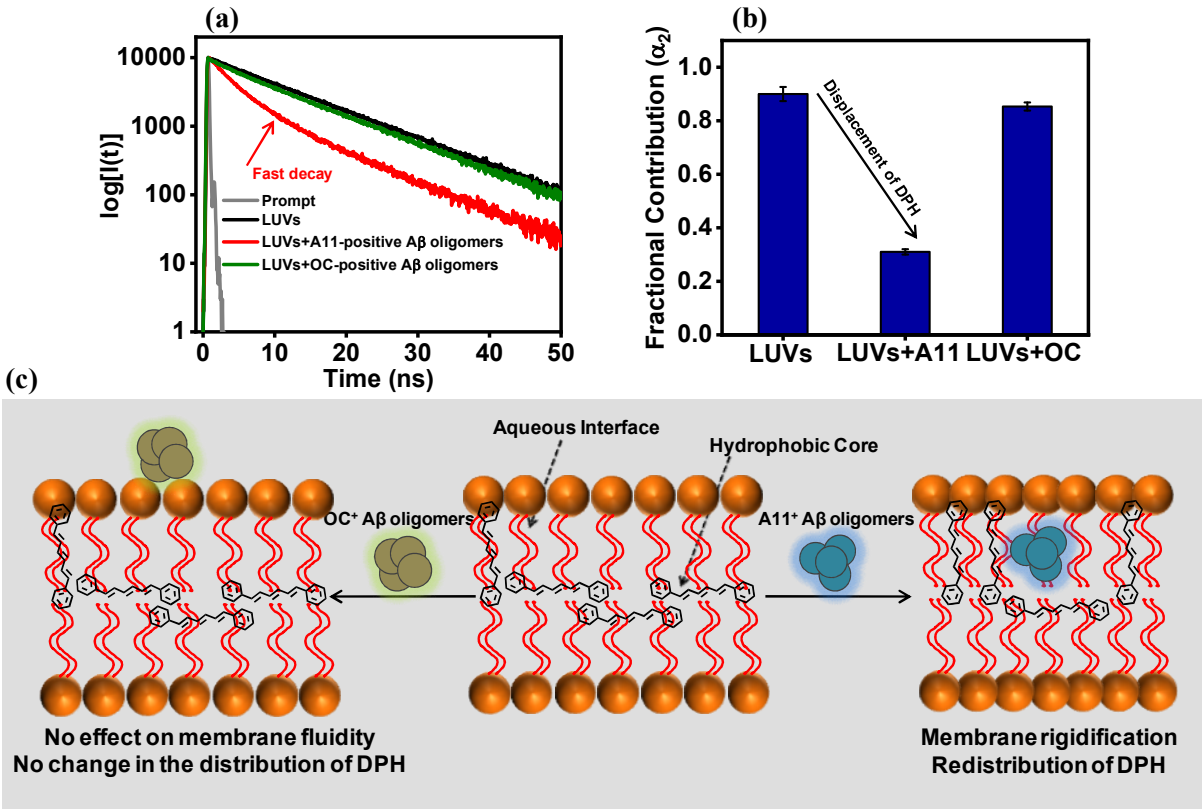

Figure 4.4. Distribution of DPH molecules in lipid vesicles. (a) Fluorescence intensity decay of DPH embedded LUVs without (black) and with A11- (red) and OC-positive Aβ oligomers (olive) at 2:1 ratio of lipid:Aβ. (b) The fractional contribution, α_2 associated with the longer fluorescence lifetime component (τ_2) of DPH embedded LUVs with and without Aβ oligomers. α_2 was calculated from three independent measurements and shown as mean ± standard deviation. See Experimental section for data analysis and Table 2 for the associated recovered parameters from the analysis. (c) Schematic of distribution of the DPH population in the vesicles upon addition of Aβ oligomers.

Table 2. Typical parameters associated with the time-resolved DPH fluorescence intensity decay of LUVs of BTLE with and without Aβ oligomers

Sample	BTLE LUVs		POPC:POPS LUVs in 3:1 ratio	
	τ_1 (ns) (α_1)	τ_2 (ns) (α_2)	τ_1 (ns) (α_1)	τ_2 (ns) (α_2)
LUVs	4.98±0.05 (0.10±0.02)	11.06±0.20 (0.90±0.02)	4.25±0.07 (0.16±0.03)	9.22±0.06 (0.84±0.03)
LUVs +A11-positive Aβ oligomers	2.84±0.04 (0.69±0.01)	9.15±0.13 (0.31±0.01)	3.14±0.05 (0.53±0.01)	8.57±0.045 (0.47±0.01)
LUVs +OC-positive Aβ oligomers	3.07±0.18 (0.15±0.01)	10.77±0.11 (0.85±0.02)	4.14±0.06 (0.23±0.01)	9.06±0.03 (0.77±0.01)

redistribution of DPH in an aqueous/non-aqueous interface, resulting in a substantial rise in the DPH population near to the membrane-water interface (Figure 4.4c). We speculate that the displacement of DPH molecules to the membrane-water interface due to the addition of A11-positive Aβ oligomers could be attributed to the membrane permeabilization. In order to probe the membrane permeabilization, we performed a well-known calcein release assay. Membrane permeabilization causes a release in the calcein from the lipid vesicles, which would result in an enhancement in the fluorescence intensity (46). We observed a very slight increase in the fluorescence intensity upon addition of both A11- and OC-positive oligomers as compared to that observed with Triton X-100, indicating a low tendency of membrane permeabilization by Aβ oligomers (Figure 4.5a). We next visualized the nanoscopic morphology of the heterotypic

assembly of lipid vesicles and Aβ oligomers using atomic force microscopy (AFM). Our AFM imaging data showed that the two structurally distinct Aβ oligomers consist of oligomeric species of various sizes, and these oligomers matured into amyloid fibrils upon interaction with the lipid membrane (Figure 4.5). Taken together, our studies revealed that both the conformationally distinct Aβ oligomers undergo lipid-induced aggregation to form fibrils; however, the mechanism by which these two structurally distinct Aβ oligomers interact with the lipid membrane is different. Therefore, we next embarked upon studies delineating the mechanism of interaction of two conformationally distinct Aβ oligomers with the lipid membrane.

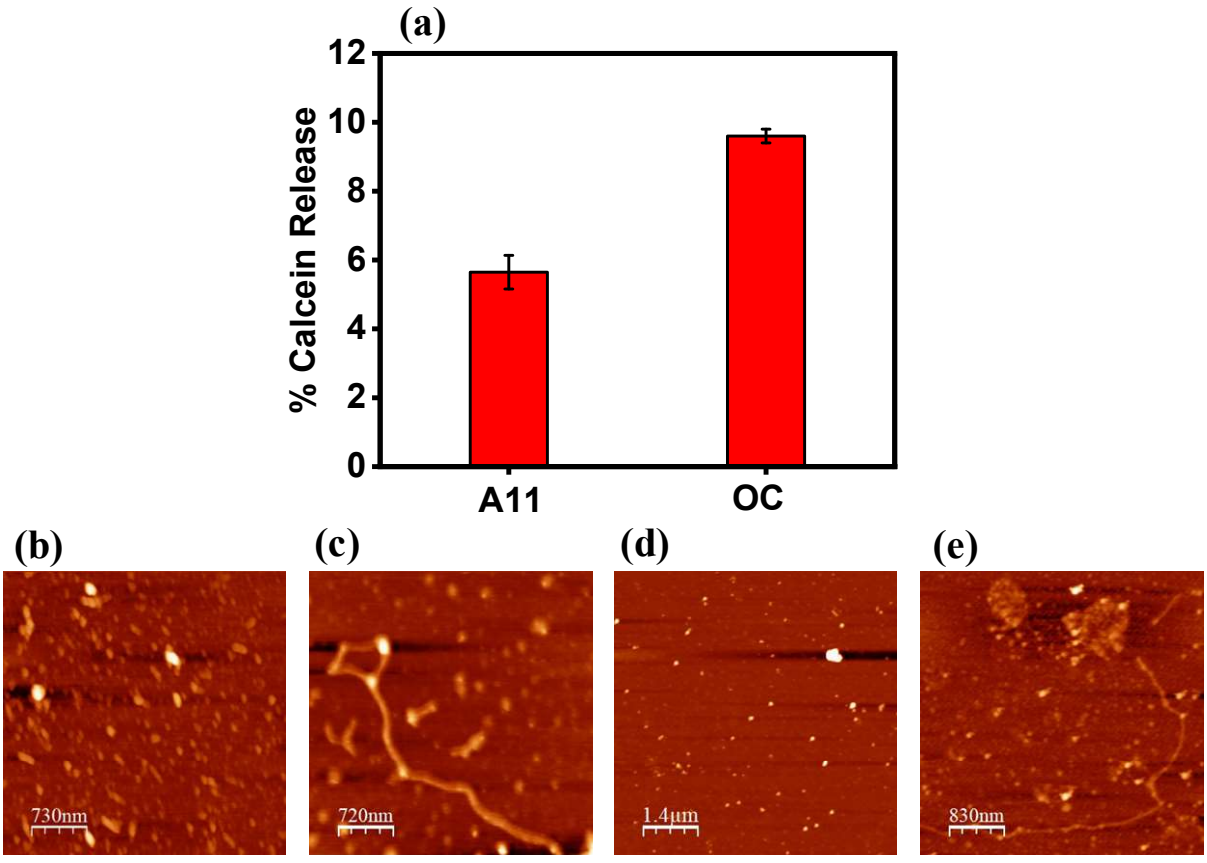

Figure 4.5 (a) Calcein release efficiency of LUVs derived from BTLE upon the addition of 4 µM of A11- and OC-positive Aβ oligomers. The calcein release efficiency was calculated using equation 7. AFM images of Aβ oligomers without and with LUVs of BTLE. (b) A11-positive Aβ

oligomers, (c) LUVs-bound A11-positive Aβ oligomers, (d) OC-positive Aβ oligomers and (e) LUVs-bound OC-positive Aβ oligomers.

4.3.2 Mechanisms of interaction of Aβ oligomers with lipid membranes

A closer look at the amino acid sequence of Aβ peptide revealed that Aβ is negatively charged. In addition, the A11-positive Aβ oligomers exhibited an increase in the DPH fluorescence anisotropy with the negatively charged LUVs, whereas, with the OC-positive Aβ oligomers, the DPH anisotropy remains unaltered (Figure 4.1c). Therefore, we conjectured that the A11-positive Aβ oligomers might interact with the lipid vesicles in a hydrophobic manner, and the OC-positive Aβ oligomers might oppose the interaction due to an electrostatic repulsion with the lipid membrane. To verify the mechanisms of interaction, we eliminated the negative charge from vesicles by preparing LUVs of a zwitterionic lipid, POPC, and monitored the steady-state DPH fluorescence anisotropy. The DPH anisotropy of lipid vesicles without the Aβ oligomers was ~ 0.09 (Figure 4.6a). We observed an increase in the DPH anisotropy of LUVs in the presence of both A11- and OC-positive oligomers. An increase in the DPH anisotropy of zwitterionic lipid vesicles with OC-positive oligomers as opposed to the negatively charged lipids suggests a critical role of electrostatic interaction (Figure 4.1c and 4.6a). On the contrary, high DPH anisotropy in the presence of A11-positive oligomers for both the lipid vesicles, zwitterionic and anionic, indicate the hydrophobic interaction between A11-positive Aβ oligomers and the lipid membrane. Aβ is an amphipathic peptide having a polar N-terminal segment and a hydrophobic C-terminal tail. Therefore, we believe that the A11-positive Aβ oligomers interact with the hydrophobic core of lipid vesicles via C-terminal, whereas the OC-positive Aβ oligomers interact with the polar headgroups of the lipid membrane through the N-terminal. We next probed the N-terminal of Aβ and examined the behavior of Aβ oligomers in the vicinity of lipid vesicles.

In order to probe the N-terminal of oligomers, we prepared two conformationally distinct Aβ oligomers using N-terminal carboxyfluorescein (FAM)-labeled Aβ42 peptide and monitored the steady-state fluorescence. In the free form, the A11- and OC- positive Aβ oligomers displayed low values of anisotropy ~ 0.05 and ~ 0.04, respectively suggests an intrinsically disordered nature of the N-terminal of Aβ oligomers, which is in line with the previous report (Figure 4.6b)

(7). Surprisingly, we observed a decrease in the fluorescence anisotropy of A11-positive Aβ oligomers upon binding to the lipid membrane, whereas the OC- positive Aβ oligomers did not show any change in the anisotropy with and without the lipid vesicles (Figure 4.6b). This observation suggests that the N-terminal of A11-positive Aβ oligomers experience less rotational

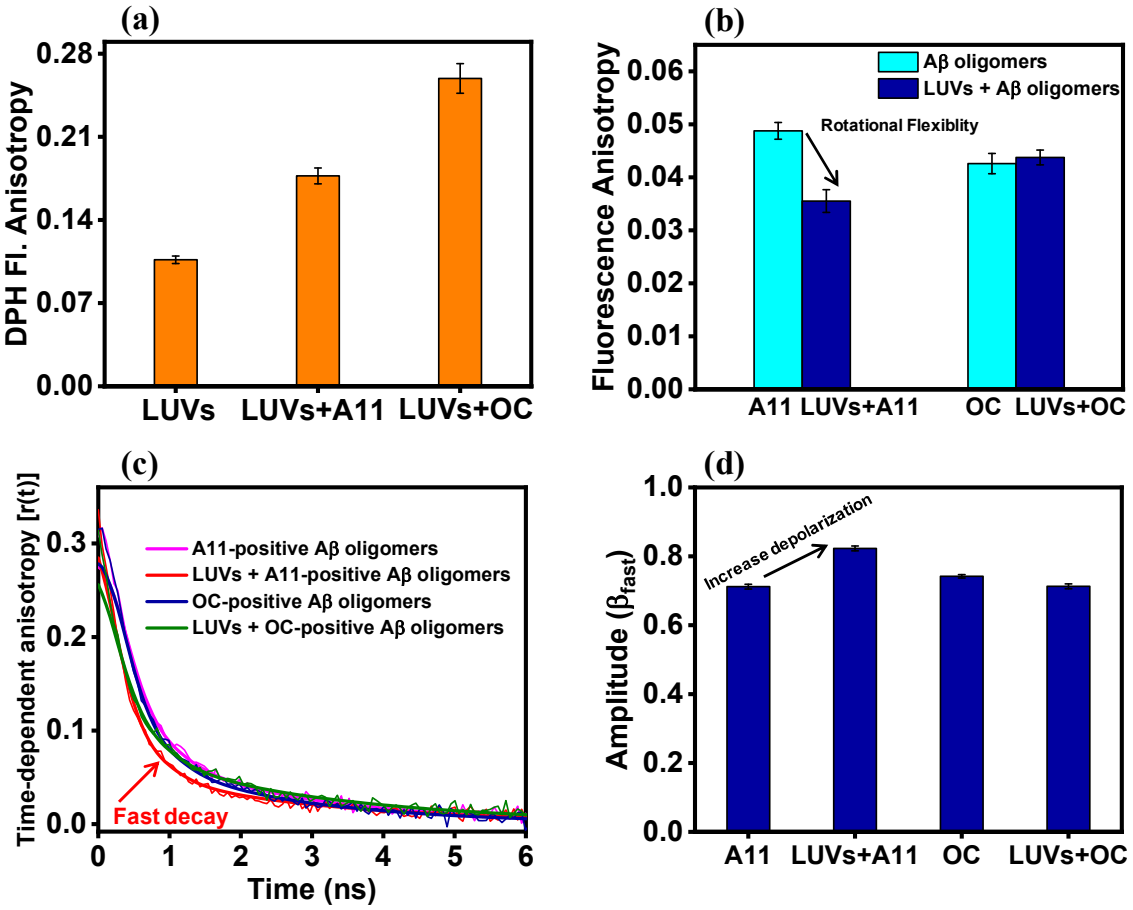

Figure 4.6 (a) Steady-state DPH fluorescence anisotropy of 100 μM of LUVs of POPC without and with Aβ oligomers at 25:1 ratio of lipid:Aβ (molar ratio). (b) Steady-state fluorescence anisotropy of N-terminal FAM-labeled Aβ oligomers without (cyan) and with LUVs of BTLE (royal blue) at 2:1 ratio of lipid:Aβ (mass ratio). The bar plot shows the mean ± standard deviation (n = 3). (c) Time-dependent fluorescence anisotropy decays of FAM-labeled Aβ oligomers without and with LUVs of BTLE at 2:1 ratio of lipid:Aβ. (d) Amplitude (β_{fast}) associated with the fast rotational correlation time of FAM-labeled Aβ oligomers with and without lipid vesicles. β_{fast} was calculated from atleast three independent measurements and shown as mean ± standard deviation. See Experimental section for data analysis.

Table 3. Typical parameters associated with the time-resolved fluorescence anisotropy decay of N-terminal FAM-labeled Aβ oligomers and lipid-bound FAM-labeled Aβ oligomers

Sample	ϕ_{fast} (ns) (β_{fast})	ϕ_{slow} (ns) (β_{slow})
A11-positive Aβ oligomers	0.368±0.015 (0.712±0.007)	2.38±0.01 (0.288±0.007)
OC-positive Aβ oligomers	0.345±0.009 (0.742±0.005)	2.28±0.12 (0.258±0.005)
LUVs + A11-positive Aβ oligomers	0.335±0.019 (0.823±0.007)	2.67±0.11 (0.177±0.007)
LUVs + OC-positive Aβ oligomers	0.370±0.020 (0.710±0.007)	2.69±0.08 (0.287±0.007)

constraint after binding to the lipid membrane, and the binding might be accompanied with a conformational change. In order to study the conformational dynamics, we next measured the picosecond time-resolved fluorescence depolarization kinetics of FAM-labeled Aβ oligomers. The anisotropy decay exhibited biexponential depolarization kinetics having two well-resolved rotational correlation times, ϕ_{slow} and ϕ_{fast} (Figure 4.6c). The fast subnanosecond component reports the local rotational dynamics of the fluorophore and the longer nanosecond component corresponds to the global rotational diffusion of Aβ oligomers with and without the lipid vesicles. We observed that the faster subnanosecond component (ϕ_{fast} ~ 0.35 ns) results in ~ 72 % (β_{fast}) depolarization of the initial anisotropy in the case of both OC- and A11-positive Aβ oligomers. This short rotational timescale with large amplitude represents the backbone segmental fluctuations in the disordered N-terminal of Aβ oligomers as shown in our previous work (34). Upon binding to the lipid vesicles, the A11-positive Aβ oligomers exhibited much

higher amplitude (β_{fast} ~ 82 %) of the local rotational mobility (Figure 4.6d), suggesting an increase in the extent of torsional mobility of the N-terminal of lipid-bound A11-positive Aβ oligomers. In contrast, the OC-positive Aβ oligomers with lipid vesicles showed no significant changes in the amplitudes (Figure 4.6d, Table 3). Our studies provide compelling evidence for a conformational change in the N-terminal of A11-positive Aβ oligomers upon interaction with the lipid membrane. On the contrary, no such conformational change was identified for the OC-positive Aβ oligomers with lipid vesicles.

4.4 Discussion

Based on all our results, we propose a model for the mechanisms of interaction of two conformationally distinct Aβ oligomers with the lipid membrane derived from BTLE (Figure 4.7). The two structurally distinct Aβ oligomers are recruited into amyloid fibrils upon binding to the lipid membrane via different mechanisms of interaction. Our results revealed that the N-terminal of A11-positive Aβ oligomers undergo a conformational change that allows the interaction of the C-terminal of Aβ oligomers with the hydrophobic core of the vesicles, resulting in an increase in the membrane microviscosity. On the contrary, the interaction between OC-positive Aβ oligomers and lipid vesicles is governed electrostatically through the polar N-terminal region of Aβ oligomers. Our time-resolved DPH fluorescence anisotropy data, along with the lifetime data, provides an important insight into the microheterogeneous environment of the lipid membrane. More preferential partitioning of DPH molecules in the hydrophobic core of the lipid vesicles with and without OC-positive Aβ oligomers results in a faster wobbling-in-cone motion of DPH within the lipid vesicles. In comparison, a substantial rise in the population of DPH near the membrane-water interface or the polar head group of the lipids due to the addition of A11-positive Aβ oligomers results in slower rotational motion of DPH within the lipid vesicles. This is due to the following reason. Two different locations of DPH in the lipid vesicles experience different rotational motions depending on the surrounding environment. The tumbling of DPH near the membrane-water interface is slower than the hydrophobic core of the lipid vesicles due to more packing density or more order in the polar head groups of the lipids. The displacement of DPH molecules to the membrane-water interface in the presence of A11-positive oligomers causes an increase in the rotational correlation time. Therefore, DPH serves as the reporter of the microheterogeneous environment of the lipid membrane. Mounting evidence,

along with our previous study, shows that the A11-positive Aβ oligomers (type 1) are more toxic than the OC-positive Aβ oligomers (type 2) (34, 47). A recent study has also indicated that the A11-positive Aβ oligomers (A+) induce Ca^{2+} dyshomeostasis in monosialotetrahexosylganglioside (GM1)-enriched cells (48). The impact of A11-positive Aβ oligomers on the dynamical properties of the lipid membrane could be a mechanism by which these Aβ oligomers induce an influx of Ca^{2+} in the cells and cause toxicity. The OC-positive Aβ oligomers might bypass the toxicity by demonstrating no significant effect on the membrane fluidity. Our findings provide a general mechanism of interaction by which the two conformationally distinct oligomers of many different amyloidogenic proteins interact with the lipid membrane.

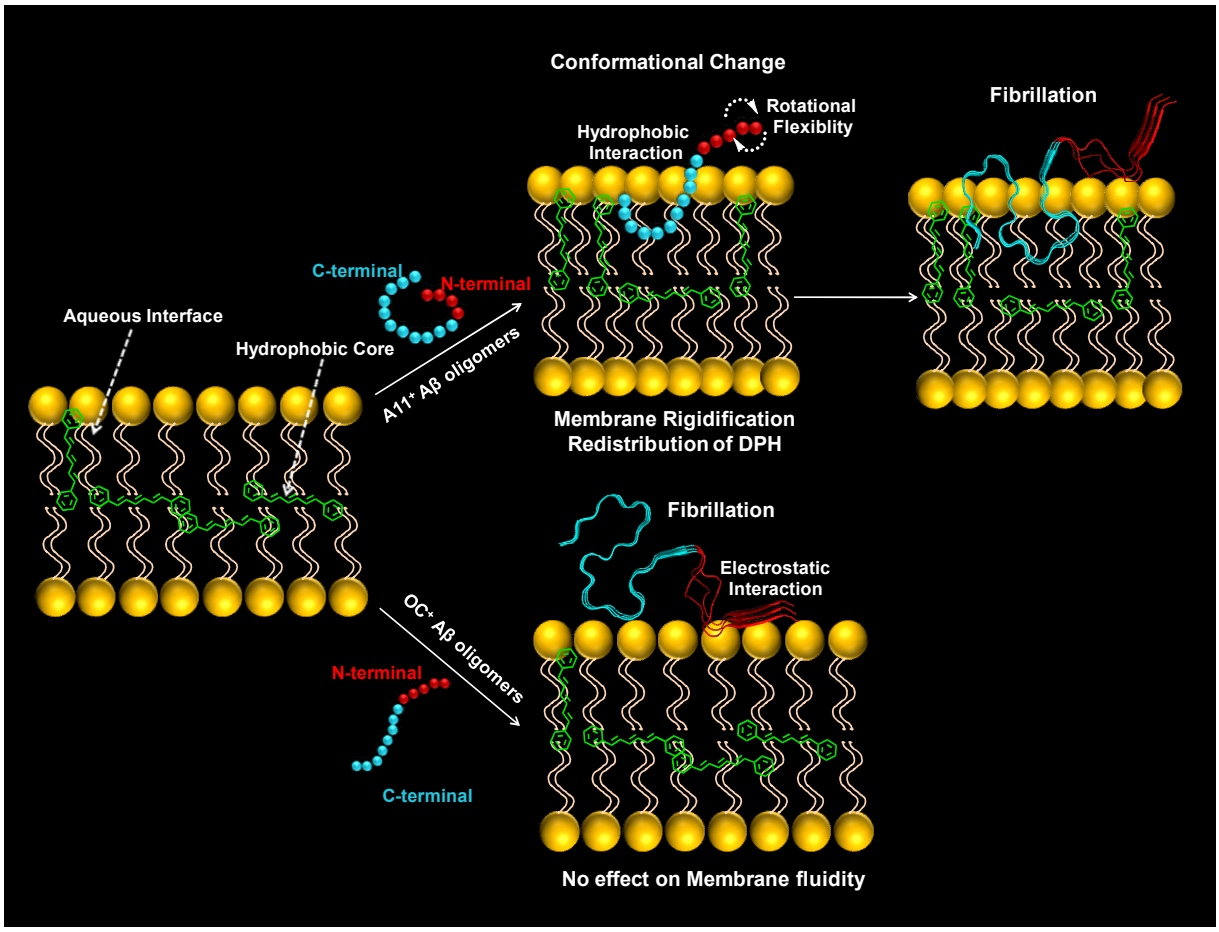

Figure 4.7 Proposed model for the mechanism of interaction of conformationally distinct Aβ oligomers with the lipid membrane. The structure of Aβ (1-42) fibril (PDB ID: 2NAO) was generated using PyMOL (Version 2.0.7, Schrödinger, LLC, New York) (49).

4.5 References

(1) Liu, P.-P.; Xie, Y.; Meng, X.-Y.; Kang, J.-S. (2019) History and Progress of Hypotheses and Clinical Trials for Alzheimer's Disease. *Signal Transduct. Target. Ther.* **4 (1),** 29.

(2) Deture, M. A.; Dickson, D. W. (2019) The Neuropathological Diagnosis of Alzheimer's Disease. *Mol. Neurodegener.* **14 (1),** 1–18.

(3) Selkoe, Dennis J. & Hardy, J. (2016) The Amyloid Hypothesis of Alzheimer's Disease at 25 Years. *EMBO Mol. Med.* **8 (6),** 595–608.

(4) Ding, Y.; Zhao, J.; Zhang, X.; Wang, S.; Viola, K. L.; Chow, F. E.; Zhang, Y.; Lippa, C.; Klein, W. L.; Gong, Y. (2019) Amyloid Beta Oligomers Target to Extracellular and Intracellular Neuronal Synaptic Proteins in Alzheimer's Disease. *Front. Neurol.* **10,** 1–16.

(5) Cline, E. N.; Bicca, M. A.; Viola, K. L.; Klein, W. L. (2018) The Amyloid-β Oligomer Hypothesis : Beginning of the Third Decade. *J. Alzheimers Dis.* **64,** S567-S610.

(6) Sengupta, U.; Nilson, A. N.; Kayed, R. (2016) The Role of Amyloid- β Oligomers in Toxicity, Propagation , and Immunotherapy. *EBioMedicine* **6,** 42–49.

(7) Breydo, L.; Kurouski, D.; Rasool, S.; Milton, S.; Wu, J. W.; Uversky, V. N.; Lednev, I. K.; Glabe, C. G. (2016) Structural Differences between Amyloid Beta Oligomers. *Biochem. Biophys. Res. Commun*. **477 (4),** 700–705.

(8) Glabe, C. G. (2008) Structural Classification of Toxic Amyloid Oligomers. *J. Biol. Chem.* **283 (44),** 29639–29643.

(9) Kayed, R.; Head, E.; Thompson, J. L.; Mcintire, T. M.; Milton, S. C.; Cotman, C. W.; Glab, C. G. (2003) Common Structure of Soluble Amyloid Oligomers Implies Common Mechanism of Pathogenesis. *Science* **486,** 486–490.

(10) Kayed, R.; Head, E.; Sarsoza, F.; Saing, T.; Cotman, C. W.; Necula, M.; Margol, L.; Wu, J.; Breydo, L.; Thompson, J. L.; Rasool, S.; Gurlo, T.; Butler, P.; Glabe, C. G. (2007) Fibril Specific, Conformation Dependent Antibodies Recognize a Generic Epitope Common to Amyloid Fibrils and Fibrillar Oligomers That Is Absent in Prefibrillar

Oligomers. *Mol. Neurodegener.* **2 (1),** 1–11.

(11) Wu, J. W.; Breydo, L.; Isas, J. M.; Lee, J.; Kuznetsov, Y. G.; Langen, R.; Glabe, C. (2010) Fibrillar Oligomers Nucleate the Oligomerization of Monomeric Amyloid β but Do Not Seed Fibril Formation. *J. Biol. Chem.* **285 (9),** 6071–6079.

(12) Laganowsky, A.; Liu, C.; Sawaya, M. R.; Whitelegge, J. P.; Park, J.; Zhao, M.; Pensalfini, A.; Soriaga, A. B.; Landau, M.; Teng, P. K.; Cascio, D.; Glabe, C.; Eisenberg, D. (2012) Atomic View of a Toxic Amyloid Small Oligomer. *Science* **335 (6073),** 1228–1231.

(13) Liu, C.; Zhao, M.; Jiang, L.; Cheng, P.-N.; Park, J.; Sawaya, M. R.; Pensalfini, A.; Gou, D.; Berk, A. J.; Glabe, C. G.; Nowick, J.; Eisenberg, D. (2012) Out-of-Register β-Sheets Suggest a Pathway to Toxic Amyloid Aggregates. *Proc. Natl. Acad. Sci. U. S. A.* **109 (51),** 20913–20918.

(14) De, S.; Whiten, D. R.; Ruggeri, F. S.; Hughes, C.; Rodrigues, M.; Sideris, D. I.; Taylor, C. G.; Aprile, F. A.; Muyldermans, S.; Knowles, T. P. J.; Vendrsucolo, M.; Bryant, C.; Blennow, K.; Skoog, I.; Ken, S.; Zetterberg, H.; Klenerman, D. (2019) Soluble Aggregates Present in Cerebrospinal Fluid Change in Size and Mechanism of Toxicity during Alzheimer's Disease Progression. *Acta Neuropathol. Commun.* **7 (1),** 120.

(15) Benilova, I.; Karran, E.; Strooper, B. De. (2012) The Toxic Aβ Oligomer and Alzheimer's Disease : An Emperor in Need of Clothes. *Nat. Neurosci.* **15 (3),** 349–357.

(16) Kayed, R.; Lasagna-reeves, C. A. (2013) Molecular Mechanisms of Amyloid Oligomers Toxicity. *J. Alzheimers Dis.* **33,** S67-S78.

(17) Mrdenovic, D.; Majewska, M.; Pieta, I. S.; Bernatowicz, P.; Nowakowski, R.; Kutner, W.; Lipkowski, J.; Pieta, P. (2019) Size-Dependent Interaction of Amyloid β Oligomers with Brain Total Lipid Extract Bilayer-Fibrillation Versus Membrane Destruction. *Langmuir* **35,** 11940–11949.

(18) Canale, C.; Oropesa-Nunez, R.; Diaspro, A.; Dante, S. (2018) Amyloid and Membrane Complexity: The Toxic Interplay Revealed by AFM. *Semin Cell Dev Biol* **73,** 82–94.

(19) Kotler, S. A.; Walsh, P.; Brender, J. R.; Ramamoorthy, A. (2014) Differences between

Amyloid-β Aggregation in Solution and on the Membrane: Insights into Elucidation of the Mechanistic Details of Alzheimer's Disease. *Chem. Soc. Rev.* **43 (19),** 6692–6700.

(20) Williams, T. L.; Serpell, L. C. (2011) Membrane and Surface Interactions of Alzheimer's Aβ Peptide – Insights into the Mechanism of Cytotoxicity. *FEBS J.* **278,** 3905–3917.

(21) Butterfield, S. M.; Lashuel, H. A. (2010) Amyloidogenic Protein – Membrane Interactions : Mechanistic Insight from Model Systems *Angew. Chem. Int. Ed.* 5628–5654.

(22) Lau, T.; Ambroggio, E. E.; Tew, D. J.; Cappai, R.; Masters, C. L.; Fidelio, G. D.; Barnham, K. J.; Separovic, F. (2006) Amyloid-β Peptide Disruption of Lipid Membranes and the Effect of Metal Ions. *J. Mol. Biol.* 759–770.

(23) Bode, D. C.; Baker, M. D.; Viles, J. H. (2017) Ion Channel Formation by Amyloid-β 42 Oligomers but Not Amyloid-β 40 in Cellular Membranes. *J. Biol. Chem.* **292 (4),** 1404–1413.

(24) Lee, J.; Kim, Y. H.; Arce, F. T.; Gillman, A. L.; Jang, H.; Kagan, B. L.; Nussinov, R.; Yang, J.; Lal, R. (2017) Amyloid β Ion Channels in a Membrane Comprising Brain Total Lipid Extracts. *ACS Chem. Neurosci.* **8,** 1348-1357.

(25) Batiste, M. S.; Ninot-pedrosa, M.; Bayoumi, M.; Gairí, M.; Maglia, G.; Carulla, N. (2016) Aβ42 Assembles into Specific β -Barrel Pore-Forming Oligomers in Membrane-Mimicking Environments. *Proc. Natl. Acad. Sci. U. S. A.* **113 (39),** 1–6.

(26) Sciacca, M. F. M.; Kotler, S. A.; Brender, J. R.; Chen, J.; Lee, D.; Ramamoorthy, A. (2012) Two-Step Mechanism of Membrane Disruption by A b through Membrane Fragmentation and Pore Formation. *Biophys. J.* **103,** 702–710.

(27) Bode, D. C.; Freeley, M.; Nield, X. J.; Palma, M.; Viles, J. (2019) Amyloid-β Oligomers Have a Profound Detergent-like Effect on Lipid Membrane Bilayers , Imaged by Atomic Force. *J. Biol. Chem.* **294,** 7566–7572.

(28) Sokolov, Y.; Kozak, J. A.; Kayed, R.; Chanturiya, A.; Glabe, C.; Hall, J. E. (2006) Soluble Amyloid Oligomers Increase Bilayer Conductance by Altering Dielectric Structure. J. *Gen. Physiol*. **128 (6),** 637–647.

(29) Valincius, G.; Heinrich, F.; Budvytyte, R.; Vanderah, D. J.; Mcgillivray, D. J.; Sokolov, Y.; Hall, J. E.; Lösche, M. (2008) Soluble Amyloid-β Oligomers Affect Dielectric Membrane Properties by Bilayer Insertion and Domain Formation : Implications for Cell Toxicity. *Biophys. J.* **95,** 4845-4861.

(30) Wang, Y.; Shi, Y.; Wei, H. (2017) Calcium Dysregulation in Alzheimer's Disease: A Target for New Drug Development. *J. Alzheimers Dis. Parkinsonism* **7 (5),** 100374.

(31) Kayed, R.; Sokolov, Y.; Edmonds, B.; McIntire, T. M.; Milton, S. C.; Hall, J. E.; Glabe, C. G. (2004) Permeabilization of Lipid Bilayers Is a Common Conformation-Dependent Activity of Soluble Amyloid Oligomers in Protein Misfolding Diseases. *J. Biol. Chem.* **279 (45),** 46363–46366.

(32) De, S.; Wirthensohn, D. C.; Flagmeier, P.; Hughes, C.; Aprile, F. A.; Ruggeri, F. S.; Whiten, D. R.; Emin, D.; Xia, Z.; Varela, J. A.; Sormanni, P.; Kundel, F.; Knowles, T. P. J.; Dobson, C. M.; Bryant, C.; Vendrsucolo, M.; Klenerman, D. (2019) Different Soluble Aggregates of Aβ42 Can Give Rise To Cellular Toxicity Through Different Mechanisms. *Nat. Commun.* ***10*****,** 1-11.

(33) Majumdar, A.; Mukhopadhyay, S. (2018) Fluorescence Depolarization Kinetics to Study the Conformational Preference, Structural Plasticity, Binding, and Assembly of Intrinsically Disordered Proteins. *Methods Enzymol*. **611,** 347-381.

(34) Jain, N.; Narang, D.; Bhasne, K.; Dalal, V.; Arya, S.; Bhattacharya, M.; Mukhopadhyay, S. (2016) Direct Observation of the Intrinsic Backbone Torsional Mobility of Disordered Proteins. *Biophys. J.* **111 (4),** 768–774.

(35) Lakowicz, J. R. (2006). *Principles of Fluorescence Spectroscopy* (3rd ed.). New York: Springer.

(36) Horcas, I.; Fernández, R.; Gómez-Rodríguez, J. M.; Colchero, J.; Gómez-Herrero, J.; Baro, A. M. (2007) WSXM: A Software for Scanning Probe Microscopy and a Tool for Nanotechnology. *Rev. Sci. Instrum*. **78 (1),** 013705.

(37) Sani, M. A.; Gehman, J. D.; Separovic, F. (2011) Lipid Matrix Plays a Role in Abeta

Fibril Kinetics and Morphology. *FEBS Lett.* **585 (5),** 749–754.

(38) Madhu, P.; Mukhopadhyay, S. (2020) Preferential Recruitment of Conformationally Distinct Amyloid-β Oligomers by the Intrinsically Disordered Region of the Human Prion Protein *ACS Chem. Neurosci.* **11,** 86-98.

(39) Bhattacharya, M.; Dogra, P. (2015) Self-Assembly of Ovalbumin Amyloid Pores: Effects on Membrane Permeabilization, Dipole Potential, and Bilayer Fluidity. *Langmuir* **31 (32),** 8911–8922.

(40) Aguilar, L. F.; Pino, J. A.; Soto-Arriaza, M. A.; Cuevas, F. J.; Sánchez, S.; Sotomayor, C. P. Differential Dynamic and Structural Behavior of Lipid-Cholesterol Domains in Model Membranes. *PLoS One* **2012**, *7* (6), e40254.

(41) Shrivastava, S.; Paila, Y. D.; Dutta, A.; Chattopadhyay, A. (2008) Differential Effects of Cholesterol and Its Immediate Biosynthetic Precursors on Membrane Organization. *Biochemistry* **47 (20),** 5668–5677.

(42) Kremer, J. J.; Pallitto, M. M.; Sklansky, D. J.; Murphy, R. M. (2000) Correlation of Amyloid Aggregate Size and Hydrophobicity with Decreased Bilayer Fluidity of Model Membranes. *Biochemistry* 10309–10318.

(43) Bhasne, K.; Jain, N.; Karnawat, R.; Arya, S.; Majumdar, A.; Singh, A.; Mukhopadhyay, S. (2020) Discerning Dynamic Signatures of Membrane-Bound α-Synuclein Using Site-Specific Fluorescence Depolarization Kinetics. *J. Phys. Chem. B* **124,** 708-717.

(44) Maiti, N. C.; Krishna, M. M. G.; Britto, P. J.; Periasamy, N. (1997) Fluorescence Dynamics of Dye Probes in Micelles. *J. Phys. Chem. B* **101 (51),** 11051–11060.

(45) Van Der Heide, U. A.; Van Ginkel, G.; Levine, Y. K. (1996) DPH Is Localised in Two Distinct Populations in Lipid Vesicles. *Chem. Phys. Lett.* **253,** 118–122.

(46) Weinstein, J. N.; Yoshikami, S.; Henkart, P.; Bluementhal, R.; Hagins, W. A. (1977) Liposome-Cell Interaction: Transfer And Intracellular Release of Trapped Fluorescent Marker. *Science*, **3,** 489–492.

(47) Liu, P.; Reed, M. N.; Kotilinek, L. A.; Grant, M. K. O.; Forster, C. L.; Qiang, W.; Shapiro, S. L.; Reichl, J. H.; Chiang, A. C. A.; Jankowsky, J. L.; Wilmot, C. M.; Cleary, P. J.; Zahs, K. R.; Ashe, K. H. (2015) Quaternary Structure Defines a Large Class of Amyloid-β Oligomers Neutralized by Sequestration. *Cell Rep.* **11 (11),** 1760–1771.

(48) Evangelisti, E.; Cascella, R.; Becatti, M.; Marrazza, G.; Dobson, C. M.; Chiti, F.; Stefani, M.; Cecchi, C. (2016) Binding Affinity of Amyloid Oligomers to Cellular Membranes Is a Generic Indicator of Cellular Dysfunction in Protein Misfolding Diseases. *Sci. Rep.* **6,** 1–14.

(49) Wälti, M. A.; Ravotti, F.; Arai, H.; Glabe, C. G.; Wall, J. S.; Böckmann, A.; Güntert, P.; Meier, B. H.; Riek, R. (2016) Atomic-Resolution Structure of a Disease-Relevant Aβ (1-42) Amyloid Fibril. *Proc. Natl. Acad. Sci. U. S. A.* **113 (34),** E4976–E4984.